

明治大学大学院先端数理科学研究科
2015年度
博士学位請求論文

Modeling and Simulation for Foldable Tsunami Pod

折り畳み可能な津波ポッドのためのモデリングとシミュレーション

学位請求者 現象数理学専攻

中山 江利

Modeling and Simulation for Foldable Tsunami Pod

折り畳み可能な津波ポッドのためのモデリングとシミュレーション

A Dissertation

Submitted to the Graduate School of Advanced Mathematical Sciences
of Meiji University

by

Department of Advanced Mathematical Sciences, Meiji University

Eri NAKAYAMA

中山 江利

Supervisor: Professor Dr. Ichiro Hagiwara

January 2016

Abstract

Origami has been attracting attention from the world, however it is not long since applying it into industry is intended. For the realization, not only mathematical understanding origami mathematically but also high level computational science is necessary to apply origami into industry.

Since Tohoku earthquake on March 11, 2011, how to ensure oneself against danger of tsunami is a major concern around the world, especially in Japan. And, there have been several kinds of commercial products for a tsunami shelter developed and sold. However, they are very large and take space during normal period, therefore I develop an ellipsoid formed tsunami pod which is smaller and folded flat which is stored ordinarily and deployed in case of tsunami arrival. It is named as “tsunami pod”, because its form looks like a shell wrapping beans.

Firstly, I verify the stiffness of the tsunami pod and the injury degree of an occupant. By using von Mises equivalent stress to examine the former and Head injury criterion for the latter, it is found that in case of the initial model where an occupant is not fastened, he or she would suffer from serious injuries. Thus, an occupant restraint system imitating the safety bars for a roller coaster is developed and implemented into the tsunami pod. As a result of the second simulation, the value of HIC is significantly reduced to be far below the safety level 1000.

Next, I conduct optimization the structural properties of the original model on the condition of minimizing mass while satisfying the maximum Mises stress on any elements for total simulation period is below the strength of CFRP.

On the other hand, parametric design method to generate the model for a tsunami pod is derived from mathematical modeling. The accurate model completely folded flat is obtained by calculating the angle of torsion which is rotated in the way each side consisting of triangle mesh on a side is not deformed. After generating models by this method, I carry out the simulation for safety verification and structure optimization again. Furthermore, the models with different number of sided polygons are generated and compared in safety evaluation.

Finally, I summarize the results obtained in this research, and mention the future works for practical applications.

Acknowledgements

I sincerely appreciate zealous support and cooperation of so many people.

Firstly, I would like to give thanks for Professor Ichiro Hagiwara, who gave me a few subjects of Origami engineering in which I have interests in. He advised how to conduct a research of numerical analysis and make a structure for a paper. Whenever we discussed, I was always impressed by his idea, logical mind, and deep consideration.

And, I have learnt a lot from Dr.Sunao Tokura how to use an analysis software “LS-DYNA”. Without his lecture and help, I wouldn’t complete my dissertation.

Moreover, I would like to give thanks for people in Hagiwara laboratory; Bo Yu, Liao Yujing, Yang Yang, and Thai Thao who all supported me to do programming, simulation.

I specially acknowledge Dr.Takamichi Sushida Takamichi who lectured me origami geometry with applying advanced mathematics. For his exceptional ability in mathematics ability of mathematics, my dissertation has been deepened in part of modelling.

I also sincerely appreciate other members at the same grade of doctoral course; Contento Lorenzo and Tanaka Yoshitaro, Dr.Nguyen Hoan. We have told each other progress of research regularly for 3 years. Having a conversation encouraged and motivated me every time.

Last but not least, I express my gratitude to my sons who give me energy all the time, which made me refresh and concentrate on my research.

My Phd journey wouldn’t have been going smoothly without supports and encouragements of all people as previously stated.

Contents

CHAPTER 1 INTRODUCTION.....	1
1.1 BACKGROUND	1
1.2 PRESENT ISSUES IN THE RESEARCH AND DEVELOPMENT OF ORIGAMI ENGINEERING	2
<i>1.2.1 Mathematical modeling of origami.....</i>	<i>2</i>
<i>1.2.2 Foldable and deployable functions</i>	<i>2</i>
<i>1.2.3 Application of origami into mathematical problem</i>	<i>3</i>
<i>1.2.4 Rigid folding</i>	<i>4</i>
<i>1.2.5 Three dimensional folding.....</i>	<i>4</i>
<i>1.2.6 Geometric solution and modeling for plants</i>	<i>5</i>
<i>1.2.7 Geometric solution and modeling for human alveoli</i>	<i>5</i>
<i>1.2.8 Strengthening origami structure: Development of new core</i>	<i>6</i>
1.3 THREE DIMENSIONAL ORIGAMI STRUCTURES	7
1.4 ORIGAMI APPLICATIONS	8
<i>1.4.1 Origami applications in science</i>	<i>8</i>
<i>1.4.2 Origami application in medical field.....</i>	<i>9</i>
<i>1.4.3 Origami architecture.....</i>	<i>10</i>
<i>1.4.4 Origami based designed clothing.....</i>	<i>10</i>
1.5 SOFTWARES FOR ORIGAMI	13
1.6 STRUCTURE OF THE THESIS	15
CHAPTER 2 ORIGAMI ENGINEERING	17
2.1 HISTORY AND RESEARCH OF ORIGAMI ENGINEERING	17
2.2 TRUSS CORE	19
<i>2.2.1 Origami Creation.....</i>	<i>19</i>
<i>2.2.2 Phase of Creation/ CAD/ Computational Mechanics.....</i>	<i>20</i>
<i>2.3.3 Forming phase of truss core structure</i>	<i>23</i>
2.3 REVERSE SPIRAL CYLINDRICAL ORIGAMI STRUCTURE.....	24
<i>2.3.1 Mathematical calculation</i>	<i>24</i>

2.4	FORMING PHASE OF TRUSS CORE STRUCTURE	30
2.5	SUMMARY	31
CHAPTER 3 SIMULATION AND OPTIMIZATION DESIGN METHOD.....		32
3.1	TECHNIQUE OF FLUID-STRUCTURE COUPLING ANALYSIS	32
3.1.1	<i>Structural vibration-acoustic coupled phenomenon</i>	<i>32</i>
3.1.2	<i>Vibration relative to structure fluid</i>	<i>36</i>
3.2	TECHNIQUE FOR OPTIMAL DESIGN.....	37
3.2.1	<i>Approximation method optimization technique</i>	<i>37</i>
3.2.2	<i>Optimization of response surface</i>	<i>43</i>
3.3	SUMMARY	51
CHAPTER 4 FOLDABLE TSUNAMI POD		52
4.1	PREVIOUS RESEARCHES AND COMMODITIES OF TSUNAMI EVACUATION	52
4.2	NEWLY DEVELOPED FOLDABLE TSUNAMI POD	54
4.2.1	<i>Generation of initial model without occupant restraint system</i>	<i>54</i>
4.2.2	<i>Theory for analysis: Fluid-structure coupling analysis</i>	<i>56</i>
4.2.3	<i>The conditions for simulation and video image shots</i>	<i>58</i>
4.3	NUMERICAL SIMULATION	59
4.3.1	<i>Verification of strength of the initial model without a restraint</i>	<i>59</i>
4.3.2	<i>Head injury criterion of the initial model</i>	<i>60</i>
4.3.3	<i>Verification of strength of the modified model with a restraint</i>	<i>61</i>
4.4	OPTIMIZATION OF STRUCTURE OF TSUNAMI POD	63
4.4.1	<i>Conditions for optimization</i>	<i>63</i>
4.4.2	<i>Result of optimization</i>	<i>64</i>
4.4.3	<i>Validation of optimal model</i>	<i>66</i>
4.4.4	<i>Consideration for simulation results</i>	<i>66</i>
4.5	SUMMARY	67
CHAPTER 5 MATHEMATICAL MODELING FOR FLAT FOLDABLE TSUNAMI POD		68
5.1	CONSIDERATION OF BI-STABLE STRUCTURE FOR A TSUNAMI POD.....	68
5.2	DESIGN METHOD OF FLAT-FOLDABLE ELLIPSOID BODY	69
5.2	SAFETY CERTIFICATION FOR THE MATHEMATICALLY DESIGNED MODEL	74
5.2.3	<i>Simulation for the mathematically designed model</i>	<i>75</i>
5.2.2	<i>Optimization for a mathematical designed tsunami pod.....</i>	<i>76</i>
5.3	COMPARISON OF THE DIFFERENT NUMBER OF SIDED POLYGONS FOR TSUNAMI POD	

.....	79
5.4 SUMMARY	81
CHAPTER 6 CONCLUSIONS AND FUTURE WORK	83
6.1 CONCLUSIONS	83
6.2 FUTURE WORK	85
<i>6.2.1 Tasks left for practical use</i>	<i>85</i>
<i>6.2.2 Consideration of generating bi-stable structure [6.4]</i>	<i>87</i>
BIBLIOGRAPHY	91
<i>CHAPTER 1</i>	<i>91</i>
<i>CHAPTER 2</i>	<i>94</i>
<i>CHAPTER 3</i>	<i>95</i>
<i>CHAPTER 4</i>	<i>96</i>
<i>CHAPTER 5</i>	<i>97</i>
<i>CHAPTER 6</i>	<i>97</i>

Chapter 1 Introduction

1.1 Background

Folding a paper is common habit among all people beyond epoch and their age, and origami is not original culture of Japan. However, multiple forms of crafts such as crane, rabbit, dog and flower created with one piece of color paper have beautiful appearances, which are known as Japanese traditional hand craft all over the world. As a result, origami is translated into English as it is. In fact, as manufactured products there have been solely honey comb core invented by British engineering who had hinted by a craft of Star Festival immediately after World War II.

Researchers of science and engineering in Japan should take it seriously. On this standpoint, Nojima proposed “Origami engineering” in November of 2002 [1.1]. Impressed by this, Hagiwara established “workshop of origami engineering” in the Japan Society for Industrial and Applied Mathematics in April of 2003. This event has been introduced in the corner of Japanese science and technology in Japan Science and Technology Science (JST) since fiscal year 2008[1.2]. The research in realm of origami engineering have been worked earnestly, and the subject of tsunami pod in this research is also included in this category. Those structures created by folding or cutting of origami paper have roughly 2 kinds of properties. One property is foldable and deployable function, and another is function to strengthen the structure of a membrane. Largely, the former primarily generates spiral shape easy to change and deform, and the latter generates symmetry shape providing stabilization. Origami engineering apply either property as mentioned as above, and as material not only paper but also plastic and metal are used which requires advanced computational science to apply origami engineering into industry.

1.2 Present issues in the research and development of origami engineering

Here in this section, the background and present issue of origami engineering is mentioned. Since “workshop of origami engineering” was established in the Japan Society for Industrial and Applied Mathematics in year 2000, there have been ever many research presentations in sessions of “origami engineering” organized in other societies such as the Japan Society of Mechanical Engineering and

These research are divided principally as below from ① to ⑩.

- ① Mathematical modeling of origami
- ② Foldable and Deployable functions of origami
- ③ Applications of origami into mathematical issues
- ④ Rigid origami
- ⑤ 3D origami
- ⑥ Geometric solution and modeling of plant
- ⑦ Geometric solution and modeling of human alveolus
- ⑧ Function to strengthen a structure by origami: development of new core material
- ⑨ Application of conformal transformation
- ⑩ origami 3D printer

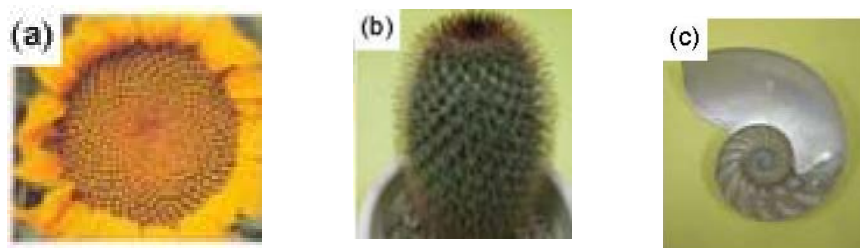
1.2.1 Mathematical modeling of origami

There is a free software “TreeMaker [1.3]” as a representative software to design origami. This had been advanced by Robert J.Lang for 10 years while taking in origami crafts by Japanese origami creators for experiment. On the basis of the theory of origami geometric, the crafts of many animals and plants devised by through trial and error were expressed by origami geometry, which have provided finer design crafts.

1.2.2 Foldable and deployable functions

There are remarkable study examples by Nojima et. al. examines thoroughly those models of cylinder[1.5] and conical shell [1.6],[1.7] which are folded in the axis direction the winding

model for circular membrane, a core structure, core panel[1.10]. These studies are based on the idea that spiral shaped folding lines provide the satisfactory ability of development for foldable structure. Furthermore, a mast of space structure for which easy folding and certain development are requested, a fundamental model for an inflatable structure to produce space structure at low cost, design of a solar sail navigated by sunlight have been considered on the basis of this theory. Many kinds of spiral structures and spiral patterns as shown in Figure.1.1 (a),(b), and (c) are observed in the nature world. Especially in plants, the number of equiangular spirals composed of 2 sequence numbers found by Fibonacci [Fibonacci sequence: 1,1, 2,3,5,8,13,21,34,55,...(each number is sum of the former 2 sequence numbers)] appear apparently in pattern. This sequence of numbers are related to cell division which is believed to evolution as well. For the reason of the ratio of successive 2 numbers are closer to golden ratio 1.618, this spiral is also called “golden spiral”. In likening the sides of cactus as shown in Figure.1.1(b) to cylinder and observing spiral structure as folding lines, this spiral has a degree of freedom to be able to escape upward. This made it possible for spiral structure to develop.



(a)spirals drawn by florets of a sunflower(34 spirals clockwise from center and 21 spirals counter-clockwise from center), (b)a side with spiral pattern of florets of cactus, (c)a section of live fossil Nautilus

Figure.1.1: Spiral structures

1.2.3 Application of origami into mathematical problem

The fact that the problems “ trisection of angle” and “Doubling the cube” whose Figures are impossible to be drawn by Euclid geometry are drawn by origami idea came to be generally known when Abe introduced his own devised folding instructions in the former of 1980s[1.12]. In expanding this instruction, the problem “Of the general solution of (real coefficient) cubic equation” have been discussed among domestic and foreign researchers [1.13]. Moreover, origami geometry mentioned as above encouraged researchers of computer science to participate in origami research. There has been a mathematical approach such as how

amount of calculation is necessary to judge whether a given folding line is folded flat or not as a subject for discussion. Uehara reported that “analogy of the number of folding” worked well corresponding to “the step necessary for calculation”, and he mentioned the problem of “maximum of working area” and “maximum of moving distance” remained to be examined for the future[1.14]. This is a substantive problem for example in developing large-scale space shuttle with origami theory, therefore the future development is strongly desired.

1.2.4 Rigid folding

Rigid folding is considered that each surface is rigid body and the parts except folding lines are impossible to be folded and be bent, therefore its condition for folding is stricter than “regular origami”. However, rigid origami is expected to wide applications such as architecture [1.16], and so active research about rigid origami has been carried out in recent years. To apply rigid origami into engineering, it is required firstly to prove obviously a continuous deformation of a form and secondly to be possible to design according to diverse factors such as function, user’s taste, and environmental condition. As a example, it is expected to resolve an inverse problem to lead a pattern from the requirements for 3D form while the possibility of rigid origami is guaranteed as well as to calculate 3D form by simulating a given pattern. Anticipating that rigid origami will be expanded to cylindrical structure and its combined structures and various designs including space will be realized to be applied widely into architecture, contained, and package, a quadrilateral mesh origami has been expanded to cylindrical structure [1.16]. On the other hand, there is a method of constructing a tetrahedral shape by folding an arbitrary triangle sheet appropriately. This method has an advantage that with relatively high strength is constituted at low cost, because a triangle is a shape which can always spread plane all over a surface and for that it is proper in taking panels from a sheet and each surface of a tetrahedral shape made of those panels without being wasted become a triangle[1.17]. In the viewpoints of industrial design, it is expected that a characteristic shaped container of tetrahedron is designed. Also, water proof sheet made of 1 triangle shaped sheet and economical simplified tend using V shaped columns are anticipated to be applied into industries.

1.2.5 Three dimensional folding

3D folding is origami which doesn't presuppose flat folding. Given certain 3D shape and considering how to express the surface of the shape with one sheet of paper, one of means is to arrange each surface which composes a polyhedron on a plane to create a pattern. Only to cut each gap generated in the 1st step, a so-called paper craft is completed which builds up to create 3D shape by gluing each side to corresponding side. On the other hand, to realize as "origami" without cutting papers, it needs to be examined that each part and folding lines are appropriately arranged. This process often makes a pattern such complex as to be unrealistic to be folded, and still remains unexamined compared to flat folding. However, in restricting "axially symmetric shape" and allowing to put the pleats between parts outside of a shape, it makes it possible to generate 3D origami with extreme simple patterns. [18]. And, clothing design applying this method is performed [1.19].

1.2.6 Geometric solution and modeling for plants

The leaves and flowers of plants are stored in their buds, and they develop and grow with increase in temperature at the beginning of spring. Hence, plants are trying diverse measures to store their leaves and petal in their buds efficiently [1.20]. For example, those leaves of beech and inushide are folded relatively with regularity in a corrugated plate shape, and in case of those leaves of poplars and platanus, both edges are stored by being enfolded into the front or back side. Not only leaves but also flowers of a morning glory are enfolded spirally into buds, while petals of a potato spread roughly in a plane whose gusset makes it folded relatively small. It is adequately considered that to research these ingenuities and characteristics expressed in nature world from engineering standpoints would provide beneficial hints with design of space developable structures such as an artificial satellite and a solar cell panel and with research about a beneficial storage form for a tent and a clothing. It needs being accelerating these researches mentioned as above.

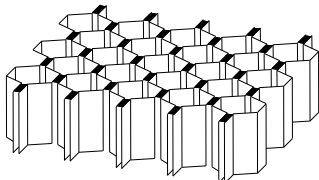
1.2.7 Geometric solution and modeling for human alveoli

The research of reproducing a structure and function of human respiratory system in a computing machine has ever been carried out [1.21]. Constructing 4D model combining 3D space and time for alveoli structure, current simulation from bronchial tubes to alveoli has been carried out. However, it is largely difficult to display the manner of complicated deformation

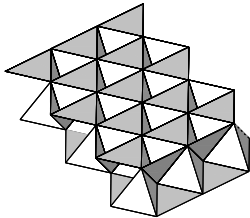
of complex structures like alveoli on 2D media such as a computer display. That's why the way of generating alveoli structure by origami paper is proposed for feeling a motion and current of alveoli during breathing are proposed. It is expected that origami alveoli model will not only contribute to improvement of respiratory research and but also become a seed for new solutions.

1.2.8 Strengthening origami structure: Development of new core

Honey comb core as shown in Figure.1.2(a) was invented by a British engineering after Wold War II by hint of an ornament of Japanese Star Festival. The rigidity of core in the height direction is maximum per weight, therefore it has numerous uses such as restraint of walls of an airplane, and ultimately it has currently been developing into industry and academics in unit of trillion Japanese yen. However, it is weak to shear and deform simply, so generally a panel is glue on upper and lower side. For usage of glue, it has disadvantages that it is difficult to be curved to a surface and inflammable in fire. On the other hand, Nojima [1.22] and Niijima



(a) Honey comb core



(b) Truss core

Figure.1.2: Comparison of rigid structures applying origami

and Saito[1.23] developed Octet typed truss core as shown in Figure1.2(b) consisting of tetrahedron and octahedron by applying space-filling theory indicated as in Figure.1.3.

The structure of space –filling form consisting of tetrahedron and octahedron by combining 2 pieces of core panels which have core shapes formed by triangular pyramid with equilateral bas, it is expected to produce structural member which is light weight and high rigid on theory. If it is the case plastic is applied for material, molding is straightforward, while it is necessary to manipulate with steel pane; and aluminum one to apply core into buildings and transportation machine. Hence, to implement origami form devised mathematically, it is essential to examine the possibility of molding from engineering standpoints, for which Tokura and Hagiwara developed multistage molding technique [1.24].

1.3 Three dimensional origami structures

There are three dimensional origami crafts designed by Dr. Nojima as shown in Figure. .The photo (b),(f), and (g) can be folded flat, while (a),(c),and (h) are not changed in form, and the others (d) and (e) are shrink to some extent.

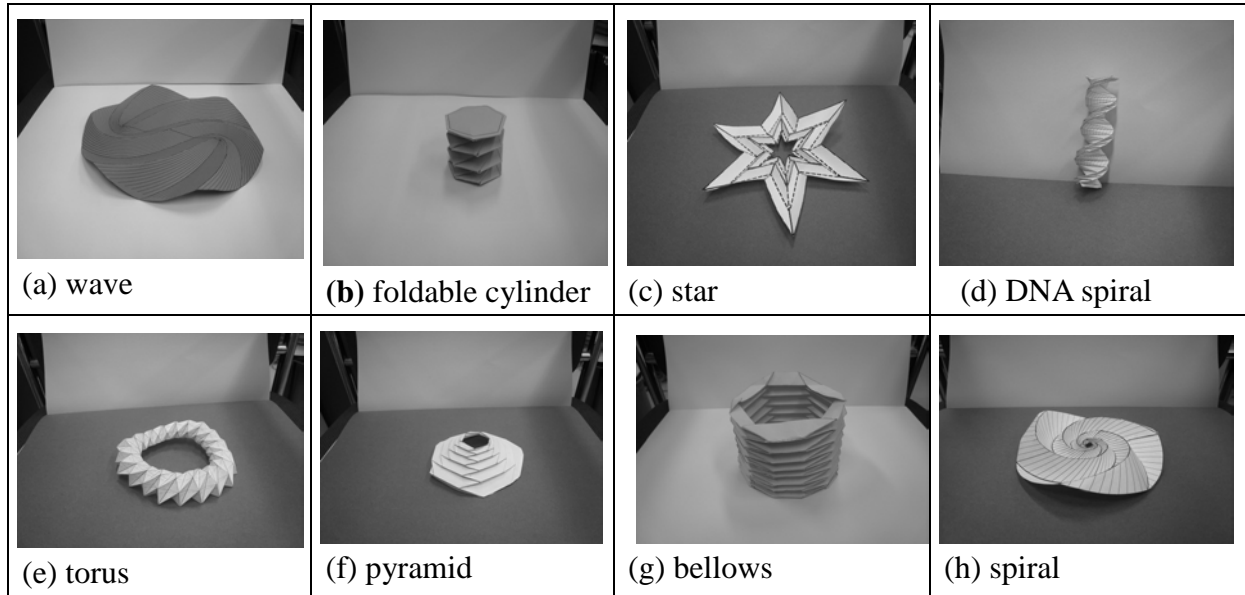


Figure.1.3: Various types of origami paper crafts

Nojima and Sugiyama developed a folding method of a circular membrane both in radial and circumferential direction like Figure 1.4 is newly developed. By gluing two circular membranes at their peripheries, fundamental foldable model for designing 3-D structure is manufactured. A novel design method of foldable spherical membranes with proper foldability was devised by using this concept [1.25].

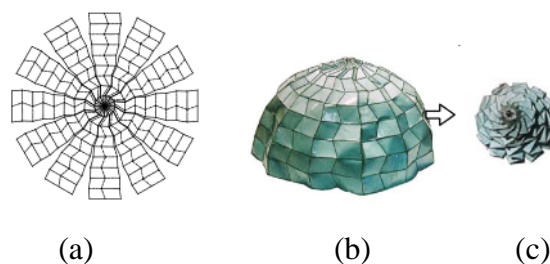


Figure.1.4: Hemisphere designed by Sugiyama and Nojima (a) Development chart (b) Foldable hemi-spherical origami model (c) Flat-folded with shrinks in radial direction

1.4 Origami applications

1.4.1 Origami applications in science

It is surprising that paper folding ideas are used in technically advanced science projects. Here are some industrial applications use which origami folding structure are applied into written as below.

In March of 1995, Japanese scientists used origami concepts to pack and deploy a solar power array in the research vessel called Space Flight Unit (SFU). On Earth, the solar array as shown in Figure.1.5 was folded into a compact parallelogram, and then in space, it was expanded into a solar sail. The method of folding the solar panels is called "Miura-ori", whose folding procedure is illustrated as in Figure.1.6 in honor of Koryo Miura, a professor in Tokyo University, who developed the fold [1.26]

The Miura-ori (translation = Miura-fold) is famous in map folding. The Miura-ori allows a square piece of paper to be folded in such a way that it can be opened (in one motion) by pulling at two opposite corners. As well, a Miura-ori folded map is less likely to tear at the crease junctions. An easy to use road map - now that's origami science.

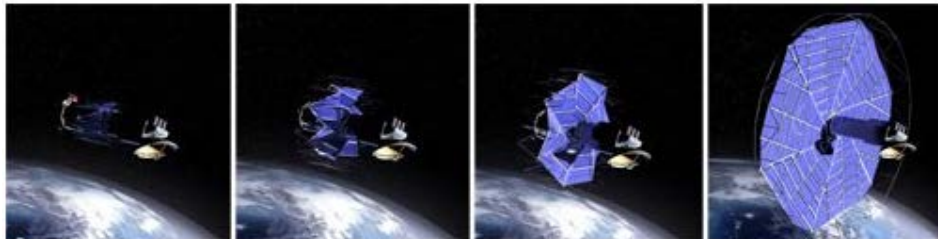


Figure.1.5: Solar array of spacecraft from Miura-ori structure (Zirbel et al.,2003)[1.27]

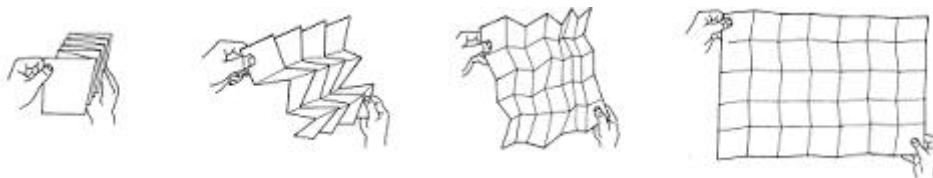


Figure.1.6: Miura folding from compact size to large flat size

A German company, EASi Engineering, was interested in finding a better fashion to pack airbags into car steering wheels. Professional origami artists, Robert Lang, helped design an algorithm which will allow computer simulations of airbag folding and deployment as shown

in Figure.1.7[1.28];[1.29]. This allowed the company to evaluate the efficiency of the airbags without actually doing a crash test. Saves money, saves time, saves lives.

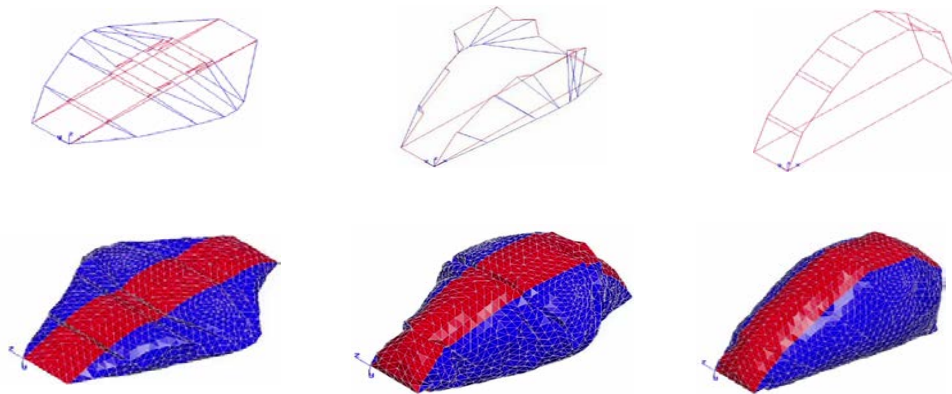


Figure.1.7: Folding airbag (upper row: framework, lower row: 3D mesh)

1.4.2 Origami application in medical field

In 2003, Zhong You and Kaori Kuribayashi from the University of Oxford developed an origami stent which may be used to enlarge clogged arteries and veins as shown in Figure.1.8. The water bomb base from origami was used to design the origami stent.

A stent is a tube which can be collapse into a smaller size. Using a balloon catheter, the stent is maneuvered through the patients' veins/arteries to the clot site. When the balloon is inflated, the stent is expanded to a larger diameter, thereby opening the vein/artery for better blood flow. Depending on the application, the tissue may grow over the stent and it remains in the patient permanently. By 2005, a self-deployable origami stent was developed.



Figure.1.8: Cylindrical tube with 0.5 mm width folds in its fully folded and expanded configurations [1.30]

1.4.3 Origami architecture

In September of 2010, Tine Hovesejian from the School of Architecture, University of Southern California developed an origami shelter made of cardboard as shown in Figure.1.9. This structure is suitable as a temporary outdoor shelter for victims of natural disasters such as an earthquake or a tsunami. These cardboard structures can serve as living spaces for the homeless. Though made of corrugated cardboard, these origami shelters are surprisingly sturdy, and are water & flame resistant. They are relatively inexpensive to make, and the units can be collapsed flat for straightforward storage & transport. Much nicer than the cardboard homes found in back alleys.



Figure.1.9: Origami shelter made of cardboard [1.31]

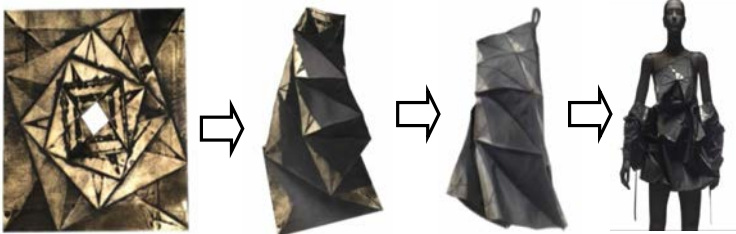
1.4.4 Origami based designed clothing

Mercedes Arocena and Lucia Benitez created fabulous origami-inspired dresses, one of which is Figure.1.10 for their thesis in 2010. The dresses used 4 types of modular origami units: water bomb tessellation, Sonobe units, and Golden Venture folding triangular units, and Electra units.



Figure.1.10: Origami-inspired dresses (Mercedes Arocena and Lucia Benitez,2010)[1.32]

While in Japan, a designer for a clothes brand “Issey Miyake” created clothes and bag on the basis of origami folding shown in Figure.1.11(a)(b)(c) hinted by Mitani’s mathematical origami theory[1.33], and sophisticated women middle aged with these items are seen in urban areas of Japan.



(a) 2D to 3D clothes [1.34]



(b)flat folding handbag [1.35]



(c)flat folding clothes [1.34]

Figure.1.11: origami based fashion designed by Issey Miyake

The pattern for a flat foldable hat was designed by an author [1.36] referring to theory proposed by Nojima explicated thoroughly in Section 2.3. Figure.1.12(a) is a pattern for flange part of this hat. The central angle of an octagonal is 45 degrees and each interior angle is 135 degrees, so the folding angle β and γ are calculated as 45 degrees collectively by assigning 8 for N in the conditional expression for flat folding (1.1) to make a folded shape octagonal. Figure.1.12(b) is a folded sample of flange part made of felt cloth by connecting each parts with sewing machine after cutting both mountain lines and valley ones. Concerning glue parts, there are glue areas in case of paper pattern, which takes time and troublesome, on the other hand there is no glue parts made on a pattern written on cloth, because sewing machine can connect each edge of parts directly.

$$\beta + \gamma = (\pi/2) (1 + 2/n) \quad (1.1)$$



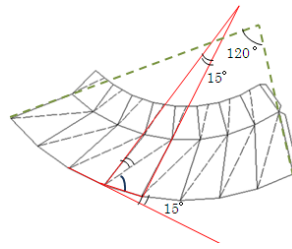
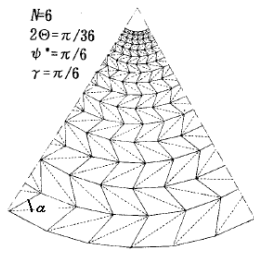
(a) Pattern of flange part

(b) Fabricated sample of flange part

Figure.1.12: Fringe part of flat foldable hat

Next, a pattern for crown part is designed on the basis of truss model as shown in Figure.1.13 (a). As far as meeting folding condition of Equation (1.2) on each node, apex angle Θ , composing angle of a triangle α , and the number of folding N are arbitrary. Figure.1.13(b) is a pattern for 2 stage truss model where the apex angle Θ between extended outlines of both end parts is 120 degrees. Therefore, in assigning 8 for N and 120 for Θ in Equation(2.2), α is calculated as 15 degrees. In similar fashion, a fabricated sample of a crown part is made as in Figure.1.13(c). Figure.1.14(a),(b),and(c) is a completed fabricated sample for a flat foldable hat which is made by connecting a flange part and crown part. I also made a flat foldable hat with vinyl chloride whose thickness is 0.1mm as shown in Figure.1.15.

$$\alpha = (2\pi - \Theta) / 2N \quad (1.2)$$



(a) Conical truss model (b) Patten of crown part (c) Fabricated sample of crown part

Figure.1.13: Crown part of flat foldable hat



(a) Folded state form from above (b) Folded state from below (c) Developed state

Figure.1.14: Combination of flange and head parts made of kilt



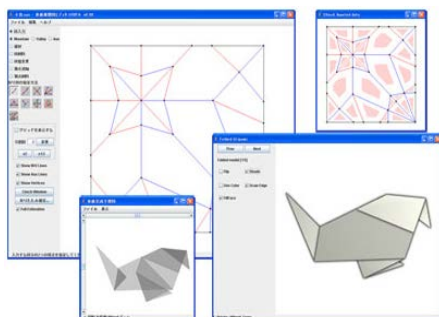
Figure.1.15: Flat foldable hat made of vinyl chloride whose thickness is 0.1mm

1.5 Softwares for origami

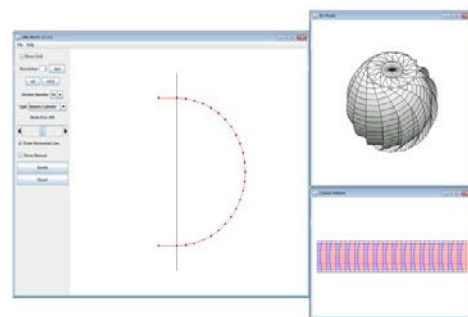
There have been several tens of software relevant to origami design developed primarily in United States and Japan by researchers who works on origami. The software which creates pattern and show complete form has already been developed by Mitani. He publishes for free in his website the editor for flat origami “ORIPA[1.37].” shown in Figure.1.16(a). However, the function of this editor is restricted to drawing folding lines on the screen referring to the marked lines on paper and displaying the predicted

completion. By this process, the correctness of folding lines drawn on ORIPA can be confirmed. It means that ORIPA is not the software which can realize all folding process included the completion, but just the editor based on the existing pattern. Mitani also developed the software called ORI-REVO [1.38] as shown in Figure.1.16(b) limited solely for the shapes based on the surface of revolution. The shapes generated with ORI-REVO are based on the surface of revolution. Actually, so far the software not depending on shapes hasn't been succeeded by any researchers because of intricate properties of origami. While there is another software; "Freeform origami[1.39]" shown in Figure.1.16(c) dealing with only rigid origami. This software shows movement transition from a flat pattern to a three dimensional form continuously.

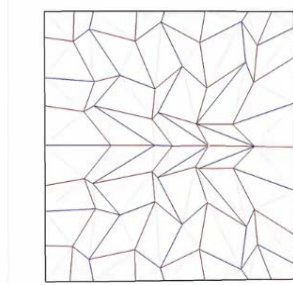
"TreeMaker [1.40]" as shown in the Figure.1.16(d) developed by Robert Lang is a program for the design of origami bases. A user draws a stick Figure of the base on the screen; each stick in the stick Figure (the "tree") will be represented by a flap on the base. A user can also place various constraints on the flaps, forcing them to be corner, edge, or middle flaps, and/or setting up various symmetry relationships. Once a user has defined the tree, TreeMaker computes the full crease pattern for a base which, when folded, will have a projection (roughly speaking, its "shadow") equivalent to that specified by the defining tree. Crease assignment (mountain or valley) are not computed, but with a few simple rules and some exploration by hand, the proper crease assignment can ordinarily simply be found. "Pepakura Designer [1.41]" developed by Tama Software Ltd. as shown in Figure.1.16(e) is to create paper craft models from 3D data which is generated by another software generating it. And finally, Hagiwara Lab in Meiji university to which an author for this dissertation belong developed "3D Origami Printer [1.42]" in 2014. This software generates 3D model from STL data, and make folding pattern from 3D model automatically. This pattern are more accurate and minute than "Pepakura Designer".



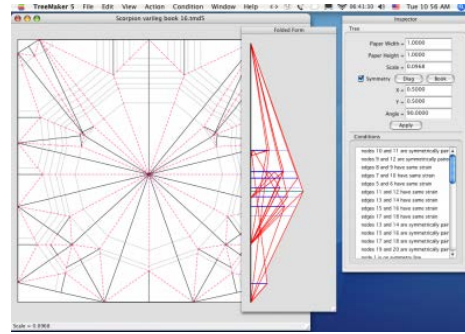
(a) ORIPA



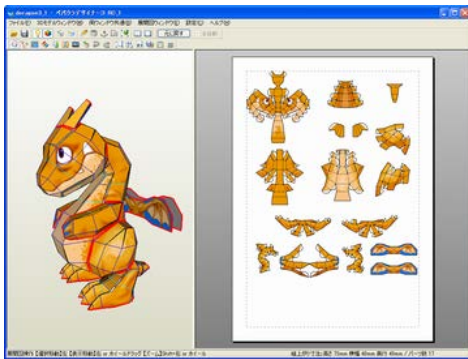
(b) ORI-REVO



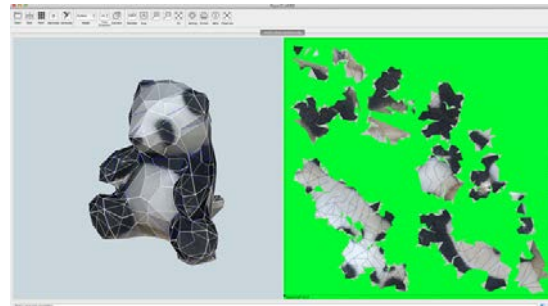
(c) Freeform origami



(d) Tree maker



(e) Pepakura designer



(f) Origami typed3D printer

Figure.1.16: Origami related software

1.6 Structure of the thesis

It can be said that this research is namely obtained by fusion of origami engineering and computational science. Hence, firstly in Chapter 1 there are history and present research subjects for origami, origami geometry, origami applications, and origami design software mentioned. And, I uncover the aim and situate this research. In Chapter 2, followed by the history and background of origami engineering, I described the numerical simulation for impact absorption with truss core and reverse spiral form. In Chapter 3, subsequently referring to simulation and optimal design method, I enlarge the safety verification for a tsunami pod and structure optimization method for it. In Chapter 4, I compare the result of simulation with a tsunami pod in case whether there is an occupant restraint system or not, and conduct structure optimization. In Chapter 5, after explicating the design method by mathematical modelling for a tsunami pod, I perform simulation optimization again for the designed model which is folded flat. Moreover, I compare the safety with the 2 kinds of

models with different sided of polygons. In Chapter 6, I summarize the all results in this research, and then mention the examinations. Finally, the problems about a mechanism and manufacturing method for making real products is mentioned.

Chapter 2 Origami engineering

2.1 History and research of origami engineering

It is necessary after creating novel origami to examine CAD and computational mechanics comprehensively in applying various materials such as paper and metal into real origami products. Specifically as shown in the Figure.2.1 there are phases with details to be examined thoroughly; ①origami creation on the basis of biotechnology and geometry,② the technique which can exalt imagination aided by CAD and CG, ③ computational mechanics, ④ manufacturing processing. Namely the steps are firstly creating diverse shapes in phase ①, and next creating CAD model from the shape obtained in phase ②, finally correcting the shape or sometimes feeding back to phase ① in aesthetic viewpoint. IT technologies of origami is to promote the imagination of phase ① furthermore. The shape obtained in this fashion is appropriated functionally in phase ③ (computational mechanics).Here, it will become necessary to collaborate closely with not only phase ② but also phase ④(manufacturing processing). It is because the function and manufacturing processing can't simply be consistent with each other. And also, close discussion with industrial group is essential to promote origami engineering.Figure.2.2 displays the origami created on the basis of plants. Here in this Chapter, two examples about truss core structure and reverse spiral cylindrical origami structure are explicated which are obtained by unifying four technologies mentioned above.

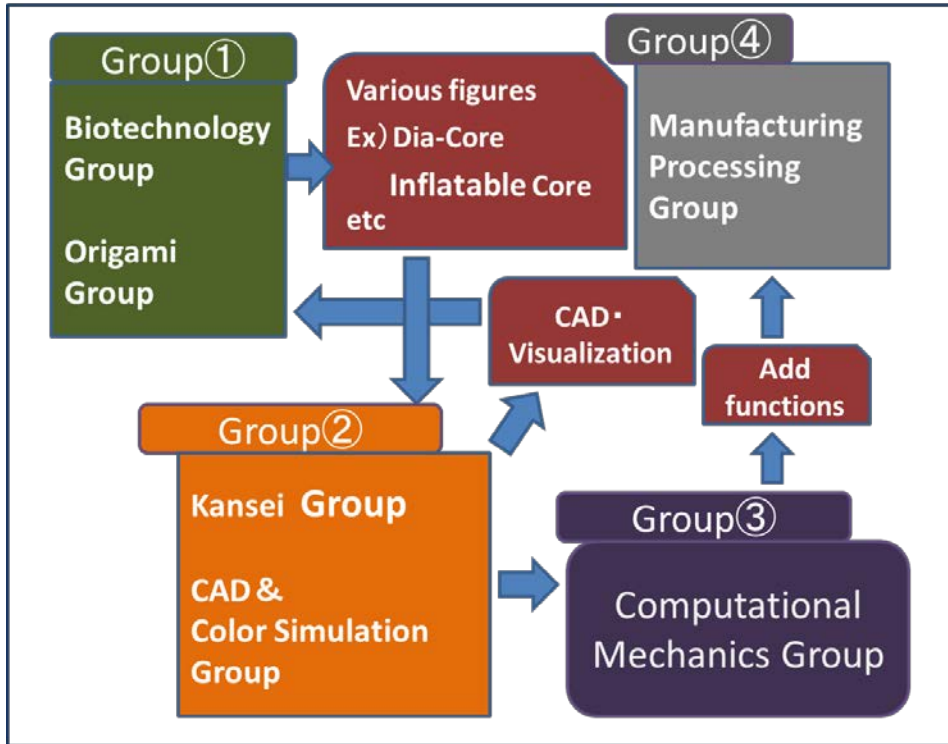


Figure.2.1: Flow of Research and Development of origami Engineering

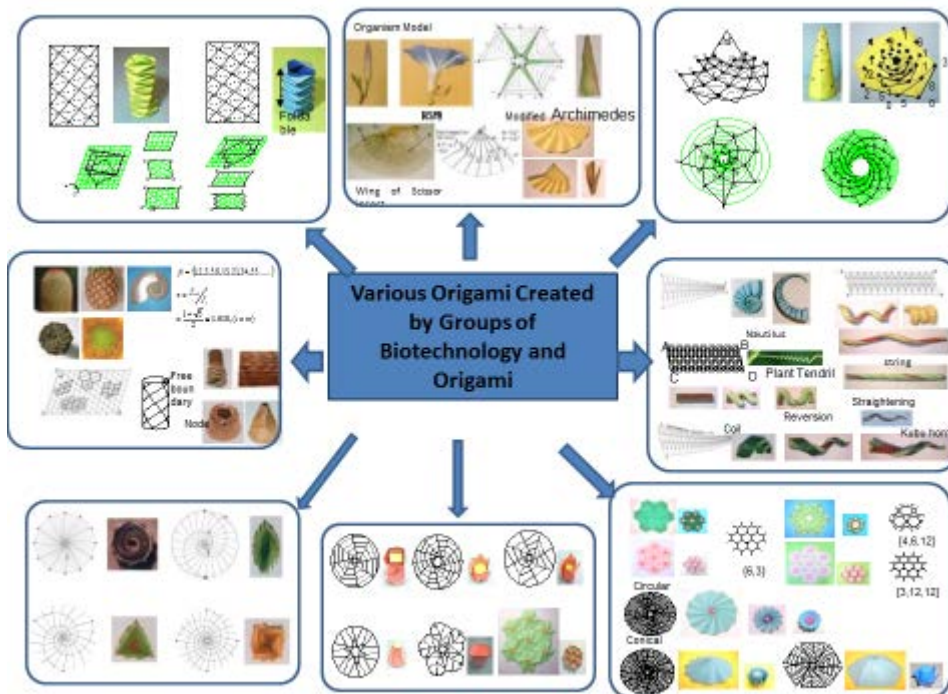


Figure.2.2: Origami based on plants

2.2 Truss Core

2.2.1 Origami Creation

Dire-core is obtained by tessellation theory shown in Figure.2.3 and space-filling theory shown in Figure.2.4. Figure.2.3 illustrates that regular polygon with all contacts uniform is referred to Archimedean polygon composed of 11 kinds of plane-filling polygons. Figure.2.4 demonstrates that there are 8 kinds of space-filling forms composed of less than 2 kinds of regular or semi-regular polyhedron. The dire-core generated by space-filling composed of tetrahedron and octahedron is called truss core displayed in Figure.2.5. The combination of tetrahedron and panel is called single core, while the space-filling between tetrahedron and octahedron is called double core. Figure.2.6 displays that numerous evolution models can be obtained from double core by origami operating such as separation and truncation. Moreover, the forming method by geometry pattern is examined in [2.1].

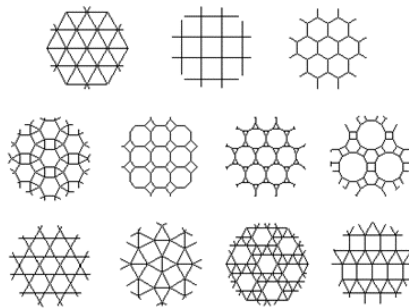


Figure.2.3: Dire-core base and diverse types obtained by origami operation

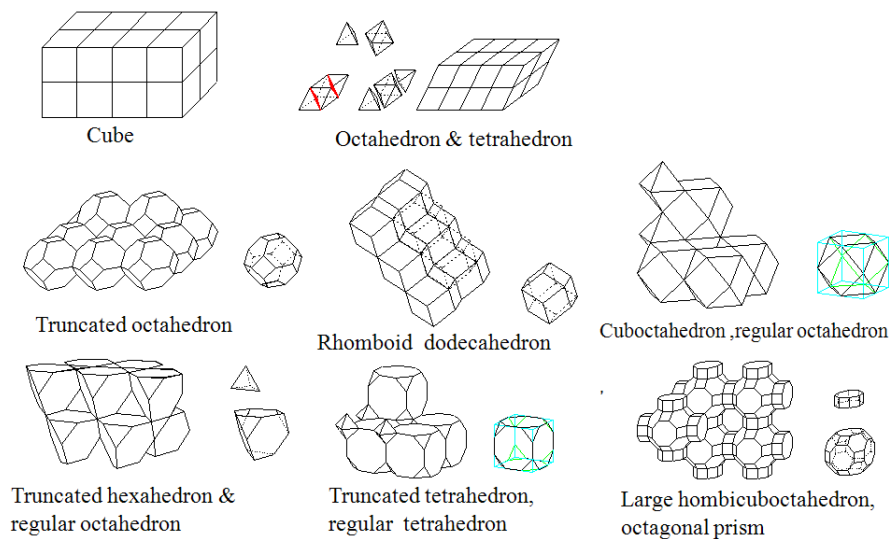


Figure.2.4: Space filling up form

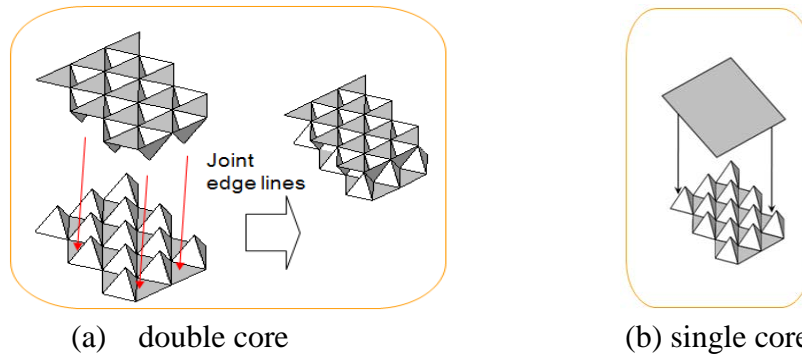


Figure.2.5: Truss core panel by space-filling composed of tetrahedron and octahedron

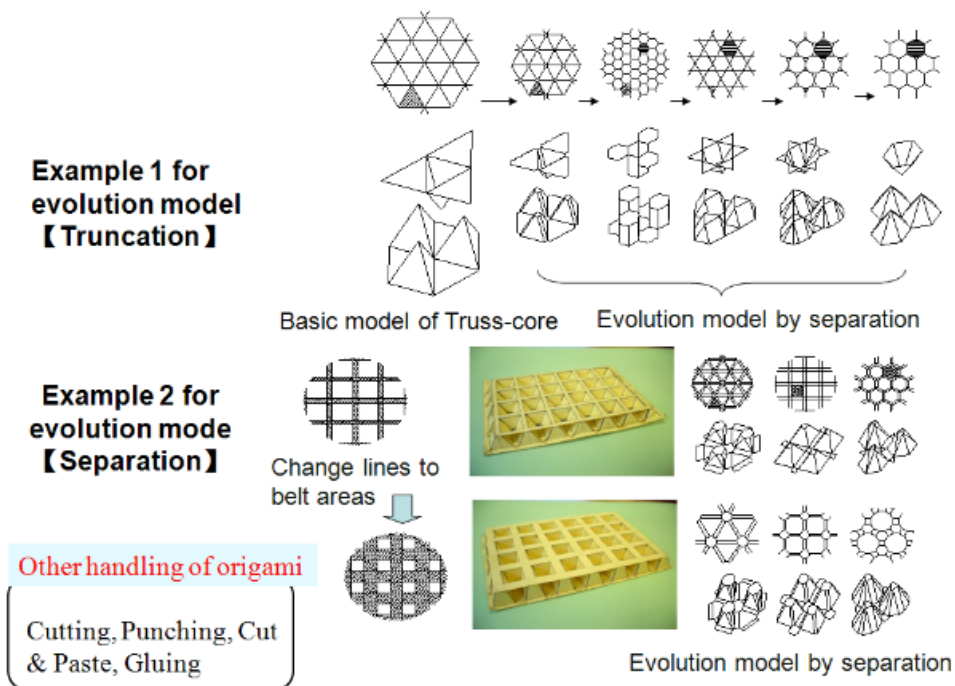


Figure.2.6: Evolution models by origami-operation

2.2.2 Phase of Creation/ CAD/ Computational Mechanics

For applying truss core into industry, those properties such as stiffness, vibration, impact, and bending compression are integral, and the property of stiffness is investigated in [2.2], the one of vibration is mentioned in [2.3], the one of impact is expatiated in [2.4], and the one of bending compression is written in [2.5]. Every property produced an excellent result.

Figure.2.7 shows the analytical procedure of bending compression property. Firstly, the flow of creating bending analytical model is written as below.

- ① Trimming the press-forming completion and then mapping onto mesh for bending analysis
- ② Copying panel and reverse upside down one sheet
- ③ Jointing two pieces of truss core panels
- ④ Defining the spot welding in the apex of triangle pyramid
- ⑤ Creating 3 points bending model

Trimming written in above ① is constituted of two tasks as below.

- 1) Defining trim line
- 2) Dividing and Re-meshing shell elements on trim line

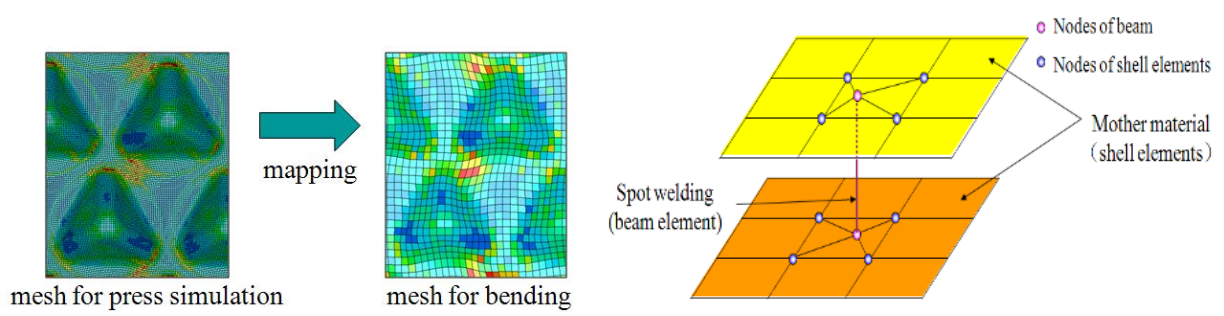
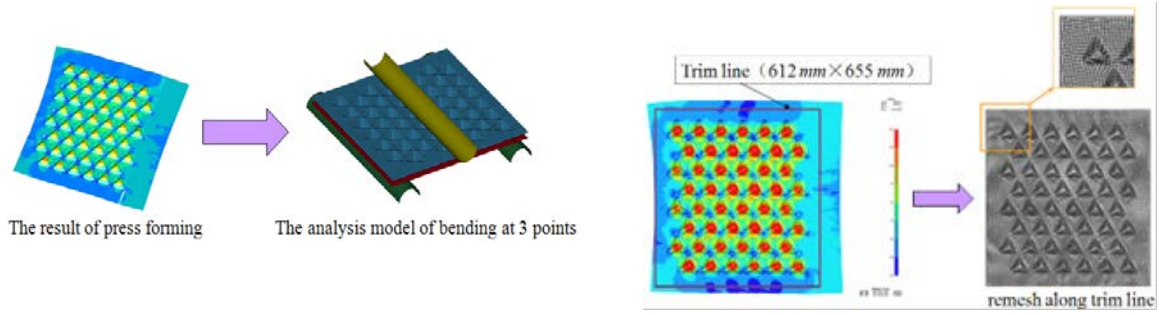
And, the mapping means that stress, deformation, and mapping of panel thickness distribution from precise mesh for press forming analysis to coarse mesh for bending analysis.

Concerning the definition of spot welding mentioned above, the apex of triangle pyramid is welded in case of real panel.

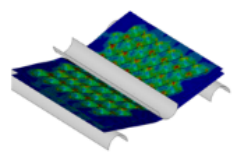
In simulation, the modeling method of spot welding (free node spot welding) which combines beam elements and the restrict condition of freedom degree of nodes is applied.

Here in case of considering work hardening and change of panel thickness, approximately 1.6 times strength has been shown, however the effect of work hardening is more significant than the one of board thickness change [2.6].

In reduced integral calculus element(BT element), even if considering work hardening, only 80 percentage of strength of complete integral element (BD element) can be achieved. It is because in BT element warpage is not reflected on element stiffness. As mentioned above, advanced computational mechanics is essential.



- Case 1: Full Int., hardening and thickness change
- Case 2: Full Int., thickness change
- Case 3: Full Int.
- Case 4: Reduced Int., hardening and thickness change
- Case 4: Reduced Int., hardening and thickness change



32% is larger than 5 deg. In warping

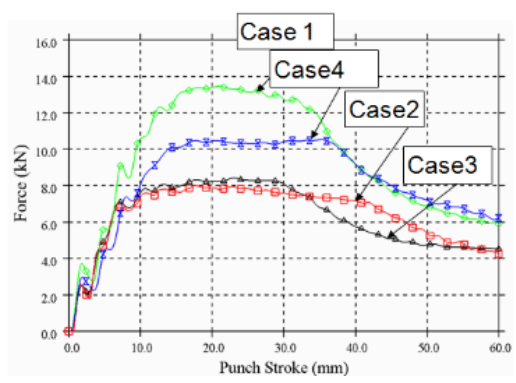


Figure.2.7: Analytical procedure of bending compression property

2.3.3 Forming phase of truss core structure

In origami field, mass production has ever been performed solely in the expand production and corrugated method for honeycomb shown in Figure.2.8, while in this paper mass production as in Figure.2.9 is achieved for truss core. This product was developed by Shiroyama Industry Co., Ltd. on the basis of the world's first multistep forming. Concerning the panel made of resin with high formability, shape is selected freely by vacuum forming, while concerning panel made of metal it is difficult to form deep crevice part, and so it is necessary to apply special forming such as traditional superplastic forming and facing hydro-forming. Manufacturing cost of these forming are high and for trying to diffusion to broad area as novel light weight means, I had aimed new forming technique at a lower price, as a consequent I've just succeeded in developing multistep press forming which can make it possible to create at a lower price aided by computational mechanics.

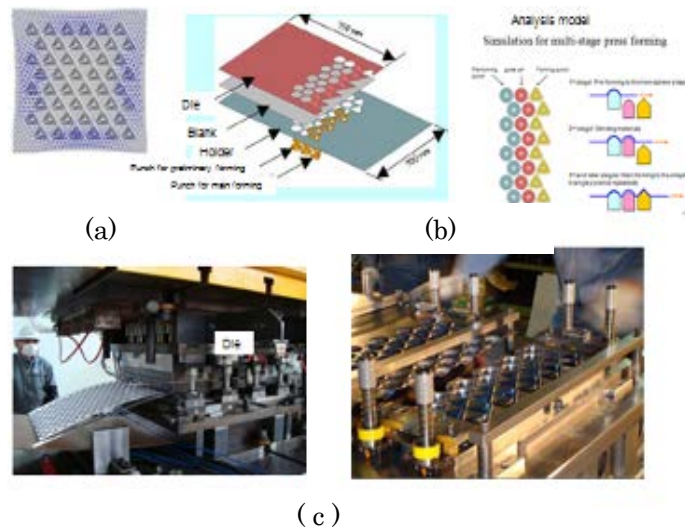


Figure.2.8: Multistep forming simulation and Mass production facility based on it
 (a) Result of single press forming, (b) Multi stage press forming, (c) Floor structure by the analysis model of multi stage forming

As shown in Figure.2.9, a good shape can't be obtained by single press forming. Figure.2.9 illustrates that multi stage press forming where in the first stage a panel is formed into hemisphere and in the next step formed into pyramid type. And, on the basis of this forming, the facility for general use was developed as shown in Figure.2.9 [2.7]. Firstly the solar cell panel consisting of single truss core developed by this facility is adopted in Town Hall Sagami-hara city, and continuously there has been one plan of mass adoption. With regard to

heliostat for solar heat generation, the current frame made of glass and steel is abolished and the structure using truss core is planned to be adopted in Japanese company. In the near future, OA floor composed of truss core is to be sold. It is concluded that truss core can take the place of honey comb core. That is to say that truss core is superior totally to honey comb considering truss core can be curved and honey comb can't. The condition is displayed as in Figure.2.10.

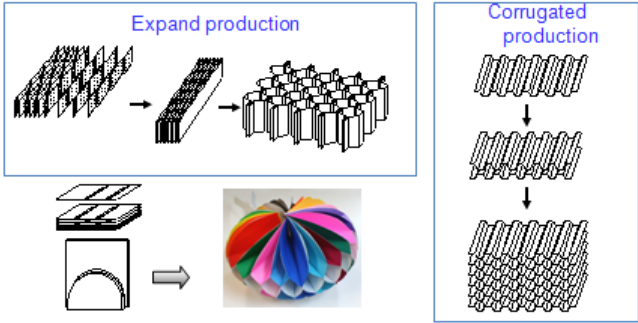


Figure.2.9: Two manufacturing methods for star festival decoration and honeycomb

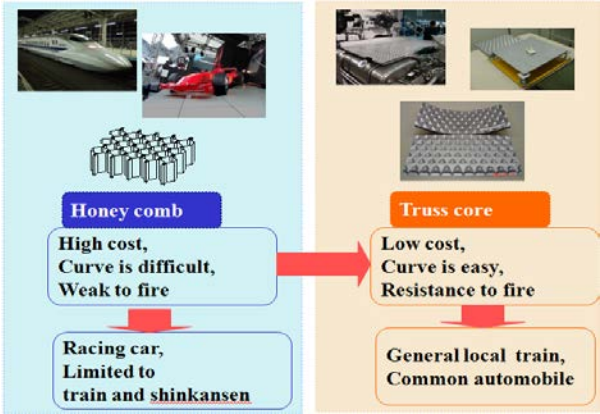


Figure.2.10: The comparison between honey comb core and truss core

2.3 Reverse spiral cylindrical origami structure

2.3.1 Mathematical calculation

Since the top and the bottom lines of cylindrical folding are desired to be equilateral polygon, the belt-like paper used for folding is well regulated as illustrated in Figure.2.11. The number

of parallelograms is labeled as m , the angle $B_1A_1B_2$ is labeled as α and the angle $B_2A_1A_2$ is labeled as β . It is obvious that the shape of cylindrical folding is determined by α and β only.

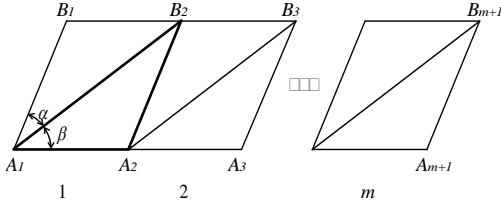


Figure.2.11: Well regulated 1-4 folding pattern

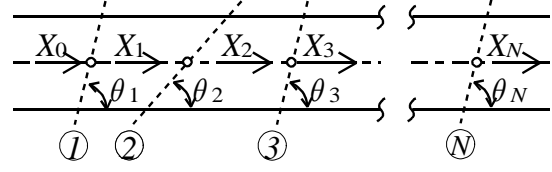


Figure.2.12: Typical 1-4 folding pattern

The value of α can be derived from Equation(2.1)

$$\theta_t = \theta_1 - \theta_2 + \theta_3 - \dots - \theta_N = \pi \quad (2.1)$$

$$\left\{ \begin{array}{l} \theta_1 = \alpha + \beta \\ \theta_2 = \beta \\ \theta_3 = \alpha + \beta \\ \vdots = \beta \\ \theta_N = \alpha + \beta \end{array} \right. \quad (2.2)$$

Then

$$\theta_t = \left(\frac{N}{2} \alpha \right) = m\alpha \quad (2.3)$$

where $N=2m$. Therefore, the solution of Equation (2.1) in this case is

$$\alpha = \pi/m \quad (2.4)$$

To know what happens during crushing, let us examine the triangle $A_1A_2B_2$ carefully. When this stripe pattern is completely folded, no matter what the value of β is, the side A_1A_2 should be fixed as one sideline of an m -sided equilateral polygon, and point B_2 should exactly fall in

on the circumscribed circle of the m -sides equilateral polygon, as illustrated in Figure.2.12. If β changes, the point of fall of B_2 should be adjusted accordingly, in order to restrict it strictly on the circumscribed circle. It has been found that if a stripe pattern can be folded into a crushable structure, the point of fall of B_2 is limited on the arc R_1R_2 . According to this, the range of β is expressed as Equation(2.5)[2.9].

$$\frac{\pi}{4} - \frac{\pi}{2m} < \beta < \frac{\pi}{2} - \frac{\pi}{m} \quad (2.5)$$

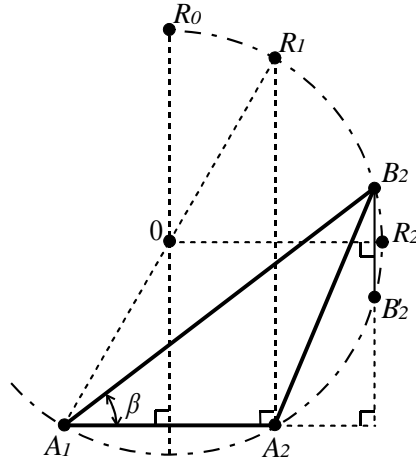


Figure.2.13: Circumscribed circle of m -sided equilateral polygon

At the same time, given the radius r of the m -sided equilateral polygon and the height h of cylindrical folding, β can be calculated by using the following formula, which is derived from geometrically deduction.

$$\beta = \alpha \tan \left[\left(\frac{h^2}{4r \cos \frac{\pi}{m}} + r \cos \frac{\pi}{m} \right) \div \left(\sqrt{r^2 - \frac{h^4}{16r^2 \cos^2 \frac{\pi}{m}}} + r \sin \frac{\pi}{m} \right) \right] \quad (2.6)$$

Let $\mu = h/r$,

$$\beta = \alpha \tan \left[\left(\frac{u^2}{4r \cos \frac{\pi}{m}} + r \cos \frac{\pi}{m} \right) \div \left(\sqrt{r^2 - \frac{u^4}{16r^2 \cos^2 \frac{\pi}{m}}} + r \sin \frac{\pi}{m} \right) \right] \quad (2.7)$$

In case of $m=6$, $0 < \mu < \sqrt{3}$; $m=7$, $0 < \mu < 1.7257$; $m=8$, $0 < \mu < 1.7123$...

When Equation (2.5) holds, a cylindrical reverse spiral structure is easy to fold. On the other hand, when Equation (2.5) doesn't hold, it is folded while producing high force and rotating. I investigated whether the former can be applied to beer can and pet bottle or not and the latter can be used for automobile energy absorption or not. In automobile collision, the hollow Half cut typed member which does sport welding between hat typed panel and flat panel is lifeline, however even if the member is crushed ideally, its own space becomes bulky, so it is crushed as long as only 70 percentage of its own length. In crash zone it is desirable for a member to be crushed as long as it can. Therefore, the use of this RSC has ever been proposed. The rapid proto-type model created on the basis of CAD data generated tearing at the edge part as shown in Figure.2.14 in case of thin panel. Therefore, by applying subdivision the improvement of forming proper has been obtained as well as aesthetic effect.

As shown in Figure.2.15, in case of RSC it shrinks to the 90 percentage of itself, however load is lower than expected. Therefore, it is difficult to replace the present energy absorption member. Even if optimized for increasing energy absorption, the form is intricate for realizing optimization. Therefore, in optimization, the subsequent examination is performed. The analytical mesh with original structured form is generated, and on the basis of that the mesh generating method for multi stages reverse spiral cylindrical origami structure is described by using the case of 2 stages shown in Figure.2.16 for example. Firstly, the forming alternation parameters (θ, R_1, R_2) are defined for the unit parts composed of 2 stages.

Practically, when one set of parameter (θ, R_1, R_2) is given in altering the form, firstly nodes coordinates shown in Figure.2.17 are altered according to new parameter values, secondly the one-to-one mapping relational expression formula is formularized by using isoparametric, and finally all of the nodes inside triangle face of original form are transformed into spiral typed forms. As the result of those processes, the analysis mesh for the cylindrical origami structure according to parameters can be obtained.

For implementing parameter study of cylindrical origami structure, it is necessary to set many combinations for form parameters (θ, R_1, R_2) , further more alter analysis mesh

automatically, finally implement analysis. For this issue, with the element information of analysis mesh maintained, the only nodes coordinated are altered every time.

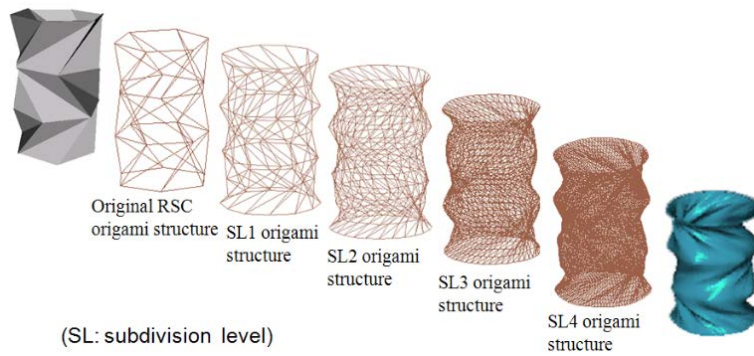


Figure.2.14: Modified RSC origami Structure

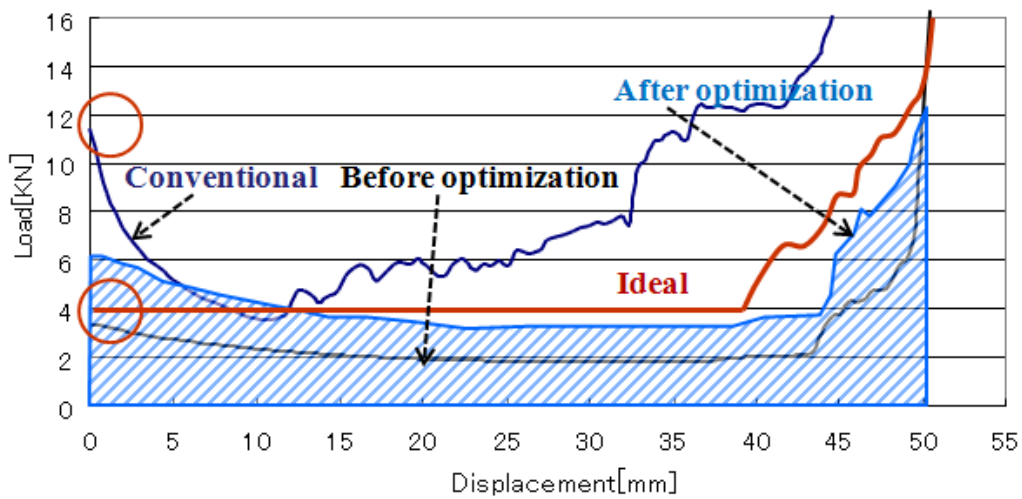
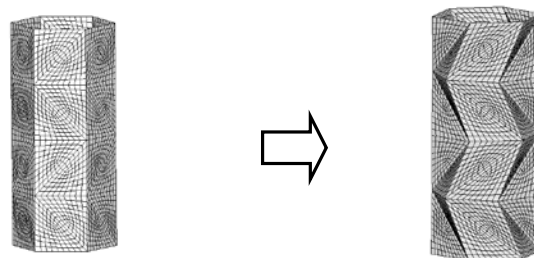


Figure.2.15: The dissimilarity between before and after Optimization



(a) Original Structure

(b) Spiral typed origami Structure

Figure.2.16: Original Structure and Spiral typed origami Structure

Then, the process where from cylinder type RSC is expressed automatically was contrived which had made optimal analysis with numerous parameters possible with RSC changing successively in the process of optimization. As a result, the design specification with 1.8 times more energy absorption than traditional structure on the condition of the same weight has been found [2.10]. Namely, the condition is as displayed the line “after optimization” in the Figure.2.15. The member shrinks more than its height and the property load-variance is flat and the load is relatively high. This feature can be advantage for driver injury index for lengthening crash time, because reaction can be controlled by oblique folding lines and member shrinks while rotating as shown in Figure.2.14 The term “without bead” in this Figure means that the bead developed by Hagiwara [2.11];[2.12];[2.13] is essential for the current half cut type member to generate satisfactory crush mode.

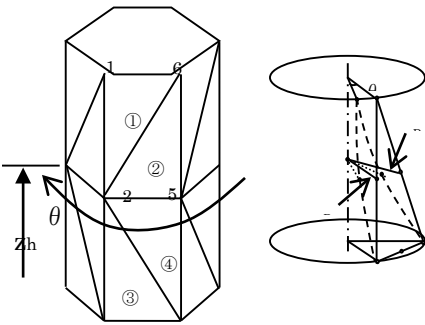


Figure.2.17: Key nodes and parameter

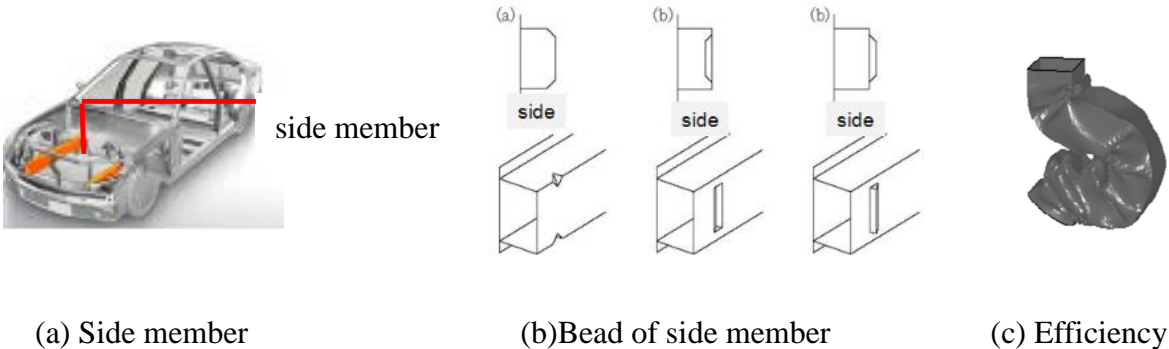


Figure.2.18: Bead and its efficiency



(a) RSC



(b) Crushed mode

Figure.2.19: RCS form by hydro forming and its crushed mode

2.4 Forming phase of truss core structure

RSC can be formed by hydro-forming as confirmed in Figure.2.20 [2.7], which house makers have an interest in RSC. While in automobile companies which are strict with cost control, RSC is still under consideration about adoption and it wasn't been accepted immediately. Therefore as displayed as Figure.2.21, if the traditional half cut type side member obtains the same property as RSC, it is estimated that more excellent property at lower cost will be achieved.

Half cut type member can't rotate as RSC does, because it's structure is joined by spot welding between one sheet of foldable panel and one sheet of flat panel. Then, as shown in Figure.2.21 by making multistep at the direction of axis and creasing along inclined direction, it has been found that transformation tendency same as RSC is generated inside internal each step and between each step [2.14] short terms, same as RSC, crush deformation mode and reaction force can be controlled freely with end and oblique folding lines, and by suitable design specification collision energy absorption property has been unconfirmed and the result has been also yielded that member is resistant to oblique directional load [2.8].

Automobile companies are concerned extremely with this member. It has demonstrated that

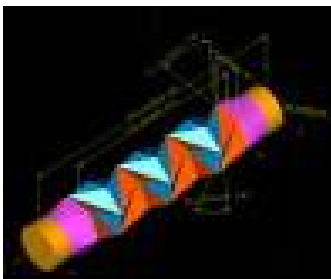


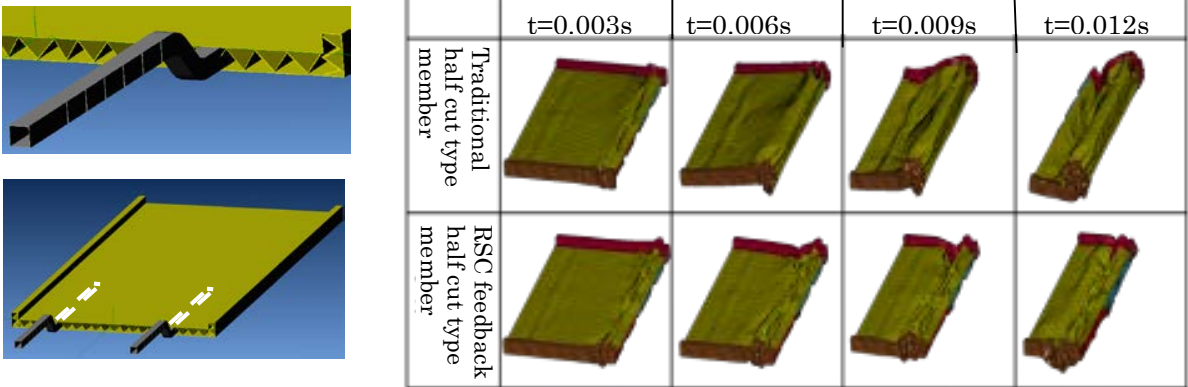
Figure.2.20: Test RSC



Figure.2.21: Half cut typed structure from RSC

traditional structure should also be reconsidered from the viewpoint of origami one. Furthermore, this new half cut type member provides totally effective crush mode as shown in Figure.2.22 not only in the traditional case of installing under floor and but also inserting member between truss core in electric automobile.

It is occasionally difficult for origami form to be processed at low price. Therefore, it is a vital aspect of origami engineering that the structural processing at low price is transformed into origami form, and as a consequent higher performance can be obtained. This example is displayed as in Figure.2.22(b).



(a) Concept of truss core electric automobile (b) High performance of half cut type RSC

Figure.2.22: Undertaking of Space utility by applying truss core into electric automobile

2.5 Summary

In this chapter, firstly I briefly describe the history and background of origami engineering, and then mention its several research areas currently being conducted. Next, two kinds of main folding structures is introduced; one is a truss core and another is a reverse spiral cylindrical origami structure. The former has the most outstanding advantage of making a structure stronger by combining two truss core panel in the way that a core of a panel fills up a hole of another panel. The latter has the advantage of absorbing more crash energy during automobile light collision or vehicles-pedestrian accidents. For a tsunami shelter in this research, I arrange the latter structure to generate a reverse spiral ellipsoid structure. It is expected that the structure has advantages of not only absorbing crash energy from tsunami and obstacles such as wall and building but also being folded compact and stored.

Chapter 3 Simulation and Optimization design method

One of characteristics for this research is to use the cutting edged simulation technique effectively. In this chapter, the positions dealt in this research of fluid-structure coupling analysis and optimization analysis are considered especially.

3.1 Technique of fluid-structure coupling analysis

3.1.1 Structural vibration-acoustic coupled phenomenon

There is structural vibration-acoustic coupled phenomenon as a representative as fluid structure coupling. For example, indoor acoustic which an occupant in an automobile feels is composed of airborne sound occurring in the way acoustic radiation generated from engine parts is transmitted to the ears of a driver and solid borne sound generated by vibration the panels of a body surrounding a cabin. The tire inputs from a road vibrate suspension to shake a body of a car. The acoustic generated by vibration of body panels is solid borne sound, and rigidity of a body panel is incommensurable larger than the one of air, therefore only vibration of panel generates acoustic generally. However, when acoustic level is large, the fluctuation of air has an effect on the vibration of panel again. This process is coupled phenomenon of structure vibration-acoustic. This coupling phenomenon is also observed in launching of a rocket for instance. In launching a rocket, roaring generated from the engine of a rocket hits on the earth whose reflected sound shakes the wall panel of a rocket and as an outcome there is huge sound pressure occurred in a rocket. This sound pressure shake the walls of a rocket to make coupling phenomenon. By this step, more loud sound possible to break a satellite inside a rocket is generated. By the way, it is considered to apply boundary element method and

statistical energy analysis into simulation of these kinds of phenomena. However, here it is standard to apply Finite Element Method which has most versatility, too. Normally, vibration and acoustic are uncoupling, therefore each of them is analyzed separately. In case of uncoupling, when vibration analysis and acoustic analysis is conducted by Finite Element Method, the obtained stiffness matrix [K] and mass matrix [M] are symmetry and possessing band property. Assuming natural frequency and eigenmode obtained by eigenvalue analysis is $w_i, \varphi_i, i = 1 \sim N$ (N: the all degrees of freedom) respectively, the displacement in frequency response is determined by Equation (3.1)

$$U = \sum_{i=1}^N \varphi_i Q_i \quad \text{and} \quad Q_i = \frac{\varphi_i^T F}{m_i(w_i^2 + 2j\varepsilon_i w_i \Omega - \Omega^2)} \quad (3.1)$$

Here, N is the total number of degrees of freedom, q_i is coordinates of mode displacement. Equation (3.1) indicates that response of vibration is obtained by superposition of modes which is called mode synthesis. When degree of freedom is very large, it is very hard to calculate eigenvalue and eigenmode in all of degrees of freedom by eigenvalue analysis. However, in observing mode closely, the lower level mode expresses vibration mode for whole structure, on the other hand higher level vibration becomes a local mode, so that Equation (3.1) is frequently expressed as Equation (3.2).

$$U = \sum_{i=1}^n \varphi_i Q_i \quad \text{and} \quad Q_i = \frac{\varphi_i^T F}{m_i(w_i^2 + 2j\varepsilon_i w_i \Omega - \Omega^2)} \quad (3.2)$$

Here, generally $n \ll N$ is true. Equation (3.2) indicates that even if mode in high level was omitted, some problems would obtain sufficient accuracy, which has been widely used as mode displacement method. In equation (3.2) there are often the case with the accuracy for the strain and stress for a first-order differential displacement is low, even though the accuracy for displacement is kept. And, Williams obtained Equation (1.3) by generating correction term in high level mode to leave out in 1945[3.1].

$$U = K^{-1} F + \sum_{i=1}^n \frac{\Omega^2 - 2j\varepsilon_i w_i \Omega}{w_i^2} \varphi_i Q_i \quad (3.3)$$

ANSYS and MSC/NSTRAN which are the leading codes for finite element method used for vibration and acoustic analysis adopt mode acceleration method. However, it isn't

straightforward to apply mode acceleration method to acoustic analysis of vehicle cabin actually. It comes to a problem when the frequency range of interior acoustic called booming noise and road noise becomes from 60Hz to 300Hz. For instance, when the form of vehicle body is determined, the frequency range which becomes a cause for noise is determined. Supposing the range between 130Hz and 180Hz becomes significant, the panel of a vehicle body in 130 Hz is already the several hundred-th mode as a large scaled model. If mode in low level can't be calculated accurately in mode acceleration method, the accuracy for Equation (3.3) can't be certified. Thus, Ma and Hagiwara obtained Equation (3.4) which compensates by leaving off the modes both in low level and in high level [3.2].

$$U = U_s + U_d \quad (3.4)$$

$$(K + j\omega_c C - \omega_c^2 M)U_s = F \quad (3.5)$$

$$U_d = \sum_{i=m}^n \varphi_i Q_i^d = \sum_{i=m}^n z_i \varphi_i Q_i \quad (3.6)$$

Here, U_s is a semi-static response and calculated by Equation (3.5). And, U_d is a complementary dynamic response as determined by Equation (3.6). Equation (3.4) is called as mode synthesis by Ma-Hagiwara. The relationship between the conventional mode synthesis and the mode synthesis by Ma-Hagiwara is as shown in Figure.3.1.

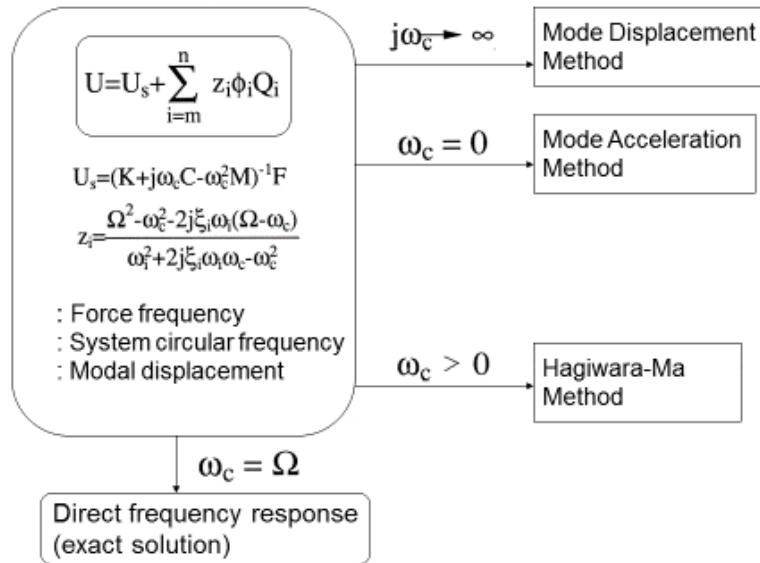


Figure.3.1: Relationship between Ma-Hagiwara method and conventional methods

Figure.3.1 illustrates that the equation by Ma-Hagiwara is most generic in the respects that it can be retrograded to the same equation as the traditional mode synthesis just by changing parameters. Though the mode synthesis is the most base for the problems of vibration and acoustic problem, both matrices for stiffness and mass are asymmetric and their band property are broken as explained by Figure.3.2 in formulating structure vibration-acoustic coupling problem by finite element method. In case matrix of stiffness and mass is symmetric, left eigenvector and right eigenvector are equal, thus Equation (4.1),(4.2),(4.3),and(4.4) are obtained by a complete orthogonality condition and a normalization condition, on the other hand in case of coupled analysis which is asymmetric, right and left eigenvectors are different which have made it hard to apply mode synthesis method into coupled problems. However, Hagiwara et al., found the relative equation of right and left given by Figure.3.3 [3.3] which express a complete orthogonality condition and a normalization condition only by right eigenvector to solve these problems as above.

$\mathbf{M}\ddot{\mathbf{u}} + \mathbf{K}\mathbf{u} = \mathbf{f} \quad (1)$	\mathbf{M}_{ss} : mass matrix of structure
where	\mathbf{K}_{ss} : stiffness matrix of structure
$\mathbf{K} = \begin{pmatrix} \mathbf{K}_{ss} & \mathbf{K}_{sa} \\ \mathbf{0} & \mathbf{K}_{aa} \end{pmatrix}$	\mathbf{M}_{aa} : inertance matrix of the sound field
$\mathbf{M} = \begin{pmatrix} \mathbf{M}_{ss} & \mathbf{0} \\ \mathbf{M}_{as} & \mathbf{M}_{aa} \end{pmatrix}$	\mathbf{K}_{aa} : elastance matrix of the sound field
	\mathbf{M}_{sa} : matrices relative to the coupling conditions
	\mathbf{K}_{sa}
	Here
$\mathbf{u}^t = \left\{ \mathbf{u}_s^t, \mathbf{u}_a^t \right\}$	\mathbf{u}_s : displacement of structure
$\mathbf{f}^t = \left\{ \mathbf{f}_s^t, \mathbf{f}_a^t \right\} \quad (2)$	\mathbf{u}_a : sound pressure level
	\mathbf{f}_s : excitation vector on structure
	\mathbf{f}_a : force vector, representees interior acoustic sources
	“s” : denoting the structural field system
	“a” : denoting the sound field system

Figure.3.2: Equations for coupled structural-acoustic system

Proposition 1: In right and left eigenvalue problem all the eigenvalues and eigenvectors are always real

Proposition 2: The left eigenvector $\bar{\phi}$ is obtained from the right eigenvector ϕ

$$\bar{\phi}_i^T = \left\{ \phi_{si}^T, \frac{1}{\lambda_i} \phi_{ai}^T \right\} \text{ (for } \lambda_i \neq 0 \text{)}$$

where $\phi_i^T = \left\{ \phi_{si}^T, \phi_{ai}^T \right\}$

λ_i : eigenvalue, s: subscript representing structural system,
a: subscript, representing acoustic system

Proposition 3: The orthogonality conditions for coupled system are

$$\phi_{si}^T K_{ss} \phi_{sj} + \phi_{si}^T K_{sa} \phi_{aj} + \frac{1}{\lambda_i} \phi_{ai}^T K_{aa} \phi_{aj} = 0, \quad \phi_{si}^T M_{ss} \phi_{sj} + \frac{1}{\lambda_i} (\phi_{ai}^T M_{as} \phi_{sj} + \phi_{ai}^T M_{aa} \phi_{aj}) = 0 \text{ (for } i \neq j \text{)}$$

Proposition 4: The normalization condition for right eigenvector ϕ_i with respect to mass is

$$\phi_{si}^T M_{ss} \phi_{si} + \frac{1}{\lambda_i} (\phi_{ai}^T M_{as} \phi_{si} + \phi_{ai}^T M_{aa} \phi_{ai}) = 1$$

Figure.3.3: The four propositions for coupled structural-acoustic system

3.1.2 Vibration relative to structure fluid

It seems that structure-acoustic coupled problem was all settled by the method by Hagiwara et al., however in a series of structure vibration relative to structure fluid, distinguished results like this haven't been obtained yet.

As an analytical method for vibration relative to structure fluid, several kinds of methods with different computational efficiency, accuracy, and stability are proposed which are classify broadly into an integrated solution and separated solution. An integrated solution is to find a solution satisfying all governing equations at respective time. It is not easy to implement, because it can be demanded a complicated algorithm, while being able to obtain high-precision solution. On the other hand, a separated solution is to solve by separating plural equations which expresses different physical phenomena independently. Its algorithm is simple and the calculation efficiency is high. Careful attention is to be paid to handing a phenomenon with strong achievement effect in a separated solution, because there are displacements occurred in the process to predict and reflect the shared physical quantity. In this research, I place great

significance on extensibility, and explain the method applying a separated solution. In fluid – structure coupling analysis, each of equation of fluid and equation of structure is solved independently, and calculated repeatedly while a boundary condition to satisfy the condition of continuity and balance on boundary is being modified.

3.2 Technique for optimal design

Considerations regarding the optimization analysis substantial for today’s design combining with the analytical software such as Finite Element Method (FEM) and Optimization software started in automobile industry. It was necessary to satisfy many functions well-balanced in automobile industry, thus there the optimization analysis stated as above started earlier around 1980 than in the other industries. There are ODDYSSEY developed by General Motors Company, LLC and OPUS by Ford Motor Company were famous for an optimization system at that time [3.4]. These software are consisting of structure analysis part and optimization analysis part to which sensitivity routine in 1 step is added. Mathematical programming is used to handle many constraint conditions. Analytical part had been limited to stiffness and eigenvalue analysis which only expressed as sensitivity analysis for a long time. 30 years passed since that time, at present I cover structure nonlinear analysis and fluid-structure coupling analysis. Optimization analyses with tens of thousands number of design variables have ever been provided for a practical use. 3 kinds of developments written in the following have contributed these progresses. 1) Objective function by Taylor series expansion originating with Schmit and approximation method-optimization technique which uses positive approximate value under constraint condition [3.5], 2) Phase optimization analysis applying homogenization method and density method, 3) Response surface approximation. Among these 3 methods, response surface method adopted in this research is detailed as follows.

3.2.1 Approximation method optimization technique

Here, the following general optimization problem is given.

$$\begin{aligned}
 & \text{Minimize } f(x) \\
 & \text{subject to } h_j(X) \leq 0 \quad (j = 1, 2, \dots, m) \\
 & \underline{X}_i \leq X_i \leq \overline{X}_i \quad (i = 1, 2, \dots, N = 2n_{ei})
 \end{aligned} \tag{3.7}$$

Among optimization techniques, SAO (Sequential Approximate Optimization) as mathematical programming method developed significantly, and become an established method in the field of structure optimization. The rudimentary concept proposed by Schmit firstly in 1974 is to convert a former complex optimization problem to a series of simple optimization one and then calculate an optimal structure step by step. Every step of optimization, objective function and constraint function are approximately expressed as a simple function. For instance, according to Taylor series expansion, an objective function can be converted to a first approximation as below.

$$f^k(X) = f(X^k) + \sum_{i=1}^n a_i^k (X_i - X_i^k) \quad (3.8)$$

where $a_i^k = \left(\frac{\partial f}{\partial x_i}\right)_{x=x^k}$. Using linear approximations such as Equation (3.8), the obtained approximation problem becomes a linear optimization problem which can be solved by a previous linear programming. By the way, in case of structure optimization it is often the case with the relationship between design variables and objective function (constraint condition) is the one of inverse. Therefore, instead of direct expansion relevant to design variables such as Equation (3.8), more strict approximation problem is obtained by expanding approximately in regards to inverse. DUAL method is on the basis of this concept. For example, expanding constraint function h by inverse of design variables while setting only i -th number active among constraint conditions,

$$h \approx h^k = h(Y^k) + \sum_{i=1}^n b_i^k (y_i - y_i^k) \quad (3.9)$$

Here, $Y = \{y_1, y_2, \dots, y_n\}^T$, $y_i = 1/x_i, (i = 1, 2, \dots, n)$

$$b_i^k = \left(\frac{\partial h}{\partial y_i}\right)_{y=Y^k} = -(x_i^k)^2 \left(\frac{\partial h}{\partial x_i}\right)_{x=X^k}$$

In this case, renewal coefficient D_i^k

$$D_i^k = \left(-\lambda \frac{b_i^k}{a_i^k}\right)^{\frac{1}{2}} = \left(-\lambda \frac{\partial h}{\partial x_i} / \frac{\partial f}{\partial x_i}\right)_{x=X^k}^{\frac{1}{2}} \quad (3.10)$$

Here, y_i is called an intermediate variable. Details are omitted, and the renewal rule

obtained by Equation (3.10) becomes the same equation as the one for optimized standard method in [3.6]. When $\frac{\partial h}{\partial x_i} / \frac{\partial f}{\partial x_i} > 0$ is held in Equation (3.10), it is impossible in theory to update design variables. In an optimization problem of static stiffness, almost of the sensitivity coefficients for design variables relevant to material become negative. It means that it is possible that sensitivity coefficients of vibration problem become positive and negative, while min-compliance is reduced in increasing the number of materials. Though the optimization method used in [3.8] is extremely effective, the fact that it hasn't been long time before optimization method by using approximation method is applied into dynamic problem is the cause for above matters.

Then, the solution of SAO have developed into improvement method for multiple versions along with the support of DUAL space theory. Among these are CONLIN (Convex Linearization) [3.7] and MMA (Method of Moving Asymptotes) [3.8] which both have most established reputations. These methods make an objective function and a constraint condition linear as intermediate variable, and then resolve a problem by separating the former optimization problem for multi variables coupling by DUAL space theory into the optimization problem with single design variable. Consequently, it has a totally efficient computational algorithm. However, the approximate optimization problem obtained by broad linearization possesses convexity to apply DUAL method. Namely, the value in a root needs to be non-negative. How to obtain convexity approach is a key point to this method. CONLIN method resolve this problem by the concept of linearizing convexity.

Method	Transformation of Design Variable	Linearity for Constrain Function ^r
SAO	$y_i = x_i$ design variable	Non-convex
Dual	$y_i = 1/x_i$	Non-convex
CONLIN	$y_i = \begin{cases} x_i & \text{if } \partial g / \partial \alpha_i > 0 \\ 1/x_i & \text{if } \partial g / \partial \alpha_i < 0 \end{cases} (i=1,2,\dots,n)$	$g \approx g^k = g_0^k + \sum_+ d_i^k x_i + \sum_- d_i^k / x_i$ Convex
MMA	$y_i = \begin{cases} 1/(U_i - x_i) & \text{if } \partial g / \partial \alpha_i > 0 \\ 1/(x_i - L_i) & \text{if } \partial g / \partial \alpha_i < 0 \end{cases} (i=1,2,\dots,n)$	Convergence faster, than CONLIN When $L_i = 0, U_i = \infty$, consistent to CONLIN
Ma et. al	$y_i = x_i - c_i ^{\xi_i} (i = 1, 2, \dots, n)$	Consistent to CONLIN and MMA on c_i, ξ_i values ^o

Figure.3.4: Comparison of SAO method, DUAL method, CONLIN method, MMA method, and a method by Ma et al.

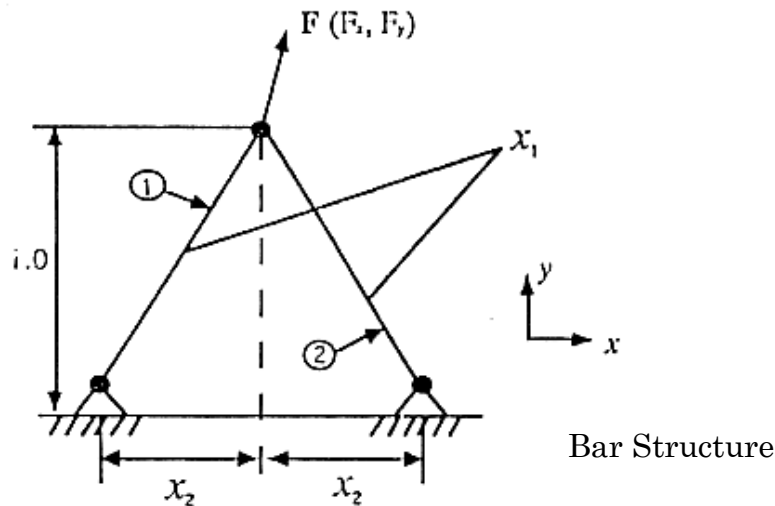


Figure.3.5: Finite element model for the minimum weight problem of a beam fastened at one end

In CONLIN method, the intermediate variables as shown in Figure.3.4 for objective function or constraint function are applied. After that, the same step as DUAL method where g is linearized by an intermediate variable y_i is followed. In [3.8], the concept of moving

asymptote by improving further the method of [3.7] is propounded. That is to say, MMA method is also on the rudiments of the concept of convexity approximation, however it utilizes the intermediate variables dissimilar from CONLIN method. In [3.8], it is revealed that it is faster to converge in using MMA method than in using CONLIN method. And, in special case that $L_i = 0$ and $U_i = \infty$, MMA method is able to be degenerated to CONLIN method. Therefore, it can be said that MMA method is improvement and extension of CONLIN method. M et al. proposed a kind of novel method to make convex in [3.9]. This method makes it possible to express CONLIN and MMA with parameters indicated as in Figure.3.4 and to make is much more stable and faster than both methods. The comparison between CONLIN method, MMA method, and the method by Ma et al. which are applied into the minimum weight problem of a beam fastened at one end is as shown in Table.3.1 [3.12]. And, the case where optimization analysis for plural eigenvalues for structure-acoustic field coupling problem is conducted by using the method by Ma et al. and sketched eigenvalue index is as shown in Figure.3.6 and Table.3.2 [3.10].

Table.3.1: Comparison of convergence between each method

Iteration number		SLP	CONLIN	MMA $\begin{pmatrix} h_1 = 1/3 \\ h_2 = 1/3 \\ : best \end{pmatrix}$	MMA $\begin{pmatrix} h_1 = 1/3 \\ h_2 = 1/20 \end{pmatrix}$	This paper (本研究)
0	x_1	1.50	1.50	1.50	1.50	1.50
	x_2	0.50	0.50	0.50	0.50	0.50
	f	1.68	1.68	1.68	1.68	1.68
1	x_1	1.38	1.39	1.39	2.17	1.41
	x_2	0.25	0.25	0.25	0.12	0.38
	f	1.42	1.43	1.43	2.09	1.51
2	x_1	1.14	1.33	1.22	1.49	
	x_2	0.50	0.50	0.50	0.28	
	f	1.27	1.49	1.37	1.55	
3	x_1	1.34	1.39	1.39	1.41	
	x_2	0.25	0.25	0.25	0.39	
	f	1.38	1.43	1.44	1.51	
4	x_1	1.15	1.33	1.37	1.42	
	x_2	0.50	0.50	0.38	0.37	
	f	1.28	1.49	1.47	1.51	
5	x_1	1.34	1.39	1.41	1.41	
	x_2	0.25	0.25	0.38	0.38	
	f	1.38	1.43	1.51	1.51	
6	x_1	1.15	1.33			
	x_2	0.50	0.50			
	f	1.28	1.49			
7	x_1	1.34	1.39			
	x_2	0.25	0.25			
	f	1.38	1.43			

Table.3.2: Change in eigenfrequency for a truck cabin

No.	initial	goal	result
1	6.2	15.0	15.0
2	8.2	20.0	19.1
3	11.7	25.0	25.0
4	14.3	30.0	29.7

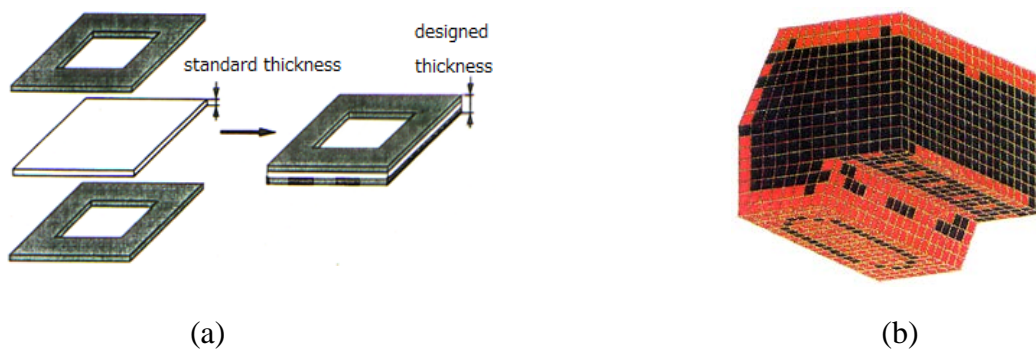


Figure.3.6: Optimal position of reinforce

Here, sketched eigenvalue index is as shown in Figure.3.7. When a structure is changed strikingly for phase optimization, it becomes extremely unstable in case that the order of eigenmode is shifted shown in the Figure.3.7, however this sketched eigenvalue index play a role in restraining not to shift its order.

Generalized Eigenvalue

“Weighted Average” of m Eigenvalues

$$\lambda^* = \begin{cases} \lambda_0 + \left(\frac{\sum_{i=1}^m w_i (\lambda_{n_i} - \lambda_0)^n}{\sum_{i=1}^m w_i} \right)^{\frac{1}{n}} & (\text{Integer other than } n=0) \\ \lambda_0 + \exp\left(\frac{\sum_{i=1}^m w_i \ln|\lambda_{n_i} - \lambda_0|}{\sum_{i=1}^m w_i} \right) & (n=0) \end{cases}$$

Parameter : $w_i, n, \lambda_{0_i}, \lambda_0^*$

- a) Maximize the designated eigenfrequency.
Max λ^*
- b) Maximize the distance between the structural eigenfrequency and the well-known frequency.
Max λ^*
- c) Maximize the difference between the eigenfrequency and the given target eigenfrequency.
Min λ^*

Figure.3.7: Sketched eigenvalue index

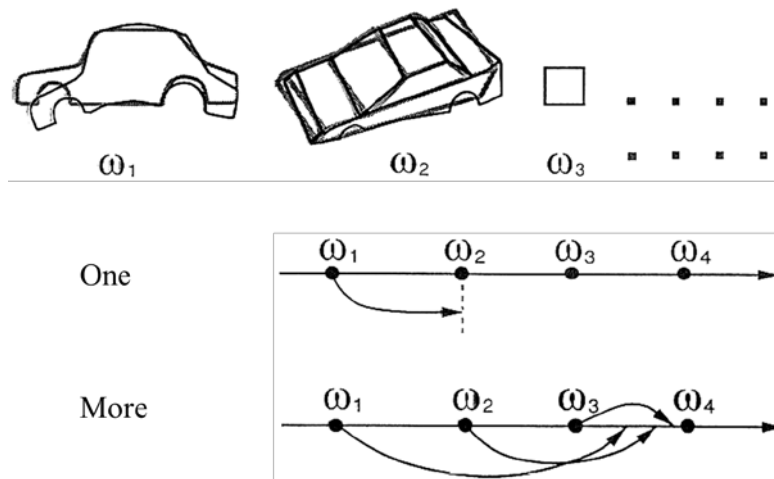


Figure.3.8: Appearance that the number of eigenmode shifts

3.2.2 Optimization of response surface

3.2.2.1 Response surface methodology applied into nonlinear problem

As for fluid analysis and structure nonlinear analysis, calculating an optimal structure is heavy, because it takes a lot of time in itself. Hence, application of optimization analysis is expected for these problems, the sensitivity isn't easy to calculate. For that reason, there are some cases that the sensitivity is calculated by difference, and CONLIN method of successive approximation optimization algorithm is utilized [3.11]. In [3.11], impact energy absorbed dose is designated for objective function, and mass is designated for constraint condition. An approximation utilized in CONLIN method is expressed to make convex space, a stable solution is obtained even in the case with strong nonlinearity as collision analysis.

Consequently, the method to calculate sensitivity by taking the difference format between amount after changing design and an amount before changing difference format, because it is hard to express sensitivity in case of nonlinear collision analysis. The calculation time for calculating sensitivity by difference becomes huge. Therefore, the method is conceived to obtain an optimal value by approximating objective function itself applying the approximation ability of Neural Network (NN). Back Propagation Learning Method based Neural Network (BNN) is most often used as NN, however Hagiwara et al., proves an overwhelming superiority of Holographic Neural Network given by Figure.3.9 [3.12].

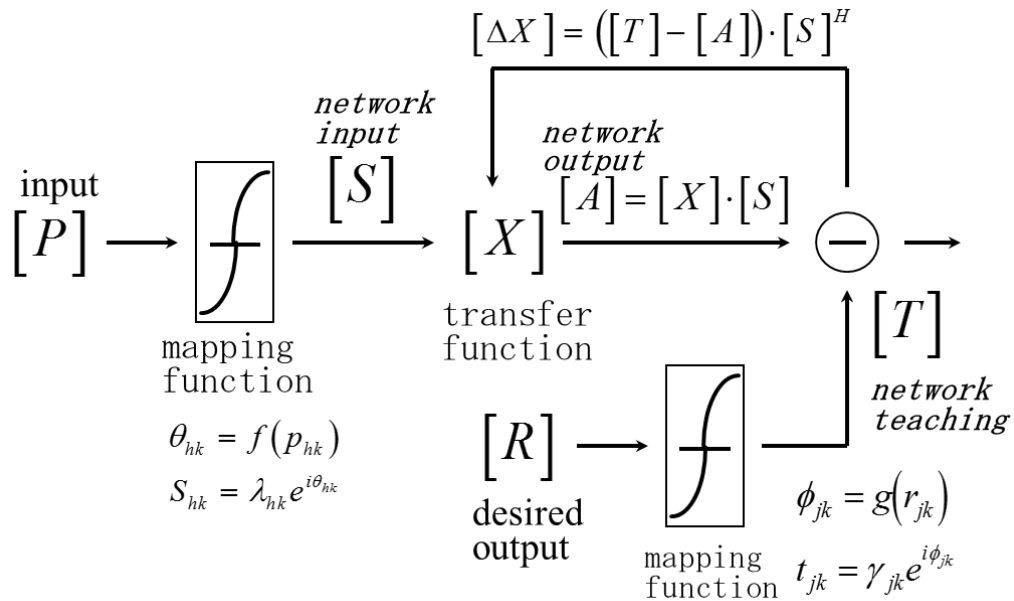


Figure.3.9: Diagram for Holographic Neural Network

3.2.2.2 Descriptions of response surface method

Response surface method is a statistical and mathematical method to provide a useful executing means in design optimization. When y for response is determined by a function composed of X for plural design variables, in response surface method, response function for behavior is expressed approximately as $y = f(X)$ with appropriate polynomial on the basis of observed data. For instance, response function with 2 variables is written by quadratic regression model as follows.

$$y = \beta_0 + \beta_1 x_1 + \beta_2 x_2 + \beta_3 x_1^2 + \beta_4 x_2^2 + \beta_5 x_1 x_2 + \varepsilon$$

Here, $\beta_0, \beta_1, \dots, \beta_5$ is regression coefficient, and ε expresses approximate error. In replacing variables more than quadratic as $x_1^2 = x_3, x_2^2 = x_4, x_1 x_2 = x_5$,

$$y = \beta_0 + \beta_1 x_1 + \beta_2 x_2 + \beta_3 x_3 + \beta_4 x_4 + \beta_5 x_5 + \varepsilon$$

Generally, regression model including arbitrary higher terms is always resolved into linear regression model by giving variables replacement as above. Supposing that a regression model has k number of regression coefficients,

$$y = \beta_0 + \beta_1 x_1 + \beta_2 x_2 + \dots + \beta_k x_k + \varepsilon$$

Hence, when the n number of observation data for design variables are expresses as matrix,

$$y = Xb + e$$

Here

$$y = \begin{bmatrix} y_1 \\ y_2 \\ \cdot \\ \cdot \\ y_n \end{bmatrix}, \quad X = \begin{bmatrix} 1 & x_{11} & x_{12} & \dots & x_{1k} \\ 1 & x_{21} & x_{22} & \dots & x_{2k} \\ \vdots & \vdots & \vdots & & \vdots \\ 1 & x_{n1} & x_{n2} & \dots & x_{nk} \end{bmatrix}, \quad b = \begin{bmatrix} \beta_1 \\ \beta_2 \\ \cdot \\ \cdot \\ \beta_n \end{bmatrix}, \quad e = \begin{bmatrix} \varepsilon_1 \\ \varepsilon_2 \\ \cdot \\ \cdot \\ \varepsilon_n \end{bmatrix}$$

Here y is observation data vector, X is matrix as observation points, b is vector of unknown coefficient, e is an error vector. Coefficient vector b is given by the following equation by the condition of minimizing the square error.

It normally needs the number of observation data much more than the number of unknown numbers to determine coefficient vectors by the equations described as above. However, in case the calculation load necessary for finite element method for a combination of design variables as in nonlinear response is large, it is important how to obtain more accurate approximate equation by less observation points. On the other hand, there are 2 kinds of approach methods. One method is to evaluate an accurate response function by less response points, and another method is to minimize the deviations of estimated response surface by minimizing the number of experiment points (in this case calculation points), while applying statistical sampling principle where response function is designated as polynomial. There are experiment method and Taguchi method as the latter method. And, as the former method there is a pioneer research applying Holographic Neural Network by Ma and Hagiwara. This research follows the former method. Thus, the method developed by Ma and Hagiwara is described as below.

3.2.2.3 Response Surface Method of Ma-Hagiwara on the basis of Holographic Neural Network

HNN is written in details in [3.13], so Most Probable Optimal Design (MPOD) is mentioned here which is utilized as mainstream currently. Ma and Hagiwara propose the case of continuous design variables in [3.14]. Here are explanations referring to that.

MPOD consists of 2 steps indicated by Figure.3.10. Firstly, random design trial points with a condition of uniform distribution are provided as initial trial points. N is the number of initial trial points, which is determined by the target problem.

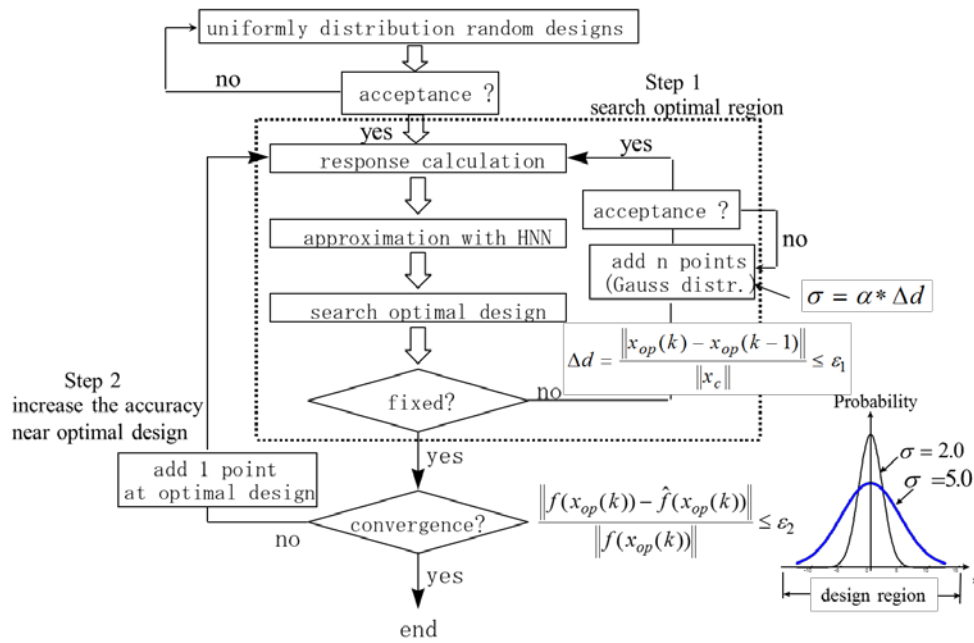


Figure.3.10: Flowchart of Most Probable Optimal Design (MPOD)

Normally, $N = n(n + 1)/2$ n is the number of design variables

However, in case higher accuracy is demanded and it doesn't take calculation cost, N is increased, to the contrary in case robustness optimization is demanded and trial calculation for 1 time is long, N is decreased. For instance, for a multi peaks function as in Figure.3.11, $d_i (i = 1,2)$ is the size for field, which is 0.7 longer interval than the maximum value in the field. In case the target is to find an optimal value from d_1 in the field A_1 (probability $p_2 + A_1/d_1$) rather than from d_2 in the field A_2 (probability is $p_2 = A_2/d_2$), N is decreased. It means robustness answer A_1 is found by making N less than d_1 and exceeds d_2 . And, in trying to find the answer A_2 which is poor in robustness and good performance function, it is possible to resolve A_2 by increasing N . However, there are numerous trial points, it takes calculation cost. The function values (objective function value and constraint function value) for these trial points are calculated, and then response surfaces ($f(x)$ and $g(x)$) followed by learning by Neural Network. Optimization is performed by applying these response surfaces. And, the accuracy to search optimal design points is being improved gradually according to the 2 steps indicated in the following.

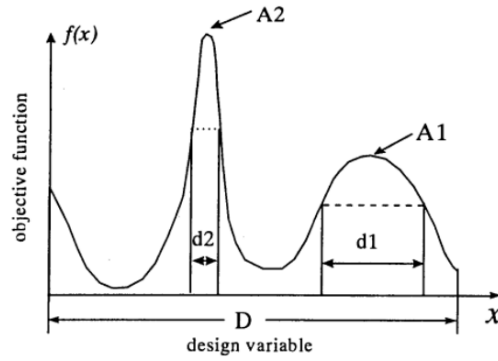


Figure.3.11: Example for multi peaks function

Step 1 is to search the field including perspective optimization, and its repeated approximation calculation is indicated as dotted line in Figure.3.12. This step conducts learning again by taking n number of random trial points in normal distribution from design field. By adding trial points successively as this way, the probability that perspective optimal position is calculated is improved. The convergence condition is given by Equation (3.11).

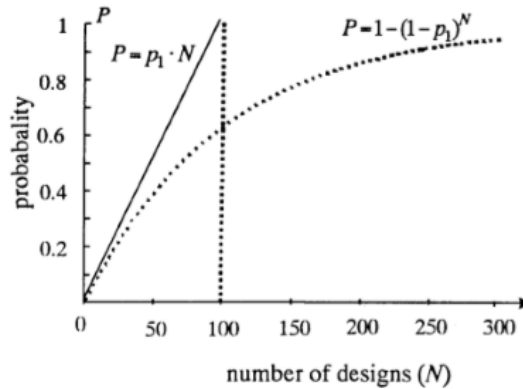


Figure.3.12: Comparison of conditional and non-conditional probability

$$\frac{\|\hat{X}_k - \hat{X}_{k-1}\|}{\|\hat{X}_{k-1}\|} \leq \varepsilon_1 \quad (3.11)$$

Here, \hat{X}_k is an optimal value after additional trial calculation, and ε_1 is threshold to converge step 1. It is repeated until Equation (3.12) is satisfied. The convergence condition for step 2 is Equation (3.12) and Equation (3.13).

$$\frac{\|f(\hat{X}_k) - \hat{f}(\hat{X}_k)\|}{\|f(\hat{X}_k)\|} \leq \varepsilon_2 \quad (3.12)$$

$$\frac{\|g(\hat{X}_k) - \hat{g}(\hat{X}_k)\|}{\|g(\hat{X}_k)\|} \leq \varepsilon_2 \quad (3.13)$$

Here, \hat{X}_k is design variable given approximation optimal value converged in step 1. $f(\hat{X}_k)$, $\hat{f}(\hat{X}_k)$, and $g(\hat{X}_k)$, $\hat{g}(\hat{X}_k)$ are objective functions, the correct answer for a constraint function, corresponding approximation values obtained from response surfaces, and ε_2 is threshold for convergence. When the convergence conditions of Equation is satisfied, the calculation is finished. Otherwise, providing additional trial point as \hat{X}_k , learning is conducted again to renew the approximation function.

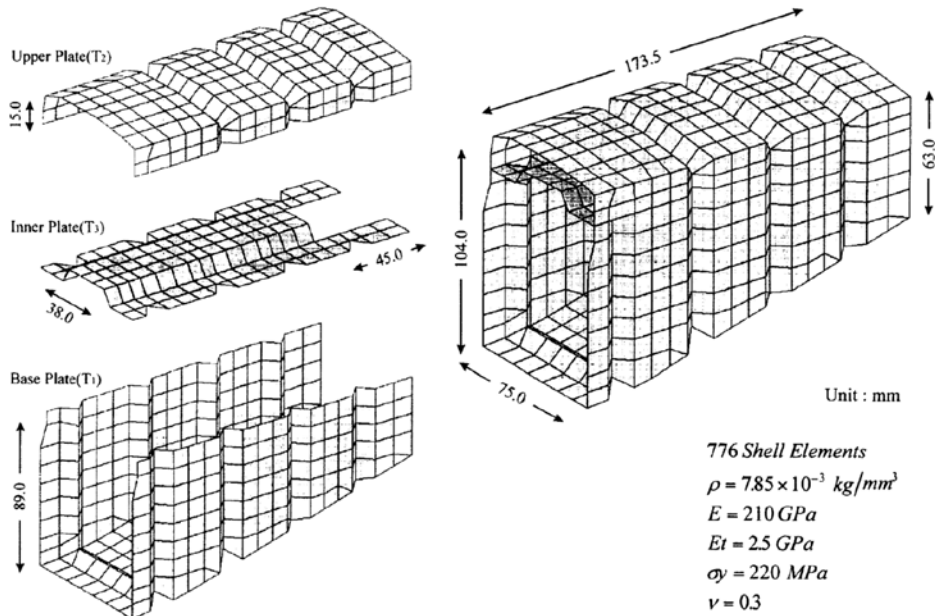


Figure.3.13: FEM model of vehicle flame

3.2.2.4 Surface response method analysis applying into this research

In this research, Radial Basis Function (RBF) is applied instead of Holographic Neural Network. In my group, CSRBF (Compactly Supported Radial Basis Functions) which provided compact sized platform is often used for structure regeneration of three dimensional data from

plural photos. For example, the function to calculate coefficients in CSRBF function is lead to diagonal matrix written as below in [3.15] for the first time.

$$f(P) = \sum_{i=1}^n \lambda_i \varphi_i(P) + v_0 + v_1x + v_2y + v_3z - f_c(x, y, z) = 0 \quad (3.14)$$

$$\begin{pmatrix} \varphi_1(P_1) & \cdots & \varphi_n(P_1) & 1 & x_1 & y_1 & z_1 \\ \vdots & & \vdots & \vdots & \vdots & \vdots & \vdots \\ \varphi_1(P_n) & \cdots & \varphi_n(P_n) & 1 & x_n & y_n & z_n \\ 1 & \cdots & 1 & 0 & 0 & 0 & 0 \\ x_1 & \cdots & x_n & 0 & 0 & 0 & 0 \\ y_1 & \cdots & y_n & 0 & 0 & 0 & 0 \\ z_1 & \cdots & z_n & 0 & 0 & 0 & 0 \end{pmatrix} \begin{pmatrix} \lambda_1 \\ \vdots \\ \lambda_n \\ v_0 \\ \vdots \\ v_3 \end{pmatrix} = \begin{pmatrix} c_1 \\ \vdots \\ c_n \\ 0 \\ \vdots \\ 0 \end{pmatrix} \quad (3.15)$$

Here, I mention RBF in the following.

In function approximation, considering the base consisting of actual value function which is spherical symmetry in respective appropriate points, respective base function is called radial basis function. The fact that function φ is radial function or spherical symmetric generally indicates that $\varphi(x) = \phi(\|x\|)$, that it the value is determined depending not on deviation components but only on radial components (a distance from an origin). Therefore, radial basis function is determined only depending on the distance from an appropriate origin point c indicated as $\phi(x; c) = \phi(\|x - c\|)$. Here, norm is considered as Euclid distance, and it is able to adopt another distance function. The approximation process for the sum of radial basis function is interpreted as a simple kind of Neural Network.

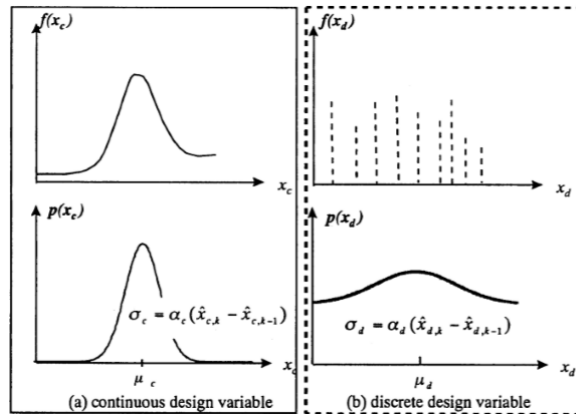


Figure.3.14: Example of function via continuous and discrete design

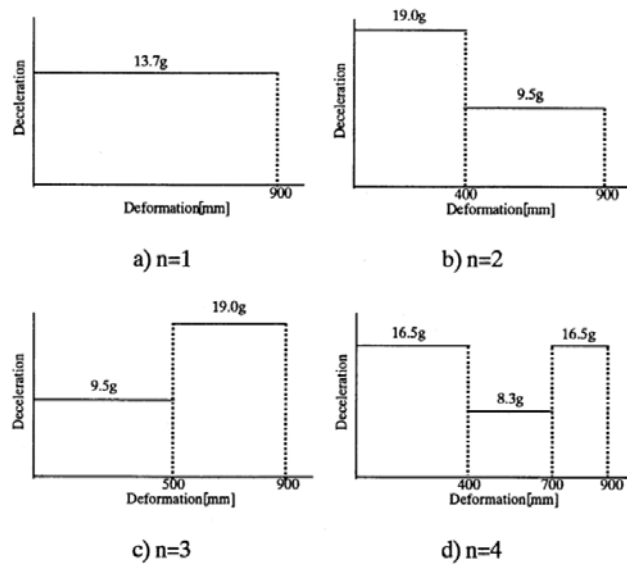


Figure.3.15: Type pf deceleration curve of vehicle

3.3 Summary

In this chapter, firstly I describe the theory of fluid-structure coupling analysis. Especially, structure vibration – acoustic coupling phenomenon for a vehicle and rocket is mentioned in details. In addition, two different kinds of ways as integrated solution and separated solution are summarized. The latter solution is arranged and applied into numerical simulation this time.

Next, new active function using holographic neural network for the response surface methodology is proposed to approximate the true structural response accurately and then to reduce the necessary design points used for searching the global optimum design. Finally, a new mode-superposition technique for calculating the frequency response of the structural systems and coupled acoustic-structural systems with modal damping is described. Those methods and techniques explained in this chapter are applied into the numerical simulation in chapter 4 and chapter 5.

Chapter 4 Foldable tsunami pod

4.1 Previous researches and commodities of tsunami evacuation

In the Tohoku earthquake on March 11 of 2011, severe damage was caused by the subsequent tsunami followed by it. In that case it is assumed that broken evacuation route would prevent people from moving, and elder people, seriously injured people, and visitors who are not familiar with the area would not readily evacuate to higher places. Therefore, how to protect people's lives from tsunami has been a big issue since the earthquake. As a countermeasure for minimizing the damage occurred by a large tsunami as the last one, there have been fixed tsunami evacuation facility such as a tsunami evacuation building and a floating type shelter proposed[4.1][4.2]. These shelters are restricted to an urgent and temporary use out of sheer necessity. As a floating type shelter, the spherical shaped shelter which has evacuation space in the upper part and weight and saving space in the lower part was proposed by Shigematsu [4.1][4.2] .





Watanabe and Kaneko[4.3] noted tsunami hybrid refuge technique and investigated to utilize floating type tsunami evacuation shelter and tsunami evacuation tower and buildings from hydraulic experiments. Namely, it is able to divide the behavior of the shelter into three types. There are the cases which a shelter moved with a wave. In addition, the floating type tsunami evacuation shelter is able to endure impulse force calculated from flow velocity and free-fall.

Mutsuda et all [4.4] have proposed and devised one kind of a large sized tsunami shelter with mooring that is capable of accommodating at least one hundred people or more to evacuate from a run up tsunami. The optimization for the shape of the tsunami shelter was examined using Particle method, Smoothed Particle Hydrodynamics As a result of numerical calculation and experiment, it is confirmed that a revolving ellipsoid body form receive the

minimum force from tsunami among other possible forms for a tsunami shelter. The form of ellipsoid body is geometrically the same as the one of my tsunami shelter.

On the other hand in commercial fields, after 3.11 earthquake, several kinds of tsunami shelters made of carbon fiber reinforced plastic (CFRP) [4.5] have been produced by Japanese companies. Table.4.1 shows those specifications for 4 kinds of tsunami shelters. Concerning form, 3 of them are sphere and one of them is semi-regular dotriacontahedron. The spherical form is assumed to avoid the crash by obstacles and pressure from outside for its curved surface and to be able to diffuse the stress. Consequently, it can decrease the load at each point, and suppress the explosion and damage to the utmost limit. CFRP used for material is made in the way epoxy resin is mixed in plastic, and has very strong durability to strengths such as bending and squashing from outside. CFRP is superior in that it is 10 times as strong as steel and one fifth as heavy as that. Furthermore, CFRP is able to save heat energy which have an occupant suffer from heat and cold, and furthermore stored outside as garden and balcony for a resistant against corrosion and deterioration. To confirm the security of breathing, oxygen concentration and air tightness have ever been examined in each shelter, and some of companies has already performed a water fall test and floating test in the sea in standpoint of strength. The product “HIKARi” in Table.4.1 is an assembling type which is carried in with each part split apart. After being carried into home, they have to put parts together into spherical form and keep it in balcony in its development state. On the other hand, I devise the pod which can be kept in foldable state and is developed instantaneously in case of emergency.

Table 4.1: Commercially available tsunami shelters

product name	Life Armour	HIKARi	Nore	Super Barrier S4
manufacturing company	Pond Co., Ltd.	Hikari Rezin Co., Ltd.	Shelter JAPAN Co., Ltd.	World Net International Co., Ltd
form on sale	integrated	integrated or assenbly	integrated	integrated
material	CFRP	CFRP	CFRP	steel
form in use	spherical body	spherical body	spherical body	dotriacontahedron
diameter	120cm	120cm	120cm	180cm
weight	80kg	80kg	80kg	500kg
maximum number of occupants	4	4	4	6
withstand load	9t	22.4t	12.5t	
price	400,000 yen	500,000 yen	670,000 yen	2,600,000yen
product photo				

4.2 Newly developed foldable tsunami pod

The form of sphere is rotated in all directions and unstable, and so an ellipsoid body rotated in 1 direction is applied into my tsunami pod. The folding way for a sphere has already been researched [1.25] and on the basis of their research the form of ellipsoid body is assumed to be possible to be folded flat. However in this Chapter, I simplify the design process, and as a result the designed form can't be folded flat. In short, I presume that there is no impact on strength by being developed and folded. Its size is set as 1200mm for major axis and 800 mm for minor axis, and examine the case where 1 occupant boards a shelter.

Firstly, I generate its 3D model for simulation by calculating the values of coordinates x , y , and z from 2D foldable pattern. And then for examining the strength of the tsunami pod, I analyze the degree of crash by von Mises stress in case the tsunami pod collides with walls and obstacles, and for verifying the safety of an occupant Head Injury Criterion (HIC) [4.6] for a passenger at the same moment.

4.2.1 Generation of initial model without occupant restraint system

I set the major axis as Z axis, the minor axis as X axis, and regard a spheroid which is obtained from the rotation around Z axis. Then, I also set the length of diameter for Z axis as a , the one of diameter for Y axis as b . The surface of the spheroid form is expressed as Equation(4.1), and each coordinate points are calculated by Equation(4.2) .

$$\frac{x^2}{b^2} + \frac{y^2}{b^2} + \frac{z^2}{a^2} = 1 \quad (4.1)$$

$$x = b \cos \theta \cos \varphi \quad y = b \sin \theta \cos \varphi \quad z = a \sin \varphi \quad (4.2)$$

(θ : latitude, φ :longitude)

To fold the spheroid form in the direction of Z axis, the foldable and deployable form is generated as shown in Figure.4.1(a). The intersection points as shown the small circle in Figure.4.1(a) are made in the fashion that the form is divided into 10 parts in the latitude direction and longitude direction and the intersection points are connected into folding lines. Those points are called key nodes here, and utilize in generating the mesh model.

I apply the 5th percentile adult female among GEBOD Dummy Model as shown in the first right side of Figure.4.1(b) (LANCEMORE Corporation) developed in the airplane industry,

because I assume an elder person and a handicapped person who have difficulty in walking as an occupant. The model for tsunami pod made in the process as above is called the initial model without an occupant restraint system. The number of nodes and elements for each part of a pod, a rigid wall, and seawater are as shown in the Table.4.2. The total number of elements for the dummy system is 36138 which are divided into 1636 for shell elements and 2648 for solid ones. The model with a laid occupant is as shown in the Figure.4.1(c). Next, each part is divided into triangle and rectangle mesh for structure analysis. The way of mesh division is as follows; firstly each side composing a triangle is divided into 5, next those nodes are connected into square meshes regularly and triangle meshes in the case of including a key mode. On the other hand, the part of a rigid wall constructed of shell elements is divided into tetrahedron mesh, and the part of seawater constructed of solid elements is divided into tetrahedron mesh whose volume is approximately 400 times as large as a pod as shown in Figure.4.2. The boundary conditions for inflow, outflow, and no-slip are set as the fluid part isn't be leak out. The total process for simulation is from the moment when seawater(tsunami) as shown the right panel in Figure.4.2 starts flowing at an initial constant velocity to the moment when a pod rises onto a wall as shown in the left panel in Figure.4.3 after hitting on it.

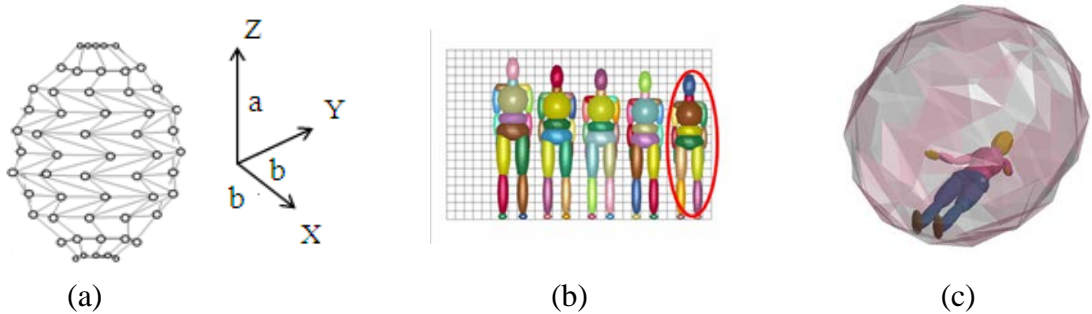


Figure.4.1: Model for tsunami pod with a dummy model

(a) Foldable ellipsoidal model, (b) the 5th percentile adult female dummy model (c) Foldable ellipsoidal model with a dummy model)

Table.4.2: Details for the whole model

part	element type	the number of elements	the number of node
pod	shell	4960	4957
wall	shell	3200	3281
seawater(tsunami)	solid	18240	20454
dummy model	shell/solid	1636/2648	7446
total number		26400	36138

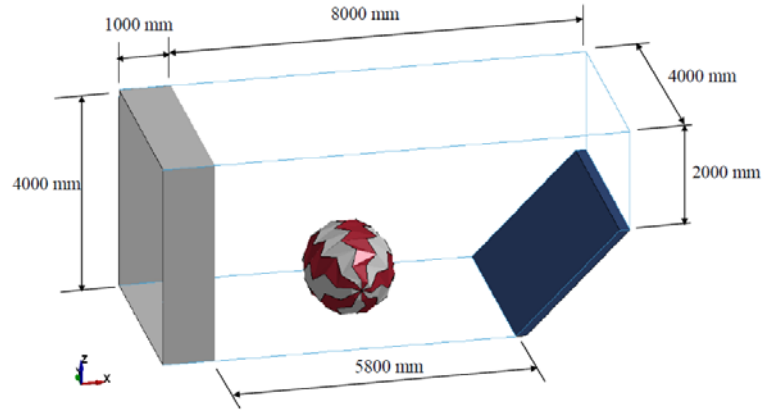


Figure.4.2: Whole model for simulation including a pod, tsunami, and rigid wall

4.2.2 Theory for analysis: Fluid-structure coupling analysis

In simulation, I utilize the software “LS-DYNA” (LSTC Corp.,2014) [4.7] which is a general-purpose finite element program capable of simulating complex real world problem. This simulation is categorized as fluid structured coupling analysis [4.8] where a fluid force transform the structure of a pod as well as the transformed structure affects a flow field. This time, seawater and air are set as fluid part, while tsunami pod is set as structured part. Those fluid parts are expressed in Arbitrary Lagrangian Eulerian (ALE) method [4.9], and those structured parts are expressed in coordinate system. The ALE method is solving simultaneous the conservation rules of mass, momentum, and energy. Each conservation rules are formally written as Equation (4.2a), Equation (4.2b) , and Equation (4.2c).

$$\frac{\partial \rho}{\partial t} + \rho \text{div}(\mathbf{v}) + (\mathbf{v} - \mathbf{w}) \text{grad}(\rho) = 0 \quad (4.2a)$$

$$\rho \frac{\partial \mathbf{v}}{\partial t} + \rho (\mathbf{v} - \mathbf{w}) \cdot \text{grad}(\mathbf{v}) = \text{div}(\boldsymbol{\sigma}) + \mathbf{f} \quad (4.2b)$$

$$\rho \frac{\partial e}{\partial t} + \rho (\mathbf{v} - \mathbf{w}) \cdot \text{grad}(e) = \boldsymbol{\sigma} : \mathbf{D} + \mathbf{f} \cdot \mathbf{v} \quad (4.2c)$$

Here, ρ is fluid density, \mathbf{v} is velocity vector of fluid, \mathbf{w} is velocity vector of mesh, e is energy per unit mass, $\boldsymbol{\sigma}$ is Cauchy stress tensor, \mathbf{D} is deformation velocity tensor, \mathbf{f} is body force. In simulation, seawater (fluid part) as shown in Figure.4.3(a) touches tsunami pod (structure

part), and then the mesh of seawater and air are deformed internally(Figure.4.3(b)), and finally the mesh is restored to the initial position(Figure.4.3(c)). In this process, the advection term including $v-w$ in Equation (4.2c) is calculated.

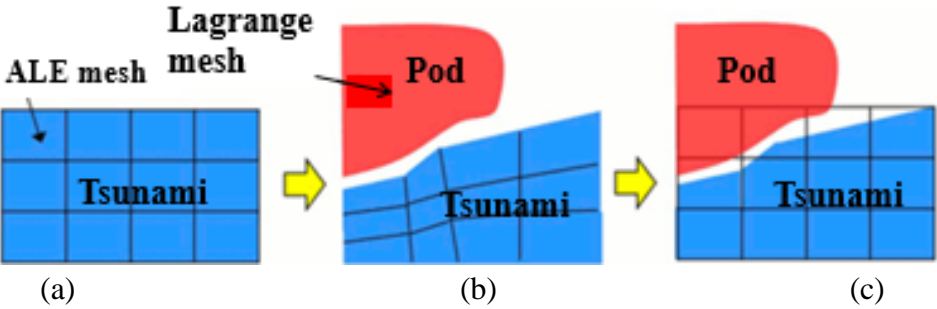


Figure.4.3: Arbitrary Lagrangian and Eulerian Method ((a)Initial mesh, (b)Deformed internal mesh, (c) Restore deformed mesh to the initial position)

The penalty method generally used in the contact calculation for structure analysis is applied into the coupling calculation method with structure part (tsunami pod) and fluid (tsunami) .As shown in Figure.4.4, those contact points are placed on the contact positions between structure part and fluid one. The contact points are shifted following the fluid transfer, however the virtual spring between the transferred point and the former point is generated. The force exerted by an extended spring expresses the pressure which a structure is exerted by fluid. The spring stiffness k for a virtual string is given as Equation (4.3).

$$k = p_f \frac{KA^2}{V} \tag{4.3}$$

Here, K is a volume modulus for a fluid element, A is average area for a structure element, V is a volume for a fluid element, p_f is scale factor. On this condition, the force P which the structure body receives is expressed as Equation (4.4).

$$P = kd \tag{4.4}$$

Here, d is intrusion of fluid into structure body. This coupling method has short time steps for an explicit method, so that intrusion into fluid for 1 step is a little.

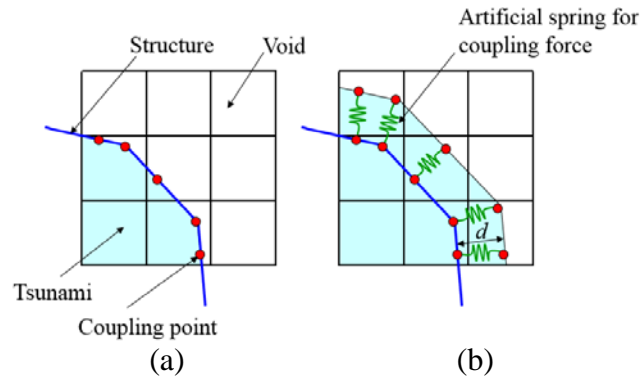


Figure.4.4: Fluid structure coupling procedure using penalty based method
 (a) Initial conFigureuration, (b) Generation of artificial spring at the next step

4.2.3. The conditions for simulation and video image shots

CFRP is compound material which has a layered structure. As a product specification for commercial CFRP, a tensile strength and a bending stress (nominal stress) are expatiated. Therefore, here a pod is dealt as a simple elastic body, and the load provided on its structure is estimated by von Mises stress to compare with the strength of an actual product on how much level of stress occur. The thickness of a tsunami pod in this simulation is set as 4.0 mm which is the minimum among the commercial products made of CFRP. The properties for CFRP as material are as follows; Young's modulus is 294GPa, Poisson's ratio is 0.12, and density is 1.8×10^{-9} ton/mm³. Tsunami velocity is calculated as follows. Tsunami velocity in transmitting on the sea is in proportion to the $\sqrt{}$ of sea depth. However, a tsunami velocity I apply into simulation is the one after flowing into the land which is slower than the one on the sea, because there are factors of reducing velocity that depth is lower and there are obstacles. The velocity for this simulation was calculated as 8 km/s by the distance which certain object move for a given period in the video taken in the Tohoku earthquake on March 11, 2011. The boundary conditions for inflow, outflow, and no-slip are set as the fluid part to prevent water from leaking out.

Figure.4.5 are 4 pieces of video image shots in simulation from the moment tsunami touches a pod to the moment the tsunami pod rises onto the wall. Figure.4.5 (c)(d) reveals that in the latter process of simulation an occupant hits on the internal wall of a tsunami pod to be injured possibly. For preventing it, I implement an occupant restraint system similar to a safety bar applied into roller coaster. In the next section, the degree of injury of an occupant is compared between the model without a restraint and the one with it.

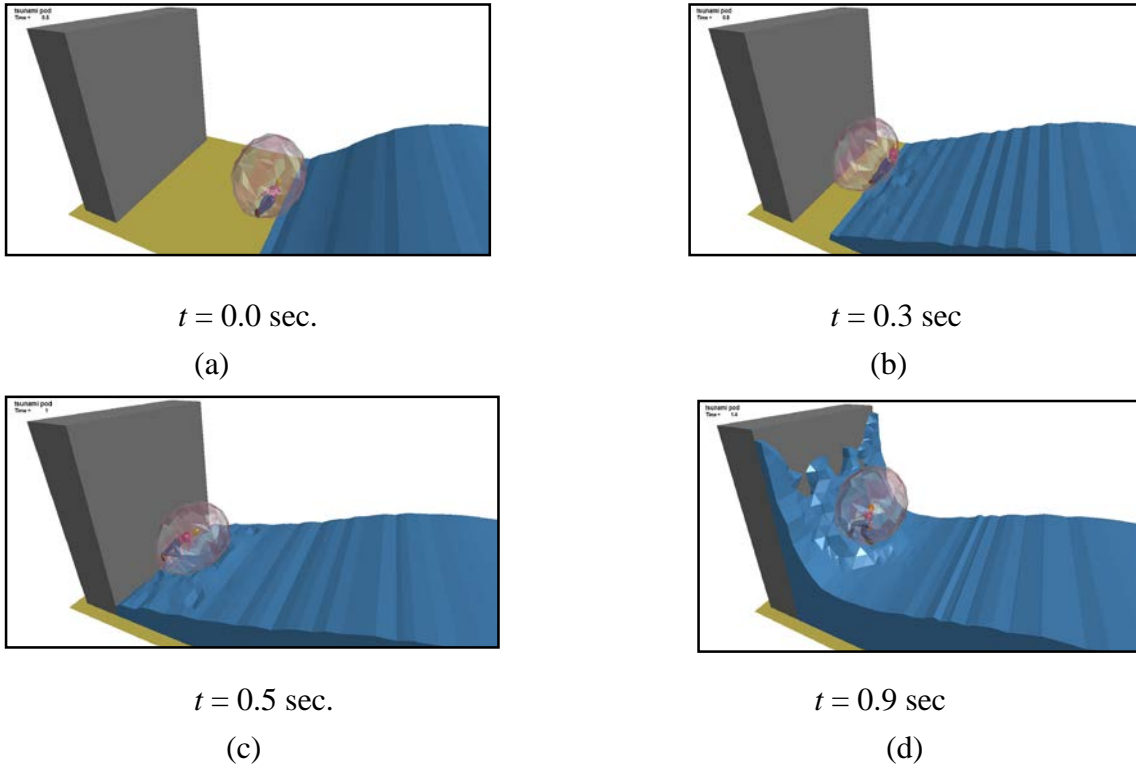


Figure.4.5: Video image shots of simulation

4.3. Numerical simulation

4.3.1. Verification of strength of the initial model without a restraint

Firstly, the strength is verified in the case of the initial model without an occupant restraint system. It is evaluated that a pod doesn't satisfy safety level, if any element of a pod exceeds von Mises equivalent stress for CFRP(500-1500Mpa). As a result of this simulation, the maximum of von Mises equivalent stress value (written shortly "Maximum Mises stress" in the subsequent sentences) is 4678Mpa observed in some elements around a central part seen from the major axis in collision illustrated as in Figure.4.6. It is assumed that a pod may be deformed or broken, because the value is more than the strength of CFRP.

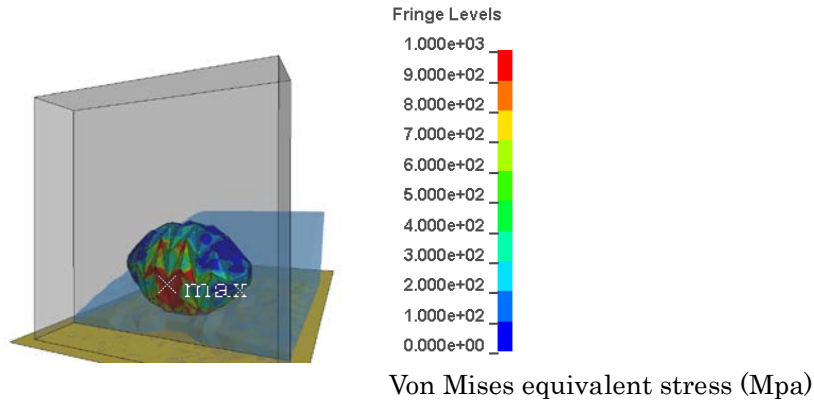


Figure.4.6: Color contour for the maximum of von Mises equivalent stress at the moment that a resultant force become maximum in case of the initial model without an occupant restraint system

4.3.2. Head injury criterion of the initial model

The Head Injury Criterion (HIC) is a measure of the likelihood of head injury arising from an impact. HIC is calculated by Equation (4.5) using head acceleration and its duration. A big acceleration value for a short duration period is allowed, because the calculated HIC value is the average of every 0.036 seconds. The value below 1000 is judged as safe where 1 of 6 people suffer a critical injury in the brain. The time transformation of HIC in case of the initial model is as exhibited by Figure.4.7. It is confirmed that the value calculated by Equation (4.5) is 9682 which is 10 times large as the safety level 1000 and it is likely that an occupant would be seriously damaged.

$$HIC = \left\{ \left[\frac{1}{t_2 - t_1} \int_{t_1}^{t_2} a(t) dt \right]^{2.5} (t_2 - t_1) \right\}_{\max} \quad (4.5)$$

- t_1 and t_2 : the initial and final times (seconds)
- a : acceleration

where t_1 and t_2 indicate the initial and final times (seconds) and a indicates acceleration. Here, I suppose that $[t_2 - t_1] \leq 0.036s$.

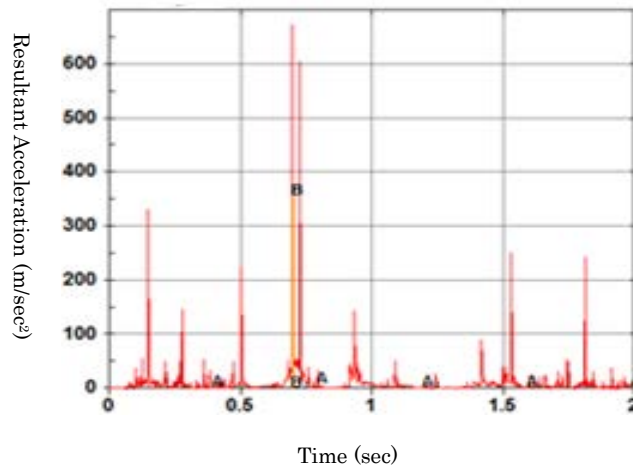


Figure.4.7: Resultant acceleration for the head of an occupant in case of the initial model without an occupant restraint system

4.3.3. Verification of strength of the modified model with a restraint

It is confirmed from the video image shots that an occupant is moving about heavily and hits on the internal wall of a pod and would be injured in the head. A tsunami pod is rotated 360 degrees, while an automobile collides head-on. Therefore, against 4-point or 5-point seat belts applied for an automobile, an restraint for an upper body and a lower body to imitate the safety bars for a roller coaster is designed as in the Figure.4.8 (a) . Figure.4.8 (b) is the modified model implemented with my designed restraint and seat. This model is called “the modified model with an occupant restraint system” subsequently. The parts of a seat and a restraint are set as rigid body consisting of 5914 nodes and 5858 shell elements totally. And, the parts of a seat and restraint are integrated into a pod by being defined having the common elements to prevent a restraint system from dropping off a pod. the thickness of an outer wall is increased from 4.0 mm to 6.0 mm for reinforcing its structure. As a result of the simulation by the modified model with an occupant restraint system, the maximum of von Mises equivalent value in some elements of a pod in collision is 2969Mpa which still exceeds the strength of CFRP and fails to improve the condition for damage enough as shown in Figure.4.9. On the other hand, HIC value is decreased by more than 90 % to become 61 in value as shown in Figure.10 which is well below the safety level 1000. Table.4.3 summarizes the comparison outcome datum between the initial model and the modified model.

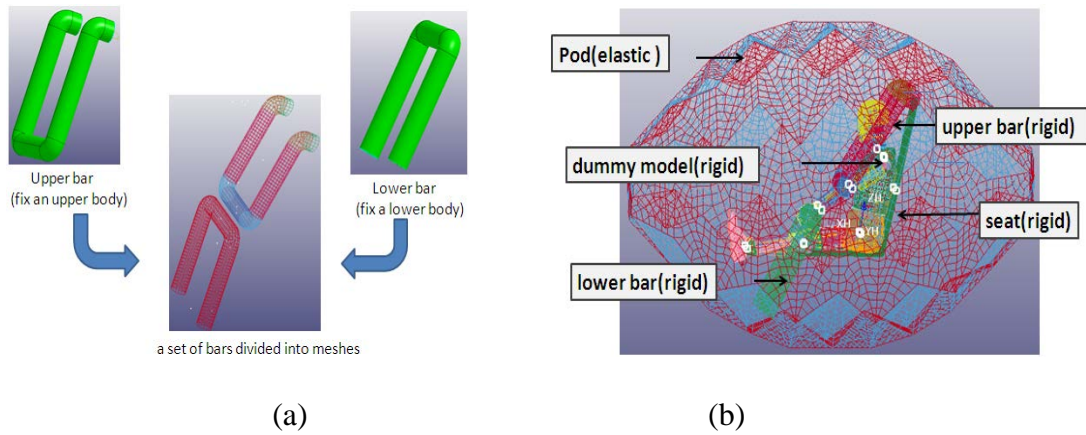


Figure.4.8: Model with an occupant restraint system
(a) upper and lower bars (b) modified model

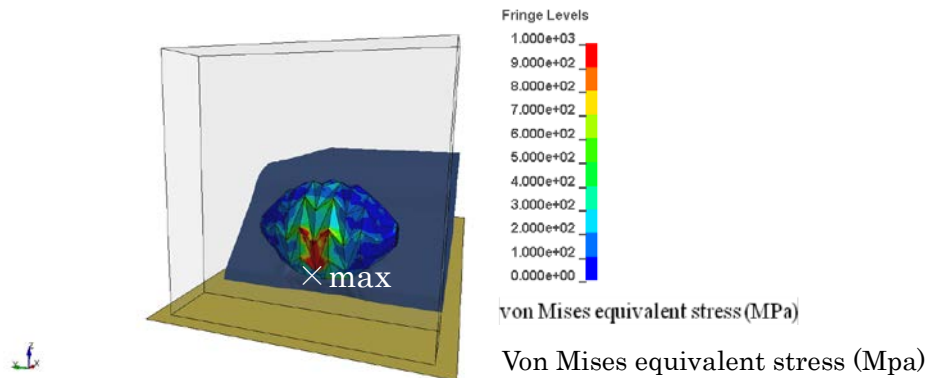


Figure.4.9: Color contour for the maximum of von Mises equivalent stress at the moment that a resultant force become maximum in case of the model with an occupant restraint system

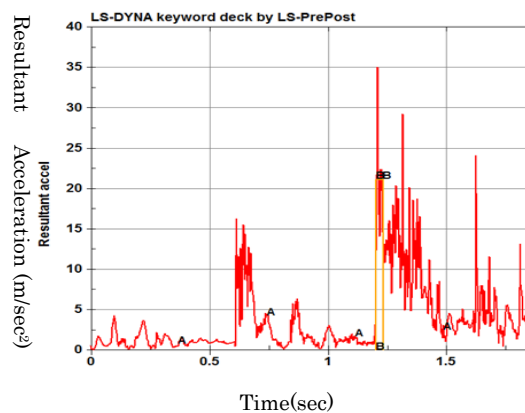


Figure.4.10: Resultant acceleration for the head of an occupant in case of the model with an occupant restraint system

Table.4.3: Comparison outcome between the initial model and the modified model

	Initial model without an occupant restraint system	Modified model with an occupant restraint system
Thickness(mm)	4.0	6
Max von Mises(Mpa)	4678	2969
HIC	9642	61

4.4 Optimization of structure of tsunami pod

4.4.1. Conditions for optimization

Applying the modified model with a restraint, the subsequent optimization is attempted. Those ranges for each design variable are as follows; $1125 < \text{major axis (a)} < 1200$, $630 < \text{minor axis (b)} < 840$, $2.0 < \text{thickness (t)} < 6.0$, $240 < \text{Young's modulus (E)} < 450$ which are all summarized in Table.4.4. In this optimization, HIC is excluded from consideration, because it has already satisfied safety level in the outcome of the simulation applying the modified model with a restraint in section 4.3.3.

Under the above conditions, respective design variables are calculated to minimize the mass of a pod. The velocity is set as constant 4m/sec in the X axis. For shortening a calculation time, a dummy model is set as rigid body, and apply decoupling analysis in optimization, and later the validity of the obtained optimal model is verified by coupling analysis. Incidentally, the calculation time for 1 step in decoupling analysis is one half as short as the one in low coupling analysis. In the PC I used for simulation (Intel(R)Core™i7-3730CPU@3.40GHz), the difference of calculation time is actually 5 hours for 1 step. Considering the number of repetition, this reduction is useful for an analyst.

For optimization, I utilize a software called LS-OPT [4.10] applying Radial Basic Function (RBF) as response surface function. Initially, 5 sample points are input and an optimum solution is searched while generating response surfaces of objective function and a constraint function by RBF network. The condition of finishing a calculation is the case where the relationship of optimal value obtained this step and the one obtained in the last step satisfies Equation (4.6). If Equation (4.6) is not satisfied, more 5 sample points are added and calculated again. The summary of this simulation is as shown in Table.4.5.

Table.4.4: Design variables, Objective function, and Constraint condition

design variable	
major axis (mm)	$1125 < a < 1200$
minor axis (mm)	$630 < b < 840$
thickness (mm)	$2.0 < t < 6.0$
Young's modulus (GPa)	$240 < E < 450$
objective function	
minimizing the mass of pod (kg)	
constraint condition*	
maximizing von Mises equivalent stress(MPa) for each element is less than the strength for CFRP	
*HIC is excluded	

Table4.5: Outline of optimization

velocity of tsunami	4m/sec (constant)
dummy model	the same amount of weight
fluid-structure coupling analysis	None
optimization	
the number of sampling points	8
the number of steps	16

[optimal value obtained in this step — optimal value obtained in the last step]

$$\frac{[\text{optimal value obtained in this step}]}{[\text{optimal value obtained in the last step}]} \leq 0.01 \quad (4.6)$$

4.4.2 Result of optimization

Table.4.6 is the summary of design variables, maximum von Mises equivalent value among elements, whether a constraint condition is satisfied or not, and the image which are output each step in optimization. The item “maxvonmises” is expressed as ○ in case maximum Mises value doesn't exceed the strength of CFRP and as × in the opposite way. In the 4th step, the constraint condition is satisfied, however the mass is twice as large as the initial model not to satisfy the objective function. Then, calculation is repeated and to converge in 16th step.

As a result of optimization process, the variables of the obtained optimal model is 41.3kg (-

24%), the length of major axis is 1200mm (-23%) , the length of minor axis is 840(-21%), thickness is 5.0mm,Young’s modulus is 245GPa.The maximum Mises value is 1299MPa (-43%) which doesn’t exceed the strength of CFRP 5000 to satisfy the constraint condition. The comparison between the initial model and the optimal model is summarized in Table.4.7. It means that by optimization the structural performance is unconfirmed while attaining the lightening by 52% which satisfied the condition of not being damaged well.

Table.4.6: Optimization processes from time step from 1to 16 (major axis, minor axis, thickness, and Young’s modulus as design variables and von Mises equivalent stress as constraint condition and mass as objective function are listed every 16 time step. And, those images for respective models are shown in the bottom.)






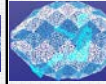

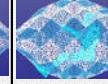

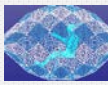
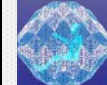
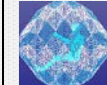

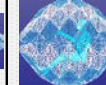


times of roop	1	2	3	4	5	6	7	8
a (scale)	1.00	0.96	1.10	0.75	1.07	0.75	1.10	0.75
b (scale)	1.00	0.75	1.07	1.10	0.79	0.75	1.10	0.75
t (mm)	4.0	6.0	2.4	6.0	5.6	2.0	2.4	2.0
Young's modulus (GPa)	294	450	240	282	240	450	450	261
mass (kg)	85	126	51	135	63	43	74	68
constraint condition(max vonmises(MPa))	× (1861)	× (1746)	× (2747)	○ (1362)	× (1895)	× (2158)	× (2253)	× (2070)
image of model								
times of roop	9	10	11	12	13	14	15	16
a (scale)	0.75	1.06	1.02	1.02	0.87	0.91	0.81	0.77
b (scale)	1.10	1.04	0.77	0.78	0.98	0.76	1.10	0.79
t (mm)	2.8	5.3	2.6	2.6	2.0	5.4	4.1	5.0
Young's modulus (GPa)	240	440	427	240	240	450	432	287
mass (kg)	97	70	76	128	62	85	51	41
constraint condition(max vonmises(MPa))	× (1558)	× (2140)	× (2264)	× (1931)	× (2061)	× (2394)	× (1611)	○(1299)
image of model								

Table.4.7: Comparison between the initial variables and the optimum variables

	initial variavle	optimal variable
design variable		
major axis(scale)	1.0	0.75
minor axis(scale)	1.0	0.82
thickness(mm)	4.0	3.7
Young modulus(Mpa)	294.0	240.0
Objective function		
weight(kg)	63.72	48.67
Constraint condition		
maximum of von Mises equivalent stress(Gpa)	2969	1299

4.4.3. Validation of optimal model

The optimal model obtained in section 4.4.2 is implemented with a dummy model, and is calculated by fluid structure coupling analysis in LS-DYNA. The maximum Mises value among the elements of a pod is 496MPa as shown in Figure.4.11 which is 70% smaller that the optimal model obtained by decoupling analysis in LS-OPT and also one sixth smaller than the modified model with a restraint obtained by coupling analysis in LS-DYNA. On the other hand, HIC in case of fluid-structure coupling analysis is 56 which is 8% lower than the modified model with a restraint, which guarantees the reliability of the optimal model.

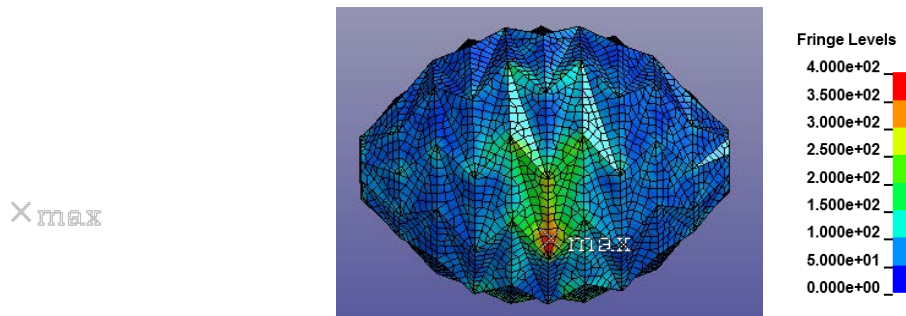


Figure.4.11: Color contour for von Mises equivalent stress when the part of element is the highest during simulation in case of fluid-structure coupling analysis applying the optimal model

4.5 Summary

In this Chapter, an ellipsoid body formed foldable and deployable structure is adopted and termed tsunami pod. Then, the model of a tsunami pod for simulation is generated, and its strength evaluation and safety examination is performed. The production obtained as a structure the outline of this research are written as follows.

1) The strength evaluation for several kinds of tsunami shelters have been performed only by experiment, and 4 point harness belt for an automobile is applied to those shelters and the injury value in collision hasn't been calculated. Here, a foldable tsunami pod is designed referring for size, material, and thickness to the present commercially products. As a result of conducting fluid-structure coupling analysis applying the initial model without an occupant constraint system, it is found that both strength of a pod and the injury value of an occupant don't satisfy safety level. The strength of a pod is evaluated by Mises condition while treated as isotropic. On the other hand, an occupant is shown in the way of being rotated 360 degrees in simulation video, so I analyzed that a 4 point harness belt is difficult to protect an occupant boarded on a tsunami pod.

2) Therefore, based on the initial model, while setting those variables as thickness, a major axis, a minor axis, and Young's modules, optimization analysis is performed under the constraint condition of Mises and the objective function to minimize a mass. As a result of optimization, the expected structure which is light weight and strong enough is obtained. In this optimization analysis, decoupling analysis is adopted instead of coupling analysis which takes twice times as decoupling analysis. Next, when the obtained optimal model is verified by coupling analysis, it is clarified that the strength of a pod is evaluated more strictly by decoupling analysis than by coupling analysis.

3) As stated as above, here I design the optimum specifications for a pod structure and develop the technique for modeling and simulation to reexamine the injury value of an occupant. Also, it is proposed that a seat and the bars which fix separately an upper and lower body of an occupant employed for a roller coaster should be useful for an occupant constraint system.

Chapter 5 Mathematical modeling for flat foldable tsunami pod

5.1 Consideration of bi-stable structure for a tsunami pod

The model of tsunami pod in Chapter 4 is generated by calculating coordinates of an ellipsoid body approximately, and it cannot be folded flat. As a way to utilize bi-stable property of folding structure, here I consider one kind of structures which utilizes the properties of folding structure can be expanded easily and difficult to be folded after expansion, while referring to [5.1]. The structure handled in [5.1] is folding cylindrical model consisting of 6 folding lines at 1 node, while the structure in this research is ellipsoid shaped folding structure. Figure.5.1(a) is its 3-dimensional folding model, and Figure.5.1(b) and Figure.5.1(c) indicates the process of being folded. This model is composed of a reverse spiral cylindrical origami structure by Nojima and an unit of triangle elements [5.2] [5.3]. Plane development is as shown in Figure.5.1(d). A solid line indicates a mountain line, and a dot line indicates a valley line. As a result of work, a cylinder is generated by closing the right and left boundaries. Here, a model is a cylinder which has regular hexagon shaped upper and lower sides, because the number of elements in the horizontal direction N is 6. And, it has 8 layers of elements in the height direction. The folding line pattern for the even number of layers is generated by mirror-reversing the folding line pattern for the uneven number of layers. Therefore, if constructing a structure in the even number of layers, the model is folded symmetrically in the longitudinal direction during the process of being, and a regular hexagon on a top moves longitudinally in the way of falling upon a bottom.

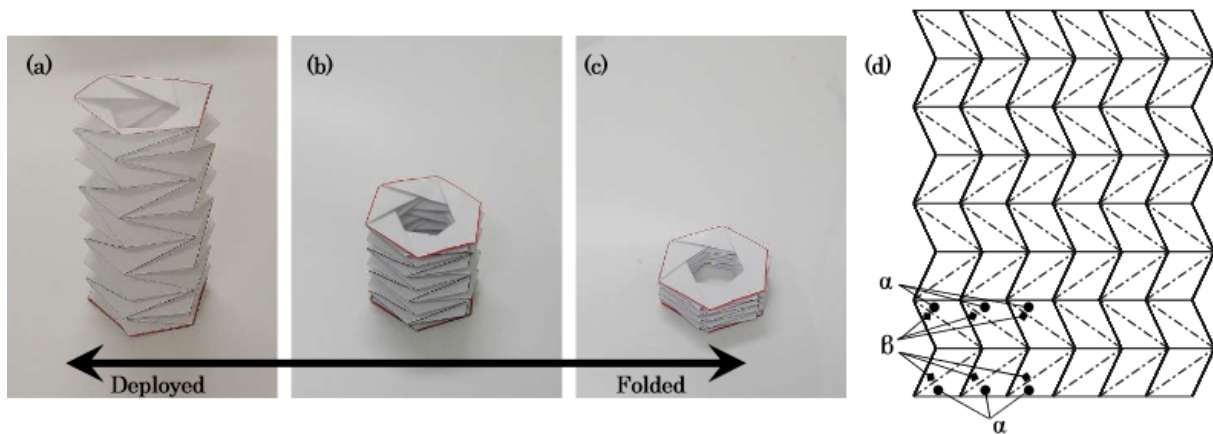


Figure.5.1: Folding behaviors of the foldable cylindrical structure based on Kresling's pattern; (a): Initial spatial state; (b): folding/expanding state; (c): Folded state; (d): Crease pattern for the structure.

When replacing all of folding lines for the model with the truss member and idealizing nodes as pinned connection, it became a truss structure consisting of three kinds of truss members in the horizontal, longitudinal, and diagonal directions. This distortion of this truss structure is zero in a 3-dimensional state, and while its members are distorted by receiving compression or strain, and finally becomes zero again in a completely folded state [5.4]. This structure is often called the bi-stability".

5.2 Design method of flat-foldable ellipsoid body

In this section, as a new model to replace the tsunami pod used in Chapter 4, I developed a triangulated ellipsoid body which can be folded flat. This triangulated ellipsoid body does not have strain in the deployed state and the folded state.

The subsequent steps give a design method of a triangulated ellipsoid body. Here we suppose that positions of vertices are the xy plane symmetry. Thus we may consider the upper-half part of this ellipsoid ($z \geq 0$), and the lower-half part is determined by the position of vertices of the upper-half part. Also I adopt the reversed spiral structure.

First I show a design method of a flat-foldable truncated cone.

(i) Consider a truncated cone with the lower radius r_1 the upper radius r_2 and the height h , where we suppose that $r_1, r_2 > 0$ and $h > 0$. Figure.5.2(a) show a truncated cone.

(ii) Replace the lower disk and the upper disk with n -regular polygons. Each vertex of the lower and the upper n -regular polygons is written by

$$A_{j,k} = (x_{j,k}, y_{j,k}, z_{j,k}) \quad (0 \leq j \leq n, k = 1, 2) ,$$

$$x_{j,k} = r_k \cos\left(\frac{2\pi j}{n} + \sum_{i=0}^k \theta_i\right), \quad y_{j,k} = r_k \sin\left(\frac{2\pi j}{n} + \sum_{i=0}^k \theta_i\right), \quad z_{j,k} = h_k,$$

where I suppose $\theta_1 = 0$ for simplicity, and $\theta_k \in \mathfrak{R}$, $h_1 = 0$ and $h_2 = h$.

(iii) Construct a lateral face by triangular faces

$$\Delta A_{j,1} A_{j,2} A_{j+1,1} \quad \text{and} \quad \Delta A_{j,1} A_{j+1,2} A_{j+1,1}$$

for $0 \leq j < n$. Figure.5.2(b) shows a modified truncated cone.

(iv) Find θ_1 such that this modified truncated cone can be folded flat, where I admit the expansion and contraction of faces in middle of deformation. Since this modified truncated cone has the rotational symmetry, I may consider the triangle $\Delta A_{0,1} A_{0,2} A_{1,1}$. The rest parts are determined automatically.

By using the rotational matrix with the rotation axis $\Delta A_{1,1} A_{0,1}$ rotate the triangle $\Delta A_{0,1} A_{0,2} A_{1,1}$ such that the z coordinate of $A_{0,2}$ is equal to 0. See Figure.5.3. I denote its coordinate by $A'_{0,2}$. Then I may find θ_1 such that the distance of the origin and $A'_{0,2}$. It is determined by

$$\theta_1 = \arccos\left(\frac{h^2}{4r_1 r_2} + (-1)^k \sqrt{1 - \frac{h_1^4}{16r_1^2 r_2^2 \cos^2\left(\frac{\pi}{n}\right)}} \sin\left(\frac{\pi}{n}\right)\right), \quad (5.1)$$

where the parameters r_1, r_2, h satisfies the condition

$$0 < h_1 \leq 2\sqrt{r_1 r_2 \cos\left(\frac{\pi}{n}\right)} .$$

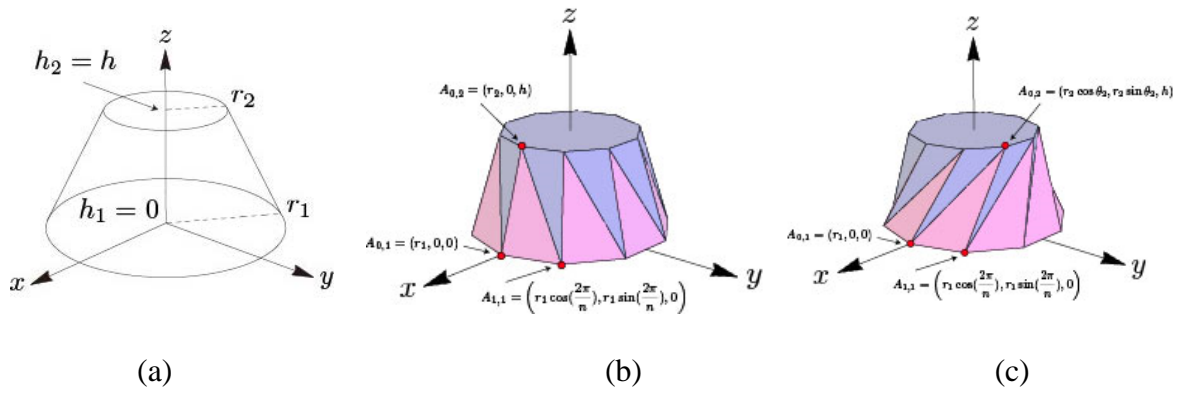


Figure.5.2: (a) A truncated cone. (b) A modified truncated cone of (a). (c) A flat-foldable truncated cone.

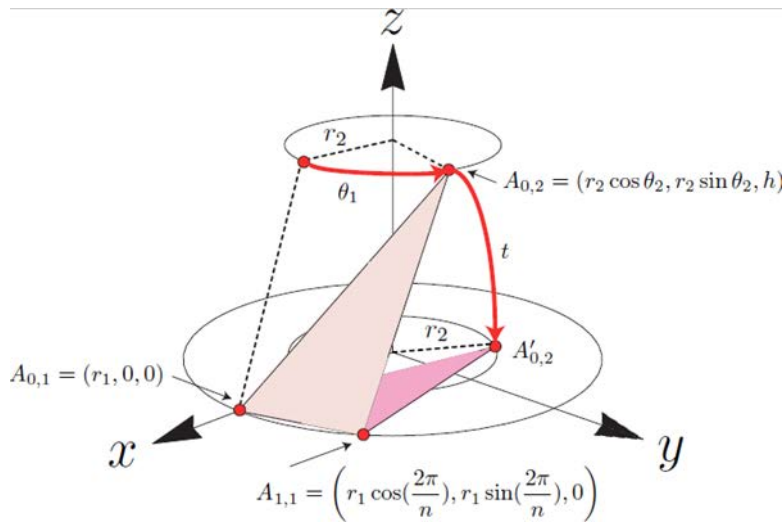


Figure.5.3: A graphical image of the determination of θ_2 .

Throughout the above steps, I can obtain a flat foldable truncated cone.

Next I show a design method of a flat-foldable ellipsoid body.

(i) Consider an ellipsoid body written by the equation $\frac{x^2 + y^2}{a^2} + \frac{z^2}{b^2} = 1$, where $a, b > 0$.

As a representation by the polar coordinates, I rewrite the above equation as $x = a \cos \theta \cos \varphi, y = a \sin \theta \cos \varphi, z = b \sin \varphi$, where θ and φ are the latitude and the longitude, respectively.

(ii) Separate this ellipsoid body by m planes which is parallel at the $x - y$ plane. Let

$P_k (k = 0, 1, 2, \dots, m - 1)$ be the boundary of a cross-section of this ellipsoid body.

Here I choose its boundary written as follows.

$$P_k = \left\{ (x, y, z) \mid x^2 + y^2 = r_k^2, z = h_k \right\}, \quad (5.2)$$

where

$$r_k = \frac{ab}{\sqrt{b^2 + a^2 \tan^2\left(\frac{k\pi}{2m}\right)}}, \quad h_k = \frac{ab \tan\left(\frac{k\pi}{2m}\right)}{\sqrt{b^2 + a^2 \tan^2\left(\frac{k\pi}{2m}\right)}}. \quad (5.3)$$

Figure 5.4 shows a graphical image of cross-sections for the side view.

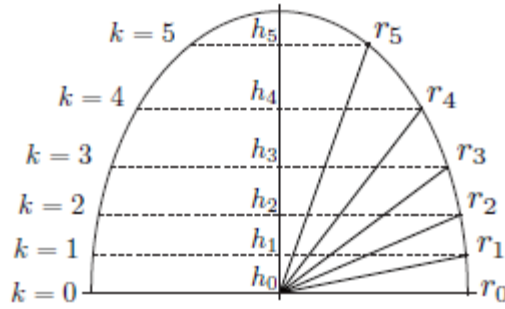


Figure.5.4: A graphical image of cross-sections for the side view. The parameters are $a = 800, b = 1200, m = 6$.

(iii) Suppose that cross-sections P_k are similar regular polygons. Let n be the number of angles of its regular polygons. Then I can obtain a separated ellipsoid body by triangular faces as follows. Each vertex is written by

$$U_{j,k} = (x_{j,k}, y_{j,k}, z_{j,k}) \quad (j = 0, 1, 2, \dots, n-1), \quad (5.4)$$

$$x_{j,k} = r_k \cos\left(\frac{2\pi j}{n} + \sum_{i=0}^k \theta_i\right), \quad y_{j,k} = r_k \sin\left(\frac{2\pi j}{n} + \sum_{i=0}^k \theta_i\right), \quad z_{j,k} = h_k,$$

where I suppose $\theta_0 = 0$ for simplicity, and By the same way of the determination of the formula 1, $\theta_k (k = 1, 2, \dots, m-1)$ is determined by

$$\theta_k = (-1)^k \arccos\left(\frac{(h_k - h_{k-1})^2}{4r_{k-1}r_k}\right) + (-1)^{k+1} \sqrt{1 - \frac{(h_k - h_{k-1})^4}{16r_{k-1}^2 r_k^2 \cos^2\left(\frac{\pi}{n}\right)}} \sin\left(\frac{\pi}{n}\right), \quad (5.5)$$

where $(-1)^{k+1}$ and $(-1)^k$ implies that a triangulated ellipsoid body has the reversed spiral structure.

Thus triangular faces of this ellipsoid body are given by

$$\Delta U_{j,k-1} U_{j+1,k-1} U_{j,k} \quad \text{and} \quad \Delta U_{j+1,k-1} U_{j,k} U_{j+1,k} \quad (5.6)$$

for $j = 0, 1, 2, \dots, n-1$ and $k = 1, 2, \dots, m-1$.

(iv) Since the lower-half is the $x - y$ plane symmetry, each vertex is determined as

$$L_{j,k} = (x_{j,k}, -y_{j,k}, -z_{j,k}) \quad (5.7)$$

Thus I obtain an ellipsoid body of the lower-half part separated by triangular faces

$$\Delta L_{j,k-1} L_{j+1,k-1} L_{j,k} \quad \text{and} \quad \Delta L_{j+1,k-1} L_{j,k} L_{j+1,k} \quad (5.8)$$

for $j = 0, 1, 2, \dots, n-1$ and $k = 1, 2, \dots, m-1$

Throughout the above steps[5.5], I can obtain a triangulated ellipsoid body where top face and the bottom face are a same n -sided polygon. Figure.5.5 shows an example of a triangulated ellipsoid body determined by the parameters $a = 800$, $b = 1200$, $n = 10$, $m = 6$. Figure.5.5 shows origami parts for Figure.5.5 and its pictures. Indicated as in Figure.5.7, it is confirmed that the paper craft for the model is able to be folded flat.

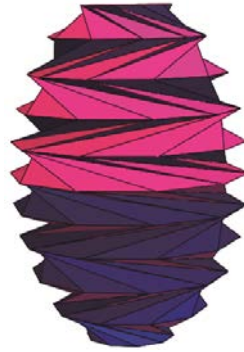


Figure.5.5: A triangulated ellipsoid. The parameters are $a=800$, $b=1200$, $n=10$, $m=6$.

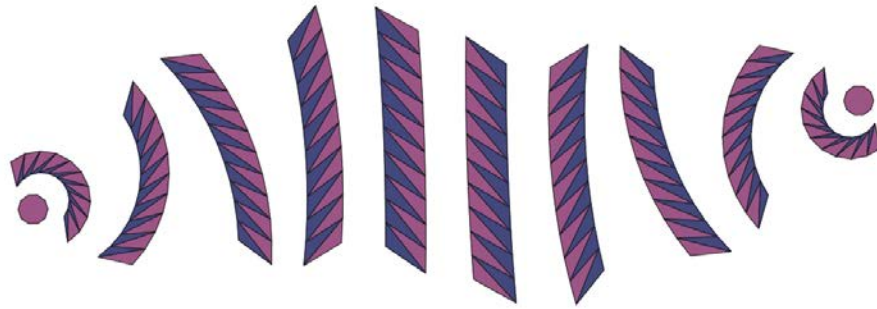
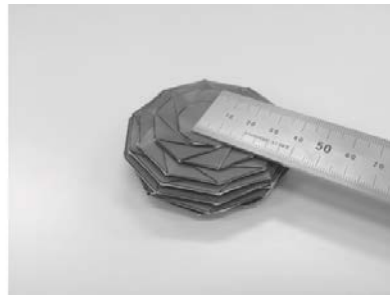


Figure.5.6: Origami parts for Figure.5.4



(a)

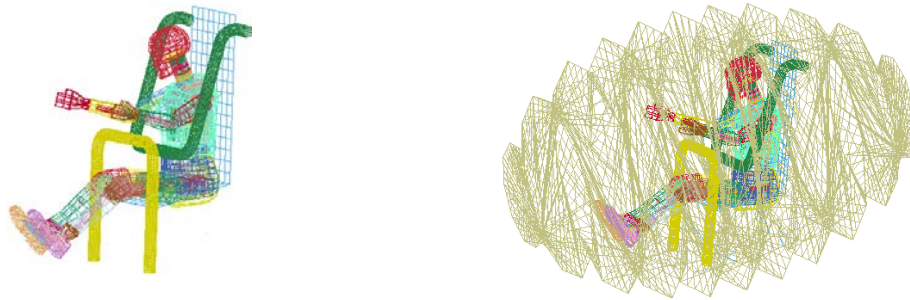


(b)

Figure.5.7: (a) Side view of an origami ellipsoid body of Figure.5.6. This can be folded by pushing z-axis direction as (b)

5.2 Safety certification for the mathematically designed model

Using the mathematical design method for design of a tsunami pod in triangulated ellipsoid body form, the pod with the same number of sides and angles as the one which is applied in the numerical simulation in Chapter 4. Regarding the other parts such as a seat, upper bar, and lower bar, and a dummy model, respective same models as the one in Chapter 4 are applied this time. The illustrations for the model are as shown in Figure.5.8 (a) and Figure.5.8 (b).



(a) Dummy fastened by occupant constrained bars on seat (b) Total pod model

Figure.5.8: Model of a tsunami pod with 10 sided polygons designed by mathematical modeling m

5.2.3 Simulation for the mathematically designed model

As a result of the simulation, the maximum of von Mises equivalent stress value among each element (written shortly as Maximum Mises stress as below) is 789 as illustrated in Fig.5.9, it is judged that a pod may be deformed or broken. While the transition of resultant force in case of the mathematical model is as shown in Figure.5.10. It is calculated that the value HIC is decreased by more than 90% to 76 which is well below the safety level 1000. Table.5.1 shows the comparison between the simplified model and mathematically designed model for a tsunami pod. The maximum of von Mises stress value of mathematical designed model is much smaller than the one of the simplified model, whose reason is considered that the former can absorb the impact energy in collision by being folded.

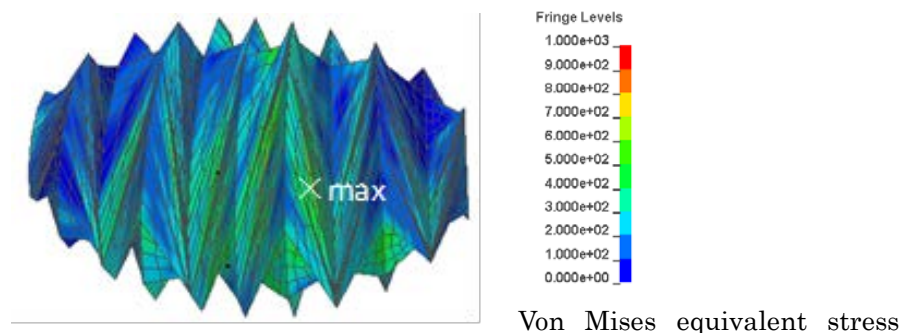


Figure.5.9: Color contour for the maximum of von Mises equivalent stress at the moment that a resultant force become maximum in case of the mathematical designed model with an occupant restraint system

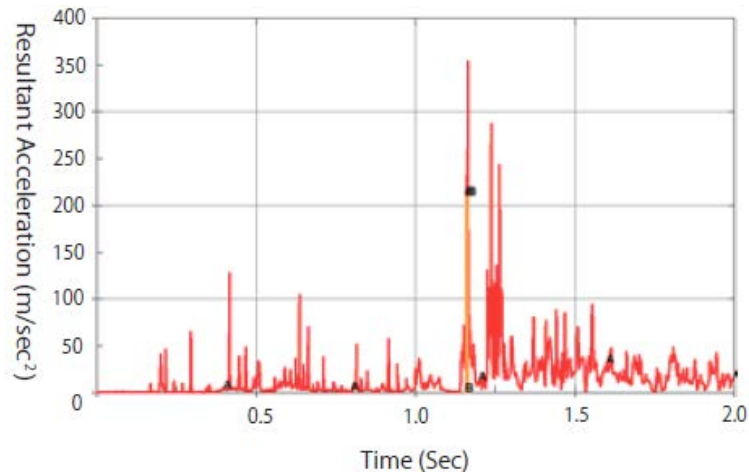


Figure.5.10: Resultant acceleration for the head of an occupant in case of the model with an occupant restraint system.

Table.5.1: Comparison outcome between the simplified model and the mathematically designed model for a foldable tsunami pod

	Simplified model with an occupant and a restraint system	Mathematically designed model with an occupant and a restraint system
Max von Mises (Mpa)	2969	789
HIC	61	76

5.2.2 Optimization for a mathematical designed tsunami pod

By applying the mathematically designed model with a restraint, the subsequent optimization is attempted. Those ranges for respective design variables are as follows: $900 < \text{major axis}(a) < 1320$, $600 < \text{minor axis}(b) < 880$, $2.0 < \text{thickness}(t) < 6.0$, $345 < \text{Young's modulus}(E) < 450$ tabulated as in Table.5.2. Here, other condition is the same as the previous optimization applying the simplified tsunami pod model in section 4.4.1.

Table.5.2: The range of design variable, objective function and constraint condition.

In this table, the mark * implies that HIC is excluded.

design variables	
major axis (mm)	$900 < a < 1320$
minor axis (mm)	$600 < b < 880$
thickness (mm)	$2.0 < t < 6.0$
Young's modulus (GPa)	$345 < E < 450$
objective function	
minimizing the mass of pod (kg)	
constraint condition*	
maximizing von Mises equivalent stress(MPa) for each element is less than the strength for CFRP	
*HIC is excluded	

Firstly, I check the correlation between respective design variables, objective variable, and the value of constraint condition as in the Table.5.3. It is found that mass of pod is higher positive correlated with a major axis and a minor axis than with thickness and Young’s modulus, so that it is necessary to reduce a size for making the model of a pod light-weighted. And, also it is found that thickness needs to be smaller and Young’s modulus needs to be lower. While the maximum Mises stress as constraint condition has a higher negative correlation with a major axis and a minor axis than with Young’s modulus, and seldom correlated with thickness. It can be said for minimizing the maximum Mises stress it is necessary to increase a size and Young’s modulus. Therefore, as a consequent of the above consideration, optimization is predicted to be under unstable process in changing the size while arranging thickness and Young’s modulus. The relationships are illustrated as in Figure.5.11 (a)(b)(c) drawn by a software for optimization “LS=OPT” with an interface to LS-DYNA. These make it easier to interpret the relationship as mentioned above visually.

Table.5.3: The values of correlation coefficient between variables

		variables				response	
		major axis	minor axis	thickness	Young's modulus	mass	maximum Mises stress
variables	major axis	1.00	0.97	-0.17	0.29	0.83	-0.90
	minor axis		1.00	-0.16	0.29	0.88	-0.90
	thickness			1.00	-0.07	0.16	0.05
	Young's modulus				1.00	0.23	-0.17
response	mass					1.00	-0.76
	maximum Mises stress						1.00

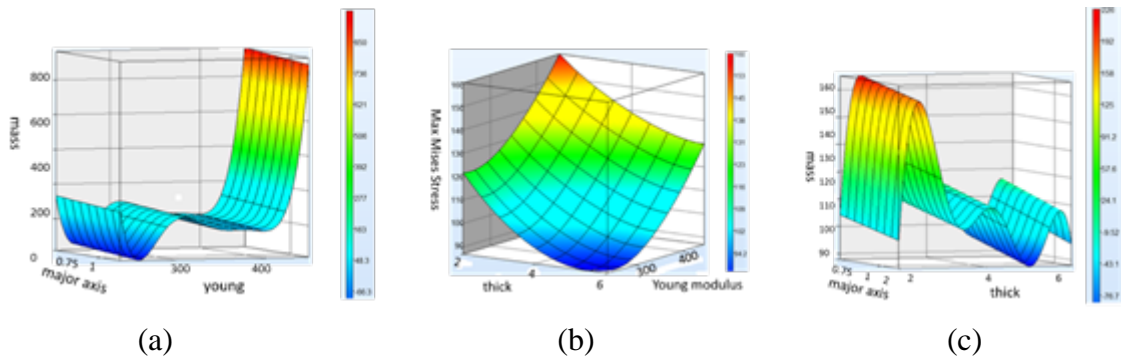


Figure.5.11: Visualized color contour for correlation between design variables, objective function, and constraint condition

The result of optimization process as shown in Table.5.4 which illustrates respective pod images during optimization process from time step 1 to 6. The calculation takes 5 days to run from step 1 to step 6. And, in checking the result, the optimization for size is converged in the 4th step, and after that thickness and Young's modulus is made to be converged in the 6th step. The comparison between the optimal model obtained in the 6th step and the initial model is as shown in Table.5.5.

Table.5.4: Optimization process from time step 1 to 6

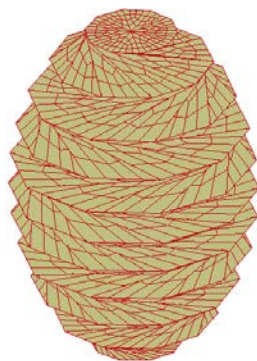
times of roop	a (scale)	a(actual)	b (scale)	b(actual)	t (mm)	Young's modulus (GPa)	mass (kg)	constraint condition(max vonmises(MPa))	image of model
1	1.00	1205	0.75	600	4.3	240	132	163	
2	0.97	1164	0.84	668	2.7	240	100	91	
3	0.98	1176	0.76	608	4.6	323	140	83	
4	1.10	1320	0.75	600	5.5	301	233	105	
5	1.10	1320	0.75	600	6.0	285	440	87	
6	1.10	1320	0.75	600	5.1	323	153	96	

Table.5.5: Comparison between the initial variables before optimization and the optimal variables after optimization

	initial variavle	optimal variable
design variables		
major axis(scale)	1.0	1.10
minor axis(scale)	1.0	0.75
thickness(mm)	4.0	5.1
Young's modulus(Mpa)	294.0	323.0
Objective function		
mass(kg)	297	153
Constraint condition		
maximum of von Mises equivalent stress(Mpa)	2969	96

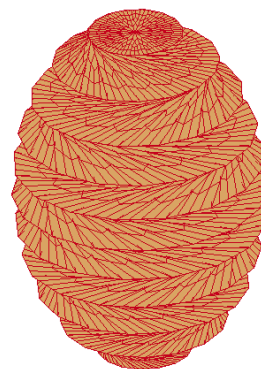
5.3 Comparison of the different number of sided polygons for tsunami pod

In the last simulation, the number of sided polygons are 10 as represented in Figure.5.10 (a). The safety for an occupant in hitting on the wall has been confirmed. Here in this Chapter, the safer form with another number of sided polygons is attempted to be found by changing the mathematical design method described in section 5.1. Considering the form is symmetry in the Z axis, the number of 16 is chosen and applied as the comparison model as shown in Figure.5.12 (b). The pod model with seat, bars, and dummy model appears as in Figure.5.13. The space is larger, therefore an occupant can stay more comfortably in the pod than the previous pod.



(a)

(a) Tsunami pod with 10 sided polygons



(b)

(b) Tsunami pod with 16 sided polygons

Figure.5.12: Comparison of ellipsoidal forms with different number of sided polygons

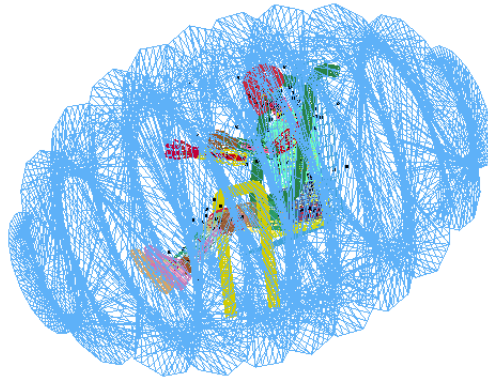


Figure.5.13: The ellipsoid body formed pod with 16 sided polygons

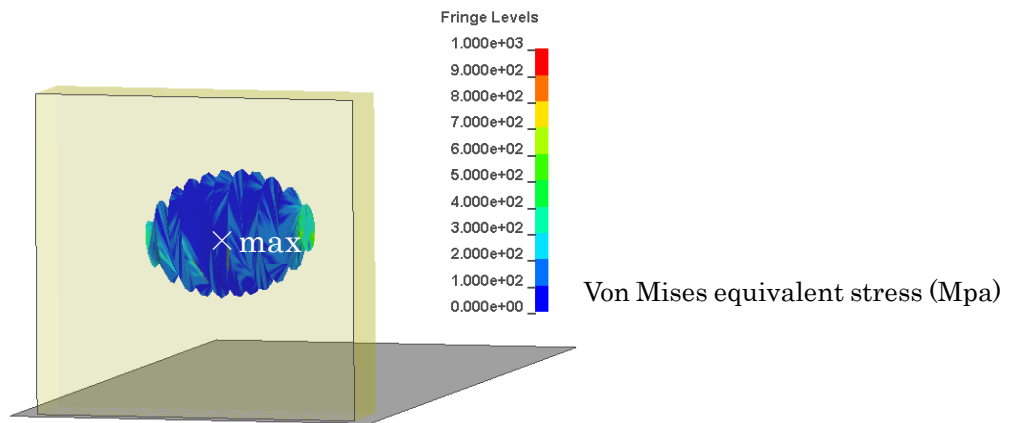


Figure.5.14: Color contour for the maximum of von Mises equivalent stress at the moment that a resultant force become maximum in case of the initial model without an occupant restraint system (maximum Mises value =1398)

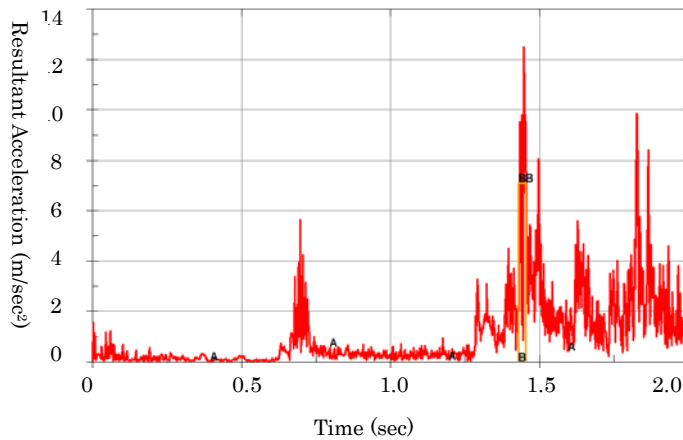


Figure.5.15: Resultant acceleration for the head of an occupant in case of the initial model without an occupant restraint system (HIC=34)

The max Mises value is 1398 while the pod ascend a wall after hitting against it displayed as Figure.5.14. Its value is smaller than the pod with 10 number of sided polygons whose max Mises value is 2969 mentioned in section 4.3.3. On the other hand, the graph shape for resultant acceleration is roughly the same, however the value of HIC is 34 calculated by time course of resultant acceleration of Figure.5.15 which is lower than the pod with 10 number of sided polygons whose HIC is 61. The comparison for outcome of safety verification between the model with 10 sided polygons and the one with 16 sided polygons are as tabulated in Table.5.6. As a result of 2 kinds of safety verifications, it is said that the safety level is enhanced for the larger number of sided polygons. It is predicted that the more number of sided polygons the pod has, the higher safety for a pod is provided. However, considering the process of manufacturing would become difficult and it is easy to break against external stress because of many nodes and sides connected with each other.

Table.5.6: Comparison between the pod with 10 sided polygons and the one with 16 sided polygons

	pod with 10 sided polygons	pod with 16 sided polygons
Max von Mises (Mpa)	2969	1398
HIC	61	34

5.4 Summary

In this chapter, the development which can be folded completely flat is designed by geometry mathematics. And, applying the generated model designed by this modeling method, the safety verification by von Mises equivalent stress and Head Injury Criterion is performed as in the same way as the simple model in chapter 4 . And then, its structure properties such as major axis, minor axis, thickness, and Young’s modulus is optimized to minimize its mass. Additionally, it is examined how the safety level differ depending on the number of sided polygons. As a result of comparison, it is found that the security of the larger number of sided polygons is enhanced for absorbing the crash energy by being folded halfway.

Here is summary of results for numerical simulation and optimization of tsunami pod in the following. In Table.6.1. It is clear an occupant restraint system improve safety which makes it possible to prevent an occupant from hitting on the internal wall of a pod.

Table.6.2 is the result of optimization for structural properties in case of both a simplified

model and a thematically designed model. Comparing the simplified model and the mathematically designed model, it is found the latter model is stronger than the former model, so that the latter model is difficult to be broken by impact. And, the optimization aimed to minimize a mass succeeded in improving the safety level in cases of both models.

Table.6.3 shows the comparison of the simulations with the different number of sided polygons. It is confirmed that the structure formed by the more number of sided polygons become weaker to impact from outer. On the other hand, the injury level of an occupant is lower than the one formed with fewer number of sided polygons, because each side and node absorb the impact energy while being folded.

Table.6.1: Result of numerical simulation in case of a tsunami pod without an occupant restraint system and the one with it

	Simplified model with 10 sided polygons without an occupant restraint system	Simplified model with 10 sided polygons with an occupant restraint system
Max von Mises (Mpa)	4678	2969
HIC	9682	61

Table.6.2: Result of optimization for structural properties of a tsunami pod in case of a simplified model and a mathematically designed model

	Simplified model with 10 sided polygons	Optimized model for the simplified model with 10 sided polygons	Mathematically designed model with 10 sided polygons	Optimized model for the mathematical model with 10 sided polygons
Max von Mises (Mpa)	2969	1299	789	96
HIC	61	56	76	-

Table.6.3: Result of numerical simulation for tsunami pods formed by different number of sided polygons in case of a simplified model and a mathematically designed model

	Simplified model with 10 sided polygons	Mathematically designed model with 10 sided polygons	Mathematical model with 16 sided polygons
Max von Mises (Mpa)	2969	789	1398
HIC	61	76	34

Chapter 6 Conclusions and future work

6.1 Conclusions

In order to put tsunami shelter into practical use which has been attracting attention since Tohoku earthquake occurred on March 11,2011, the form was transformed in the way an occupant is able to lie down and as an occupant restraint system to fix an upper body and a lower body separately which is developed by referring to the safety bars used for a roller coaster. CFRP which is adopted for material was treated as isotropy, and new modeling methods such as configuration of injury value. On the other hand, weak coupled analysis between shelter and tsunami and response surface method which was devised so as to obtain an objective value by as few as trial points were examined as simulation techniques, and the design method which ensure an user's safety was proposed. The concluding remarks about each chapter of this dissertation are summarized as follows.

Chapter 1 "Introduction" stated the problems of the previous relative researches and the aim of this research. The previous tsunami shelters take space while not in use, because they are not able to be folded. Therefore, it is difficult to become widespread, so that in place of them a foldable and deployable structure was suggested and the importance of applying an occupant restraint system in order to enhance safety was indicated.

Chapter 2 "Origami engineering" discussed the 2 types of origami shapes according to origami superior properties. One superior property is that a structure generated by tessellation space-filling possesses lightweight and high stiffness. Truss core panel is introduced as a representative for a tessellation composed of tetrahedron and octahedron. Truss core is assumed to be applied into the floor of a vehicle and a train. Considering its practical use, truss core is superior in the respects of not only lightweight and high stiffness but also low cost and fire resistance than conventional forms such as honey comb. Another superior property origami has is that a structure is deployable and foldable alternatively. Reverse spiral cylindrical structure

is a representative to utilize this property effectively. Each angle consisting of mesh triangle in its pattern is calculated exactly by mathematics on the basis of geometric theory for folding. More complex theory and calculation is conducted to apply other material with thickness beside a thin paper for producing an industrial goods. There are a side member for a vehicle which absorb the impact in crash as an example. From these instances, In this dissertation, I apply this kind of structure into a tsunami pod to utilize its superiority in the points of storage and absorption of impact.

Chapter 3 “Simulation and Optimization design method” described fluid-structure coupling analysis and response surface method optimization technique. As a representative for fluid-structure coupling analysis there is structure acoustic coupled system. While a matrix obtained by finite element method is symmetry and possesses band property, in case of structure acoustic coupled system a matrix becomes asymmetry and arrayed finely. Corresponding to this problem, it was proved that the relationship between right eigenvectors and left eigenvectors was obtained and a matrix was converted to another matrix which was symmetry and possesses band property only by right eigenvector, which enabled to treat strong coupled analysis in structural and acoustic system. On the other hand, in case of general fluid structured coupling analysis there has never been such a distinguished method discovered, so that weak coupled analysis where the single analysis for fluid part and structure part is solved sequentially and the external force by one part is treated as the power to another part. In this research, this weak coupled analysis was adopted. Not mathematical programming using weak coupled analysis but response surface method is appropriate for optimization of a nonlinear problem. In the case of the period for one time of simulation is long, it is important to select trial points in accordance to the goal followed by the decision of the range where an appropriate value exists instead of following a response surface completely.

Chapter 4 “Foldable tsunami pod” made of CFRP (Carbon Fiber Reinforced Plastics) which is dealt as isotropy is proposed. Large-scaled model whose total number of nodes is 36000 is generated which consists of an occupant restraint system modeled by shell elements, an occupant and fluid modeled by solid elements. In simulation, von Mises equivalent stress is used as failure condition, and HIC (Head Injury Criterion) is used as the injury value of an occupant which is adopted in automobile industry. As occupant restraint system, it was indicated that the safety bars used for a roller coaster rotated in 360 degrees to fix upper and lower bodies separately instead of 3 points seatbelt for an automobile ensured safety of an occupant. Moreover, as a result of performing optimization, large reduction in weight for a pod was realized.

Chapter 5 “Mathematical modeling for flat foldable tsunami pod” derived a mathematical

principle for foldable structured ellipsoid body to express the structure of a tsunami pod parametrically in large scaled simulation in Chapter 4. This principle was very useful to solve a new question whether a model composed of the more number of consisting nodes and sides would enhance the safety level or not. By this principle, a model with 10 sided polygons and a model with 16 sided polygons are generated and compared in evaluating safety. Consequently, it is predicted that the more complex folding model has higher safety for an occupant because it is possible to absorb external energy more effectively. To the contrary, a pod is weaker against external pressure, so that a new problem about manufacture is raised to produce a strong structure at a low cost and for short time. However, it is essential to determine an optimal model for each model to compare genuinely, which remains for one of future works. At least in this chapter, the importance of parametric expression to generate models in this kind of large scaled model was represented.

In Chapter 6, conclusions and future works are mentioned. This research investigate mathematical modeling and analysis to design a tsunami pod which is not broken on expanded state and prevent an occupant from dying. However, there are many issues remained for practical applications, say, design to give ease to an occupant and how to get out a pod after tsunami passes, and how to keep the shape from external water pressure. Corresponding to these issues, the novel design method to utilize bi-stability characteristic for foldable structures is mentioned. Higher simulation techniques than ever is necessary to realize it, which would contribute to advancement of research in this field.

6.2 Future work

6.2.1 Tasks left for practical use

Originally, a tsunami shelter should be folded into flat in normal period and be expanded quickly in case of emergency. However, the tsunami pod in this research is dealt as being expanded from the first time. And, there is a concern that it is folded easily depending on the direction of the load it receives. Corresponding to this problem, I haven't discussed its mechanism and ignored the impact of that on the strength of a pod to simplify this research yet. In the future, I will propose a mechanism to be foldable and deployable for a tsunami pod with CFRP, and optimize the model considering the mechanism. I can refer to a type of motor called actuator as represented in Figure.6.1 [6.1] that is responsible for moving or controlling a mechanism or system utilized for solar panel in space and a string moving upward or forward

in a single quick motion by elastic potential energy to return to the former state employed for a pop up tent as represented in Figure.6.2 [6.2].

Another problem is how to connect each part of a pod. While glue and cellophane tape are used in case of paper, a special device is integral to connect an object made of CFRP, because it is rather thick and provide a connecting space to correspond a load in crash and folding. The hinge structure connecting with bolt nuts are developed for generating truss core panel by Terada as shown in Figure.6.3 [6.3]. The bending stiffness of the trial product made of steel is certified by measurements and FEM analysis.

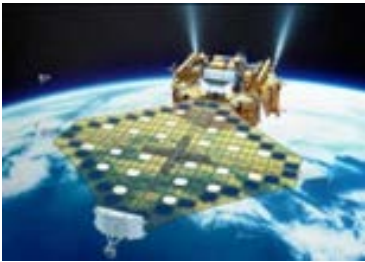


Figure.6.1: Solar panel implemented with artificial satellite



Figure.6.2: Pop up tent



Figure.6.3: Hinge structure connecting each part with bolt nuts

Another challenge is decreasing the thickness of a pod to be folded even by a weak force and to make a folded state as thin as possible. Likewise, it is necessary to calculate the value of thickness not to be strained and broken in crash. The minimum thickness for CFRP is 4mm at the present, hence, other materials which is thin and strong such as carbon fiber called Toreka developed by TORAY Industries, Inc recently.

Final task is to have an occupant stay in a shelter safely and comfortably. There are several issues to be solved in the following.

- To implement an entrance and exit. The places will be determined as around the strongest elements where von Mises equivalent value is the lowest for the complete duration of simulation.
- To implement a suction port for oxygen

- To construct a space which gives an occupant a sense of safety while evacuating
- Certify the stiffness along Z axis direction, because this time the impact only from the X and Y axis directions are examined
- Decrease the thickness of a pod to be folded even with a weak force and make a completely folded state as thin as possible. At the same time, it is necessary to keep the value of thickness not to be strained and broken by impact.

6.2.2 Consideration of generating bi-stable structure [6.4]

In [5.1], on the assumption that all of the same kinds of members only receive strain or compress and bending deformation isn't caused, the process of expansion and contraction is simulated and those distortions which occur in truss member in the horizontal, longitudinal, and polygonal are calculated. For simplification, here the number of layers for the structure is set as two which is the minimum even number, and bar element is assumed to be a circular in cross-section. The shape and material are indicated as in Figure.6.4 and Table.6.1. The height of the truss structure in the initial state is 0.155m. Figure.6.5 shows the behavior of folding in giving the displacement in the height direction to the nodes node composing the hexagon on the top layer, while fixing the positions of nodes composing the hexagon on the bottom layer. And, Figure.6.6 gives the mean values for the distortions caused on each truss member. It is indicated that the truss members in the horizontal and longitudinal directions are compressed, while the ones in the polygonal direction are strained by receiving tension. However, the truss structures in the upper and lower layers are not folded longitudinally symmetrically, but the upper layers which receive displacement input is folded ahead and then the deformation of the truss structure in the lower layers is small given as in Figure.6.5 (b). As a result, on the condition that the height of truss structure is 0.0775 m which is half of the initial value, the truss structure in the upper layers are folded flat and the hexagon on the top falls on the hexagon on the bottom indicates as Figure.6.5(c). Moreover, in continuing the displacement input, the upper layer is not folded, but the hexagon on the top goes past the middle hexagon as shown in Figure.6.5 (d).

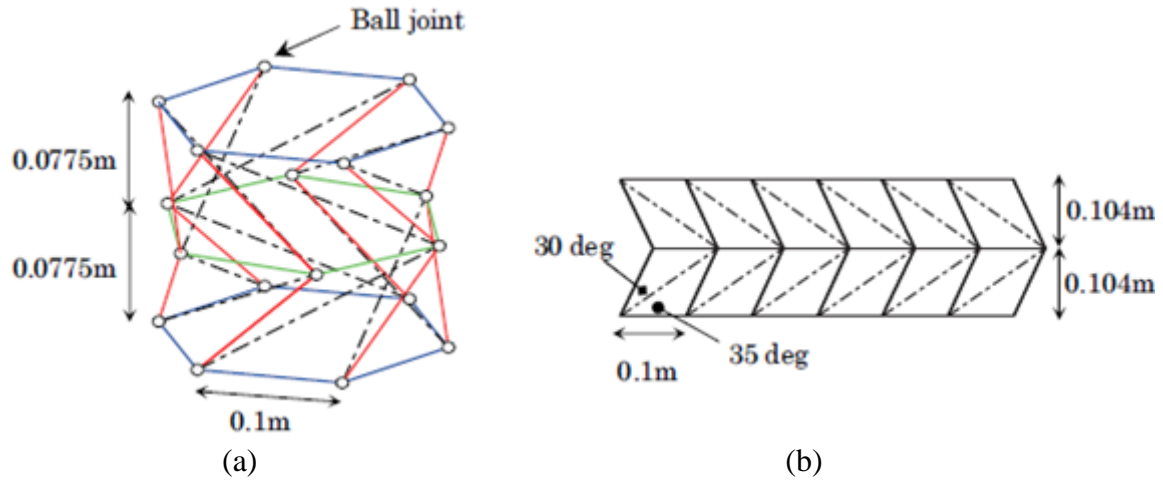


Figure.6.4: Computational model for foldable truss structure; (a): computational truss model consists of horizontal bar elements (blue and green), longitudinal bar elements (red) and diagonal bar elements (black), which are connected by ball joints; (b): crease pattern of the model.

Table.6.1: Specification of the bar elements.

Material	Young's modulus [N/m^2]	Diameter of the cross section [m]
Steel	2.058×10^{11}	2.000×10^{-3}

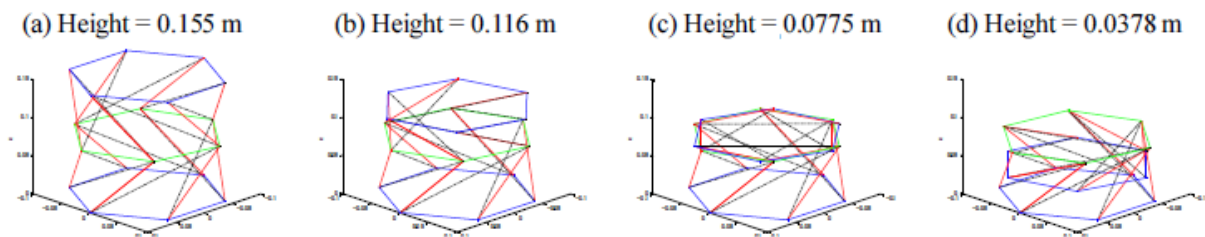


Figure.6.5: Structure shapes through folding process; (a): the initial state without elongation of the bar elements; (b): the intermediate state during folding process; (c): the intermediate state during folding process, where the upper part is perfectly folded; (d): the intermediate state during folding process, where the upper hexagon goes past the middle hexagon (green).

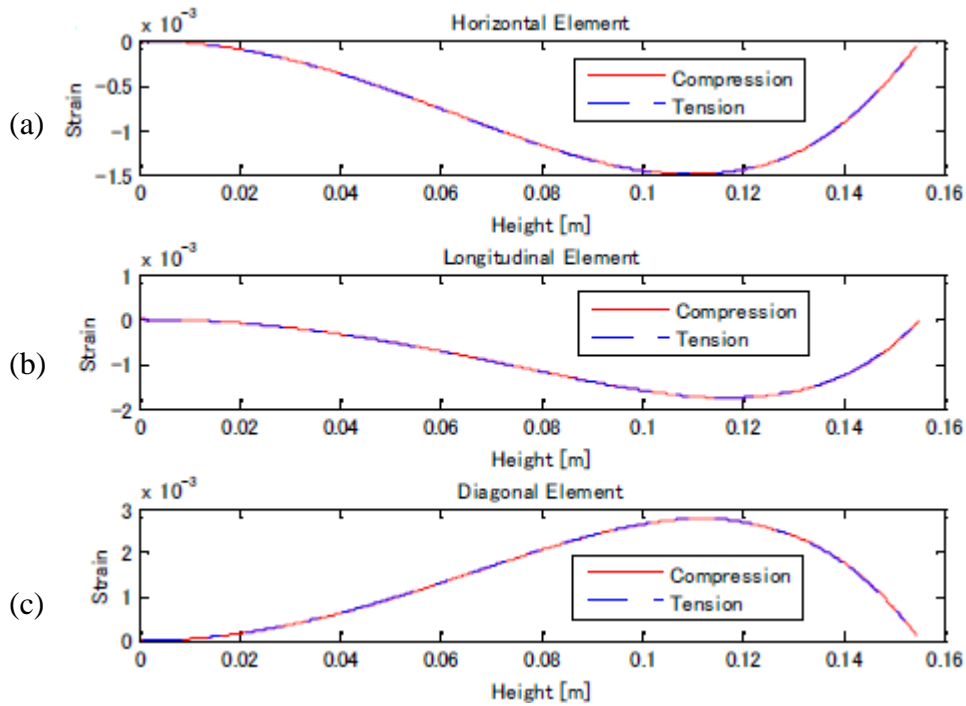


Figure.6.6: Strain of bar elements through folding/expanding processes; (a): a horizontal bar element; (b): a longitudinal bar element; (c): a diagonal bar element. Horizontal and longitudinal elements are tensioned through folding/expanding processes, whereas diagonal elements are compressed.

The above model is devised to prevent the folding structure from buckling, which is considered to be necessary for a tsunami pod [5.1]. If this kind of measure is made, the property of compression tension given as in Figure.6.7 is obtained. In this Figure, in taking the maximum value as small as possible and taking the minimum value as large as possible, a tsunami pod is designed in the way that in case of emergency it is expanded with small force, difficult to be folded in tsunami disaster, and folded with enough force after disaster. This kind of S shaped curve is unstable in the first place, therefore it needs more accurate nonlinear analysis, on which I'd like to work in the future.

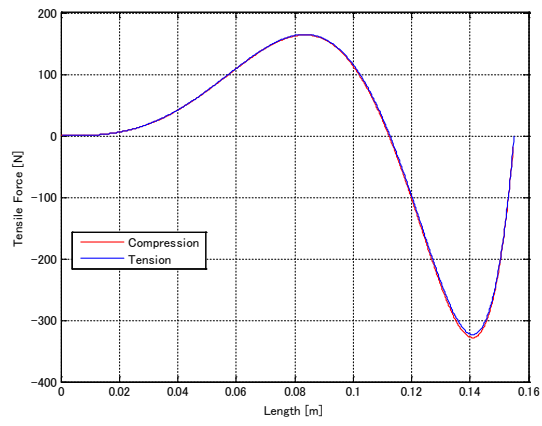


Figure.6.7: Property of compression-tension

Bibliography

Chapter 1

- [1.1] Nojima, T. Structural model by mathematical origami, Faire in INTERNATIONAL INNOVATION CENTER, KYOTO UNIVERSITY (IIC), November 26, 2002.
- [1.2] <http://sciencelinks.jp/content/view/656/260/> (English)
<http://sciencelinks.jp/fr/content/view/592/260/> (French)
<http://sciencelinks.jp/ch/content/view/619/261/> (Chinese)
- [1.3] Robert J. Lang, Tree Maker, <http://www.langorigami.com/science/treemaker/treemaker5.php4>
- [1.4] Kwasaki, T. Dissertation titled as "Theory for deformation of origami crane", 1999, Kyusyu University.
- [1.5] Mojima, T. Modelling of Folding Patterns in Flat Membranes and Cylinders by Using Origami, Transactions of the Japan Society of Mechanical Engineers A, Vo.66, No.643, pp.1050-56(2000)(in Japanese).
- [1.6] Nojima, T. Development of Foldable Conical Shell, Transactions of the Japan Society of Mechanical Engineers A, Vo.66, No.647, pp.2463-69(2000)(in Japanese).
- [1.7] Nojima, T. Origami-Modellings of Foldable Conical Shells Consisting of Spiral Fold Lines, Transactions of the Japan Society of Mechanical Engineers A, Vo.66, No.647, pp.1009-14(2002)(in Japanese).
- [1.8] Nojima, T. Modeling of Facilely Deployable Folding/Wrapping Method of Circular Flat Membrances by using Origami (Foldings in Radial Direction and Wrapping by Archimedean Spiral Arrangement), Transactions of the Japan Society of Mechanical Engineers A, Vo.67, No.653, pp.270-75(2001)(in Japanese).
- [1.9] Nojima, T. Modelling of Compact Folding/Wrapping of Flat Circular Membranes : Folding Patterns by Equiangular Spirals, Transactions of the Japan Society of Mechanical Engineers A, Vo.67, No.657, pp. 1667-74(2001)(in Japanese).

- [1.10] Nojima,T.and Saito,K.,Development of Newly Designed Ultra-Light Core Structures, JSME Inter. J. A,Vol.49, No.1, P38-42 (2006)
- [1.11] Sugiyama,F. and Nojima,T., Development of folding method of spherical membrane in both radial and axial directions, Transactions of the Japan Society of Mechanical Engineers A,Vo.80, No.814, DR0170-DR0170 (2014)(in Japanese).
- [1.12] Abe,K. “Great origami~Enjoy geometry by imagination of origami”, NIPPON HYORON SHA CO.,LTD. PUBLISHERS (2002) (in Japanese)
- [1.13]Moritsugu,S. and Nakamura,R., Computer Algebra : Design of Algorithms, Implementations and Applications
- [1.14] Uehara R., Computational Complexity of Origami, Simulation, Vol.29,No.3,pp.96-101(2010-9) (in Japanese).
- [1.16]Arzu Gonenc Sorguc,Hagiwara,I. and Semra Arslan Selcuk, origamics In Architecture: A Medium Of Inquiry For Design In Architecture, Middle East Technical University, Journal Of The Faculty Of Architecture, Vol.26, No.2, pp.235-247, (2009-12)
- [1.16] Tachi,H., Design Method of Rigid Origami Based on Quadrilateral Mesh,Simulation, Vol.29,No.3,pp.102-107(2010-9).
- [1.17] Takashima,N., The ways to fold triangle into tetrahedron, Simulation, Vol.29,No.3,pp.108-113(2010-9)(in Japanese).
- [1.18] Mitani,J., A Method for Designing 3D Origami Which Envelop an Axisymmetric Shape,Simulation, Vol.29,No.3,pp.114-120(2010-9) (in Japanese).
- [1.19] Designing magazine “Domus ITA”, Architecture of Italy, No. 974, (November 2013).
- [1.20] Kobayashi,H., and Horikawa,K., Deoloyable Structures in Plants,Advances in Science and Technology,Vo.58,p;31-40,(2008)
- [1.21]H.Kitaoka,G.F.Nieman, Y. Fujino,D.Carney,J.DiRocco and I.Kawase,A 4-dimensional model of the alveolar structure,J Phisiol Sci 57,pp.175-185(2007).
- [1.22] Nojima,T., Panel and panel piece, Number of patent application:2005-245045, Patent number: 4451366.
- [1.23] Nojima,T. and Saito,K., Development of Newly Designed Ultra-Light Core Structures、 JSME Inter. J. A,Vol.49, No.1, P38-42 (2006).
- [1.24] Tokura,S. and Hagiwara,I., Forming Process Simulation of Truss Core, Transactions of the Japan Society of Mechanical Engineers A,Vo.74, No.746,pp. 1379-1385(2008)(in Japanese).
- [1.25] Sugiyama, F. and Nojima, T., Development of folding method of spherical membrane in both radial and axial directions, Transactions of the JSME (in Japanese), Vol.80,No.814(2014),DOI:10.1299/transjsme.2014dr0170.
- [1.26] Miura,K.,Zeta-core sandwich-its concept and realization, Inst.of Space and Aeronautical

Science, University of Tokyo,(480):137-164.

[1.27] Zirbel,S.A.,Lang,R.J.,Thomson,M.W.,Sigel,D.A., alkemeyer,P.E.,Trease,B.P.,Magleby,S.P.,and Howell,L.L., Accommodating thickness in origami-based deployable arrays, Journal of Mechanical Design,135(11):111005.

[1.28] Hoffmann, R., et al. "A Finite Element Approach to Occupant Simulation: The PAM-CRASH Airbag Model", SAE-Paper 890754, International Congress and Exposition, Detroit, Michigan, 1989 (also SAE Transactions 1989)

[1.29] Gärtner, Torsten; Eriksson, Magnus; Fältström, Jonas; EASi GmbH, Advanced Technologies for the Simulation of Folded Airbags, 2nd European LS-DYNA Conference, Gothenburg, Sweden, June 1999

[1.30]Kuribayashi,K., A novel foldable stent graft,Phd thesis,University of Oxford.

[1.31] Official website of “Cardborigami”,<http://cardborigami.org/>. Accessed 8 January 2016.

[1.32] Official website of “Mercedes Arocena & Lucia Benitez”,
<https://www.notjustalabel.com/designer/mercedes-arocena-lucia-benitez>, Accessed 8 January 2016.

[1.33]Mitani J (2009) A design method for 3D Origami based on rotational sweep. Computer Aided Design Applications 6(1):69–79

[1.34] Official website of “132 5. ISSEY MIYAKE”,
http://www.isseymiyake.com/brand/132_5.html,Accessed 8 January.

[1.35] Official website of “BAO BAO ISSEY MIYAKE”,
http://www.isseymiyake.com/brand/bao_bao.html,

[1.36] Nakayama,E, Ishida,S, Liao,Y. and Hagiwara, I., Clothes skirt designed on conical truss model, Advances in Manufacturing,Vol.1, No.2,Page 130-135,DOI 10.1007/s40436-013-0019-0 (2013).

[1.37] Software “ORIPA”: <http://mitani.cs.tsukuba.ac.jp/oripa/>. Accessed 8 January 2016

[1.38] Software “ORI-REVO”: http://mitani.cs.tsukuba.ac.jp/ori_revo/.Accessed 8 January 2016

[1.39] Software “Freeform Origami”: <http://www.tsg.ne.jp/TT/software/>.Accessed 8 January 2016

[1.40] Software “Tree Maker” ,
“<http://www.langorigami.com/science/computational/treemaker/treemaker.php>” .Accessed 8 January 2016

[1.41] Software “Pepakura Designer”, <http://www.tamasoft.co.jp/pepakura-en/>.

[1.42] Software “Origami typed 3D printer”, <http://www.i-locus.com/product/other/>.

Chapter 2

- [2.1]Saito,K. Takeda,S. Tokura,I. Hagiwara , Relation between Geometrical patterns and Press Formabilities in Newly Developed Light-Weight Core Panels, Transactions of the Japan Society of Mechanical Engineers(A), Vol.75,No.751, (2009), pp.111-117.in Japanese.
- [2.2]Saito, K., Nojima, T. , Tokura, S. and Hagiwara, I. ,Relation between Geometrical Patterns and Mechanical Properties in Newly Developed Light-WeightCore Panels,Transactions of the Japan Society of Mechanical Engineers(A), Vol.74, No.748, (2008), pp.1580-1586.in Japanese.
- [2.3]Tanaka,S.,Saito, K.,Morimura, H.and Hagiwara,I., Research on the Vibration Analysis of Truss Core Panel ,Transactions of the Japan Society of Mechanical Engineers(C), Vol.76,No.765, (2010), pp.1050-1055.in Japanese.
- [2.4] Tokura, S. Hagiwara, ,I. Shape Optimization to Improve Impact Energy Absorption Ability of Truss Core Panel,Journal of Computational Science and Technology,Vol.5,No.1,(2011-1),pp.1-12.
- [2.5]Saito, K., Nojima, T. , Morimura, H. and Hagiwara, I. ,Evaluation of Bending Rigidity in Newly Developed Light-Weight Core Panels,Transactions of the Japan Society of Mechanical Engineers (A), Vol.75,No.750, (2009), pp.259-265.in Japanese.
- [2.6]Tokura, S. and Hagiwara, I., A Study for the Influence of Work Hardening on Bending Stiffness of Truss Core Panel, J.Appl.Mech.,Vol.77/031010-1-031010-6(2010-5).
- [2.7]Tokura, S. and Hagiwara, I. Forming Process Simulation of Truss Core Panel, Journal of Computational Science and Technology ,Vol. 4(2010),No.1,pp.25-35 (Release Date: March 30, 2010)
- [2.8]Truss core panel by Tokyo Institute of Technology has been applied Sollar panel, Newspaper of Nikkan-kogyo on 20th of July ,2010.
- [2.9]Wu,Z.,Hagiwara,I.and Tao, X.,Optimization of crush characteristics of the cylindrical origami structure, Int. J. Vehicle Design, Vol.43,Nos.1-4(2007), pp66-81.
- [2.10]Zhao, X., Hu,Y.and Hagiwara,I.,Shape Optimization to Improve Energy Absorption Ability of Cylindrical Thin-Walled origami Structure,Journal of Computational Science and Technology,pp. 148-162, Release Date: November 30,2011.
- [2.11]Hagiwara, I.,Tsuda,M.,Kitagawa,Y. and Futamata,T.,Method of Determining Positions of Beads, United States Patent,Patent Number 5048345.)
- [2.12]Kitagawa,Y., Hagiwara,I. and Tsuda,T., Development of a Collapse Mode Control Method for Side Members in VehicleCollisions, SAE 910809 1991 Transaction Section 6 (1992-4 月),pp1101-1107.
- [2.13]Hagiwara,I.,Tsuda,M.,Kitagawa,Y.and Futamata,T.,Method of Determining Positions of Beads,United States Patent,Patent Number 5048345.
- [2.14] Zhao, Z.,Hu,Y.and Hagiwara,I.,Study on Crash Characteristics of Half Cut Type Vehicle Side

Member Structure of Energy Absorption Ability by Using origami Engineering, Journal of Computational Science and Technology, Vo.5, No.1, (2011-1), pp.13-25.

Chapter 3

- [3.1] Williams, D, Dynamics loads in aeroplanes under given impulsive loads with particular reference to landing and gust loads on a large flying boat, Great Britain RAE Reports SME 3309,3316(1945).
- [3.2] Z.D.Ma and I.Hagiwara, Improved Mode-Superposition Technique for Modal Frequency Response Analysis of Coupled Acoustic-Structural Systems, AIAA Journal, Volume 29, Number 10 (1991-10月), pp.1720-1726.
- [3.3] I.Hagiwara and Z.D.Ma, A. Arai and K. Nagabuchi, Reduction of Vehicle Interior Acoustic Using Structural-Acoustic Sensitivity Analysis Methods, 1991 SAE 910208 Transaction Section 6(1992-4月), pp.267-276.
- [3.4] Hagiwara, I., Trends of optimization research in automobile industry, Symposium organized by society of automotive engineering "Structure analysis in optimization technique" (1985) (in Japanese).
- [3.5] Shmit, A. and Farsh, B., Some Approximation Concepts for Structural Synthesis, AIAA J., 12, 692. (1974)
- [3.6] Bendsoe, M.P. and Kikuchi, N., Generating Optimal Topologies in Structural Design using a Homogenization Method, Computer Methods in Applied Mechanics and Engineering, Vol.71, pp.197-224(1988).
- [3.7] Fleury, C. and Braibant, V., Structural Optimization: a New Dual Method Using Mixed Variables, International Journal for Numerical Methods in Engineering, Vol.23, pp.409-428(1986).
- [3.8] K.Svanberg: The Method of Moving Asymptotes a New Method for Structural Optimization, International Journal for Numerical Methods in Engineering, Vol.24, pp.359-373(1987).
- [3.9] Z.D. Ma., Kikuchi, N., Hagiwara, I. and Torigaki, T., Development of Structural Optimization Method for Vibration Reduction : 2nd Report, An Improved Algorithm for the Optimization Problem, Journal of the Japan Society of Mechanical Engineering C, Vol.60, No.577, pp. 3018-3024, (1994).
- [3.10] Torigaki, T., Hagiwara, I., Kitagawa, Y., Ueda, M., Z.D. Ma. and N.Kikuchi, Development and Application of a Shape-Topology Optimization System Using a Homogenization Method, 1994 SAE Transactions Journal of Passenger Cars(SP-1035, SAE940892).
- [3.11] Z.D.Ma, Kikuchi, N. and Hagiwara, I., Structural topology and optimization for a frequency response problem, Computational Mechanics(1993)13, pp.157-174, Springer-Verlag 1993.
- [3.12] Hagiwara, I., Shi, Q. and Takashima F., Function Approximation Method for Crash Optimization Using Neural Network(2nd Report, Application to Vehicle Component), Journal of the Japan Society of Mechanical

engineering A, Vol.64,No.626,pp.2441-2447,(2008)(in Japanese).

[3.13]Shi Q.,Hagiwara,I.,Takashima F. and Tokura S., A Study on Deformation Behavior of Vehicle Cabin and Safety Belt Using a Most Probable Optimal Design Method, Journal of the Japan Society of Automobile Engineering,Vol.31,No.3(2000)(in Japanese).

[3.14]Z.D.Ma. and Hagiwara,I.,Development of New Mode-Superposition technique for Truncating The Lower-and/or Higher frequency Modes Part 1: Frequency Response Analysis for Damped System, Transactions of the Japan Society of Mechanical Engineering C,Vol.57,No.536,pp.1148-1155(1991)(in Japanese).

[3.15]Kojekine,N.,Savchenko,S.,Senin,N.and Hagiwara,I. An approach to surface retouching and mesh smoothing,Visual Computer(2003)19,pp.1-16.

Chapter 4

[4.1]Shigematsu, T., Akechi, K. and Koike, T., Basic experiment about the development of a float typed tsunami shelter, Journal of civil engineering in the ocean,Vol.24(2008),pp.105-110(in Japanese).

[4.2]Shigematsu, T. and Nakahigashi, D., Experimental research about the motion property of double float typed tsunami shelter,Journal of civil engineering,B2 (Coastal engineering), Vol. 67,No. 2(2011),pp.751-755 (in Japanese).

[4.3]Watanabe, K., and Kaneko Y., INVESTIGATION OF TSUNAMI EVACUATION USING FLOATING TYPE TSUNAMI EVACUATION SHELTER ON THE BUILDING, Japan Society of Civil Engineers B3, 71(2), I_701-I_706, 2015.

[4.4]Mutsuada,H, Fujii, S., Kamata,T., and Tsuchii Y.,Reduction of Tsunami Force Acting on a Floating/Submerged Tsunami Shelter and Its Motions, Journal of the Japan Society of Naval Architects and Ocean Engineers, No.20(2014).

[4.5] SANKYO MANUFACTURING Co.,Ltd. >CFRP>Data collection for performance comparison I (online),available from <<http://www.sankyo-ss.co.jp/about-cfrp/performance.html>>, (accessed on 15 May, 2015) (in Japanese).

[4.6]Wikipedia, the free online encyclopedia for the term" Head injury criterion" https://en.wikipedia.org/wiki/Head_injury_criterion

[4.7]LS-DYNA KEYWORD USER'S MANUAL VOL.I-III, LIVERMORE SOFTWARE TECHNOLOGY CORPOTATION (LSTC Corp.,) (2014).

[4.8]Mitsume, N., Yoshimura, S. and Murotani, K., Fluid-structure coupled analysis using finite element method and particle method, Proceeding of computational engineering and science,B-4-2(2012) (in Japanese).

[4.9]Souli, M., Ouahsine, A. and Lewin, L., Arbitrary Lagrangian Eulerian formulation for fluid-structure interaction problems. Computer Methods in Applied Mechanics and Engineering, Vol.190 (2000) ,pp. 659-675 .

[4.10]Stander, N., Willem, R., Goel, T., Eggeleston. and Craig, K.,LS-OPT user's manual design optimization and probabilistic analysis tool for the engineering analyst, Ver.4.2(2012), Livermore software technology corporation.

Chapter 5

- [5.1] Ishida, S., Uchida, H. and Hagiwara, I., Vibration isolators using nonlinear spring characteristics of origami-based foldable structures, Transactions of the Japan Society of Mechanical Engineers A Vol. 80, No. 820, p. DR0384 (2014) (in Japanese).
- [5.2] Kresling, B., Natural twist buckling in shells: from the hawkmoth's bellows to the deployable Kresling-pattern and cylindrical Miura-ori, Proceedings of the 6th International Conference on Computation of Shell and Spatial Structures (IASS-IACM 2008): Spanning Nano to Mega (2008).
- [5.3] Hunt, G. W. and Ario, I., Twist buckling and the foldable cylinder: an exercise in origami, International Journal of Non-Linear Mechanics, Vol. 40 (2005), pp. 833-843.
- [5.4] Nagashima, G., and Nojima, T., Development of foldable triangulated cylinder, in Proceedings of the 7th JSME Materials and Processing Conference (M&P) (1999), pp. 153-154 (in Japanese).
- [5.5] Sushida, T., Huzume, A. and Yamagishi, Y., Design methods of origami tessellations for triangular spiral multiple tilings, Origami6: I. Mathematics, pp. 241-252 (2016).

Chapter 6

- [6.1] Robert, L., presentation slides titled as "The math and magic of origami", TED talk, (2008).
- [6.2] <http://www.h2.dion.ne.jp/~td-imp/main/popuptent.htm> . Accessed 8 January 2016
- [6.3] Terada, K., Tokura, S., Satou, H., Makita, A. and Hagiwara, I., Evaluation of the bending stiffness on assembled light weight and high strength panel, Transactions of the Japan Society of Mechanical Engineers, No. 15-00039 (2015) (in Japanese)
- [6.4] Hagiwara, I., Ishida, S. and Uchida, H., Origami based vibration control structure, patent application number: 2013-220548 (October, 23, 2013) , patent publication number: 2015 - 81655 (April 27, 2015) (in Japanese).